TRIGGERING MECHANISMS OF A RAINFALL-INDUCED RESIDUAL SOIL SLOPE FAILURE

by

Mariely Mejías Santiago

A thesis submitted in partial fulfillment of the requirements for the degree of

MASTER OF SCIENCE
in
CIVIL ENGINEERING

UNIVERSITY OF PUERTO RICO
MAYAGÜEZ CAMPUS
2011

Approved by:

_____	_____
Miguel A. Pando, Ph.D. President, Graduate Committee	Date
_____	_____
Ismael Pagán Trinidad, MSCE Member, Graduate Committee	Date
_____	_____
Ricardo Ramos Cabeza, Ph.D. Member, Graduate Committee	Date
_____	_____
Luis R. Pérez-Alegría, Ph.D. Graduate School Representative	Date
_____	_____
Ismael Pagán Trinidad, MSCE Chairperson of the Civil Engineering and Surveying Department	Date

ABSTRACT

This MS thesis entails an experimental and analytical study of a slope failure that occurred in the city of Mayagüez after a heavy storm on June, 2005. The slope failure case history is considered a representative event of the recurring shallow landslides that often occur in residual soil slopes of Western Puerto Rico. The experimental component of this work involved field reconnaissance, surveying of the failed slope, geotechnical drilling and testing, soil sampling, laboratory testing, long term field monitoring of rainfall, soil moisture, and soil suction. The study also included laboratory tests to evaluate the soil-water characteristic curve. The research also included an analytical component to investigate the triggering mechanism of the slope failure.

RESUMEN

Esta tesis de maestría trata de un estudio experimental y analítico de un talud fallado en la ciudad de Mayagüez, PR luego de una lluvia fuerte en junio del 2005. El deslizamiento se considera como un evento representativo de los deslizamientos superficiales que ocurren frecuentemente en pendientes con suelos residuales en el oeste de Puerto Rico. El componente experimental de este trabajo envolvió reconocimiento de campo, agrimensura del talud fallado, muestreo, pruebas de laboratorio, monitoreo a largo plazo de lluvia, succión, y contenido de humedad. La investigación también incluyó un componente analítico para investigar el mecanismo de falla del talud.

.

To God
To my family
To my son, Eriam Yael
To my husband, Henry

ACKNOWLEDGEMENTS

During the development of my graduate studies at UPRM several people collaborated directly and indirectly with my research. Without their support it would have been impossible for me to finish my work. I dedicate this section to recognize their support.

I want to start expressing a sincere acknowledgement to my advisor, Dr. Miguel A. Pando because he gave me the opportunity to do research under his guidance and supervision. I received motivation, encouragement and support from him during all my graduate studies. The last stages of this work were done from the distance while working full-time for the U.S. Army ERDC. Even in the distance he kept giving me support and motivation to finish this work and I am really thankful for that.

I also want to thank my committee mentors, Prof. Ismael Pagán and Dr. Ricardo Ramos for their motivation and support during my graduate studies and also during the process of finishing this work. Special thanks go to Dr. Victor Snyder for his generosity for providing most of the equipment necessary to perform the field work. Dr. Snyder provided valuable suggestions for the field instrumentation portion of this thesis. Special thanks also go to my friend and class-mate Anibal Mercado for all his unconditional support during the experimental work for this research. I would also like to give special acknowledgments to the laboratory technicians Jaime, Monse, and Elvis, and my "field crew": Lennie González, Cesar Ramírez, Omar Esquilín and Ruth Dendariarena.

I would also like to acknowledge the financial support I received from a fellowship from the NASA Puerto Rico Space Grant Consortium. This fellowship provided partial funding and resources for the development of this research, thus I am very grateful for their support.

And last, but not least, I would like to thank my family for their unconditional support, inspiration and love: my mom Tere; my dad Francisco; my brothers and sisters, Ivy, Kary, Frances, Frankie, Paquito, Coralis; my son Eriam Yael; and, my husband Henry.

TABLE OF CONTENTS

LIST OF TABLES

Tables **Page**

LIST OF FIGURES

Figures **Page**

1 INTRODUCTION

1.1 Background and Justification

Landslides triggered by episodes of intense rainfall constitute a serious natural hazard for many regions of the United States and worldwide (NRC, 2004). In Puerto Rico, rainfall-induced instabilities also constitute a common and recurrent problem (Larsen and Torres-Sanchez, 1998, Pando et al. 2005). For the region of Puerto Rico one main area of interest is related to the behavior of residual soil slopes that are typically in unsaturated state and have a complex shear strength behavior that depends on matric suction levels, which in turn is a function of rainfall infiltration.

Similar instabilities have been reported in Singapore, where failures in both natural and cut slopes that involve residual soils are usually brought about during monsoon season which is characterized by heavy rainfall (Low et al., 2000). In Puerto Rico, slope instabilities are generally reported with intense and persistent rainfall events, better known as wet or rainy seasons. For example, the hurricane season in Puerto Rico tends to be wet, but also there are other periods like winter fronts with equal critical rainfall events.

Landslides are usually sudden, occurring after heavy rainfall. This is a serious recurring problem partly related to Puerto Rico's hilly and mountainous terrain which covers more than 70 percent of its territory. The problem is accentuated due to the presence of problematic soils such as weathered residual soils, the effect of human activities, such as road

construction through and around natural slopes, and recurrent episodes of intense rainfall. Clearly, landslide hazards are a serious concern for state and local government agencies, universities, and the engineering community in PR. To implement effective mitigation schemes requires a good understanding of the triggering mechanisms involved in these rainfall-induced slope instabilities involving tropical residual soils. Unfortunately, current state of knowledge is insufficient as highlighted by a study lead by a national expert panel (NRC, 2004).

Recent research in this area suggests that the main triggering mechanism involved in residual soil slope failures is that the infiltration of rainwater causes a reduction of matric suction in the unsaturated soil zone and increases the weight of the landsliding mass. The shear strength of the residual soil varies in a complex fashion during rainfall infiltration (Low et al., 2000; Zhan et al., 2003; Pando et al., 2007; and, others). The shear strength decreases due to loss of apparent cohesion related to matric suction and due to decrease of effective stress levels.

The main focus area of this MS thesis is rainfall-induced instabilities in residual soil slopes of Western Puerto Rico. Specifically, this thesis will focus on a case history where several landslide events were triggered during a heavy storm on the 10^{th} of June 2005. The events occurred in the city of Mayagüez, located in the Western end of Puerto Rico. The total rainfall for this storm was 9.3 cm and the maximum intensity was 6.7 cm/hr. During this storm at least 10 shallow landslides were initially reported within the Mayagüez area. However, later past-storm surveillance of the area revealed many more failures. This research

is mainly focused on a detailed study of one of the landslide events that occurred near the UPRM campus during this June 2005 heavy rainfall storm.

The experimental component of this work involved field reconnaissance, surveying of the failed slope, geotechnical drilling and testing, soil sampling, laboratory testing, long term field monitoring of rainfall, soil moisture, and soil suction. The study also included laboratory tests to evaluate the soil-water characteristic curve. The research also included an analytical component to investigate the triggering mechanism of the slope failure.

1.2 Objectives

The main objective of this research was to carry out a detailed investigation of a rainfall-induced slope failure located in Western Puerto Rico, which was comprised primary of tropical unsaturated residual soils. More specific objectives of this study include the following:

1) Design and implement a field instrumentation plan for long term monitoring of soil suction as a function of rainfall and time.

2) Develop and implement a laboratory experimental plan to determine the soil water characteristic curve of soil samples retrieved from the slope.

3) Perform an analytical study to investigate the triggering mechanism involved in the slope instability case study. This objective included unsaturated infiltration ground water modeling coupled with slope stability analyses.

1.3 Thesis Organization

This thesis is divided into eight chapters including this introduction. Chapter 2 presents background information on the triggering mechanisms of rainfall induced landslides and the basic concepts of unsaturated soil mechanics applied to slope stability. Chapter 3 presents a literature review summarizing the most important and relevant work related to previous studies carried out to evaluate the effects of the rainfall infiltration on unsaturated soil slopes. Chapter 4 presents a description of the slope under study, Chapter 5 describes the experimental methodology, Chapter 6 presents the experimental results and Chapter 7 discuses the analytical models and results. Conclusions and recommendations are presented in Chapter 8, and the references are listed at the end.

2 BACKGROUND AND DEFINITIONS

2.1 Rainfall-Induced Landslides

Rain is the most common cause of landslides. Rainfall-induced landslides typically occur in mountainous landscapes, and cover a wide range of failure mechanisms. In tropical and subtropical areas, for example, a large number of steep, natural and engineered slopes have been observed to remain stable for a long time and then suddenly fail during heavy rainstorms (Tsaparas et al., 2002). In Puerto Rico, landslides in residual soil slopes are usually sudden and tend to occur after events of heavy rainfall.

Several authors have suggested that conventional methods for the design and construction of soil slopes that are based on the assumption of saturated behavior cannot be applied for slopes under unsaturated conditions (Fredlund, 1979; Fredlund and Rahardjo, 1993; and, Zhou et al., 2005). Slope stability analysis of unsaturated soil slopes typically requires seepage analysis because the failures involve complex heavy rainfall and infiltration.

The triggering mechanism of rainfall-induced failures on unsaturated soil slopes is related to the infiltration of rainwater that causes an increase in the soil unit weight and a reduction of the soil matric suction (or an increase in the negative pore-water pressure). This complex process results in an increase of the driving force and a decrease of the resistance force which is a function of the shear strength of the soil.

The next section of this chapter presents a review of the basic concepts of unsaturated soil mechanics as they relate to the slope stability problem being studied in this research.

2.2 Review of Unsaturated Soil Mechanics

The general field of soil mechanics can be subdivided into the portion dealing with saturated soils and the portion dealing with unsaturated soils (Fredlund and Rahardjo, 1993). A major distinction that is made between saturated and unsaturated soils is the negative pore pressures (suction) that develop in unsaturated soils (Figure 2.1). Any soil near the surface will be subjected to fluctuation in water content (and saturation) as shown in Figure 2.1. This zone is often referred as to the vadose zone.

An unsaturated soil sample within the vadose zone will have three phases: 1) solids, 2) water, and 3) air. For simplicity, the air-water interphase or contractile skin (Fredlund and Morgenstern, 1977) will not be included in this review discussion, but the reader should be aware that this is often referred to as a fourth phase in unsaturated soil mechanics.

Climate plays an important role in whether a soil is saturated or unsaturated. Evaporation from the ground surface or evapotranspiration from a vegetative cover produce an upward flux of water out of the soil. On the other hand, rainfall and other forms of precipitation provide a downward flux into the soil. The difference between these two conditions coupled with regional ground water condition, dictates the pore-water pressure conditions in the soil

within the vadose zone. Climatic changes highly influence the water content of the soil near the ground surface. Upon wetting, the pore-water pressures increase, tending toward positive values. As a result, changes occur in the volume and shear strength of the soil. Many soils are known for their significant loss of strength upon wetting. As mentioned in the previous section, changes in the negative pore-water pressures associated with heavy rainfalls are the cause of numerous slope failures.

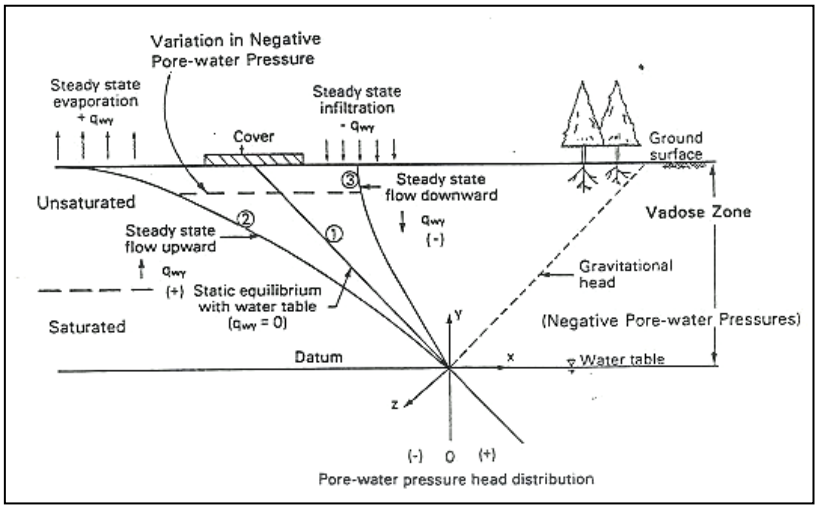

Figure 2.1 Negative pore-water profiles in the vadose zone (from Fredlund, 1993).

2.2.1 Soil-Water Characteristic Curve

The soil-water characteristic curve (SWCC) is the relationship between the soil matric suction and the volumetric water content, gravimetric water content, or degree of water saturation. This curve is characteristic for different types of soils and can be determined using the method described by the ASTM D 6836. The SWCC is a key consideration for

hydrological characterizations of unsaturated soils and is also required for most analyses of water movement in unsaturated soils. The reliability of estimated unsaturated soil properties is to a large extent related to the accuracy of the SWCC (Fredlund and Houston, 2009).

The shape of the SWCC has been studied by several researchers (e.g., Burdine, 1953; Gardner, 1956; Brooks and Corey, 1964; Brutsaert, 1966; Mualem, 1976; van Genuchten, 1980; McKee and Bumb, 1987; Kosugi, 1994; and Fredlund and Xing, 1994). However, a good mathematical expression should have only a few parameters with clear physical meaning and be easy to use (Zhou et al., 2005). The van Genuchten (1980) expression is widely used to characterize the shape of the SWCC due to its flexibility and simplicity and is given as follows:

$$\theta(\psi) = \theta_r + \frac{\theta_s - \theta_r}{\left[1 + \left(\alpha|\psi|\right)^n\right]^{1-\frac{1}{n}}} \qquad \textbf{(2.1)}$$

where, $\theta(\psi)$ is the water retention curve, $|\psi|$ is the suction pressure, θ_s is the saturated volumetric water content, θ_r is the residual volumetric water content, α is a constant ($\alpha>0$), and n is a measure of the pore size distribution ($n > 1$).

In this model, parameter n is related to the pore size distribution index. The more uniform pore sizes in soil have larger n values. Also the larger the value of n the steeper the curve in the de-saturation zone will be. The uniformity in the pores allows for a quicker loss of

saturation. Parameter *a* does not affect the shape of the curve, but shifts the curve towards the higher or lower suction regions of the plot.

Figure 2.2 shows typical SWCC for a silty soil. At suctions close to zero, a soil is close to saturation, and water is held in the soil primarily by capillary forces. As the water content decreases (during the desorption process), binding of the water becomes stronger and at small suctions (more negative) water is strongly bound in the smallest of pores, at contact points between grains and as films bound by absorptive forces around particles.

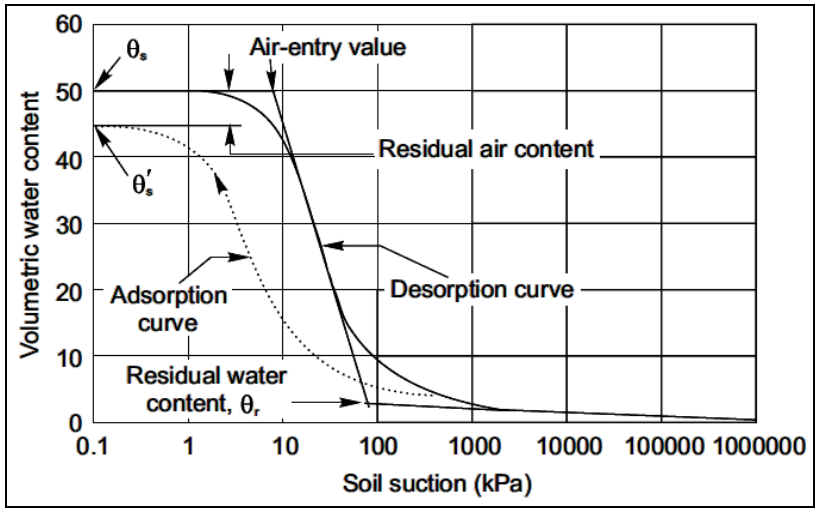

Figure 2.2 Typical desorption and absorption curves for a silty soil (adapted from Fredlund and Xing, 1994).

The suction-water content relationship varies with the water flow process which flow into or out of the soil section (Konyai et al., 2009). When water is flowing into the soil section it is called absorption (or wetting) process. The water retention curve of the absorption process from the initial stage of air-dry soil until saturated condition is a unique curve, called the

primary absorption curve. Similarly, the primary desorption (drying) curve is obtained from a draining process of saturated soil until the soil is very dry. Wetting and draining processes of soil water conditions between saturated and air-dry condition, produce the scanning curves. The two primary curves form the boundaries of all scanning curves are shown in Figure 2.3. This phenomenon is called hysteresis.

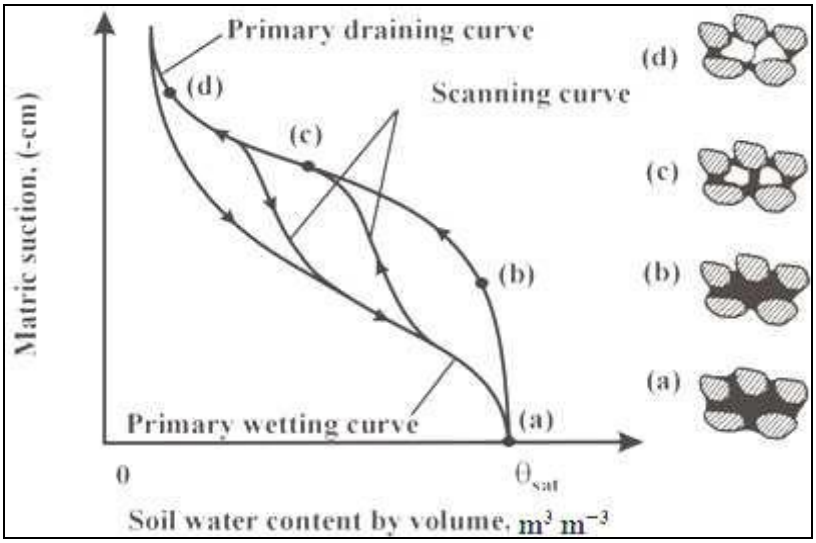

Figure 2.3 The characteristics of hysteresis retention curve (from Konyai et al., 2009).

There is a limit to the negative pore water pressure a soil can sustain without drawing in air through any surface exposed to the atmosphere. This limiting negative pore water pressure is known as the air entry value (*AEV*). *AEV* for a soil increases if the soil pore size decreases and it can be estimated by considering the equilibrium of a hemispherical water meniscus in a circular pore of diameter *d* using the following equation and Figure 2.4:

$$\pi d T = \frac{\pi d^2}{4} AEV$$
$$AEV = \frac{4T}{d} \quad \textbf{(2.2)}$$

where T is the surface tension.

The force due to surface tension around the rim of the meniscus is equal to the force due to difference between pore water and air pressure. When the suction is larger than the air-entry value then the soil starts to desaturate. The amount of water in soil decreases significantly with increasing suction in the transition state. Eventually a large increase in suction leads to a relatively small change in the water content and is the residual stage. The hysteresis can affect the accuracy of unsaturated flow calculations.

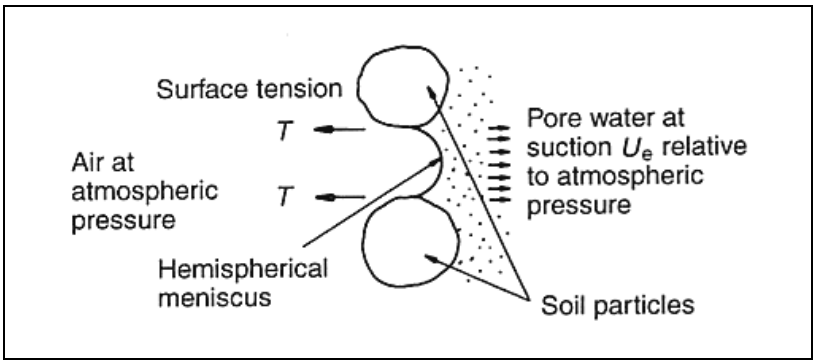

Figure 2.4 Estimation of the AEV from equilibrium of a hemispherical water meniscus in a circular pore (adapted from Konyai et al., 2009).

Sandy soils will involve mainly capillary binding, and will therefore release most of the water at higher suctions, while clayey soils, with adhesive and osmotic binding, will release water at lower (more negative) suctions. The water holding capacity of any soil is defined by

the porosity and the nature of the bonding in the soil. Table 2.1 lists some typical AEV for different soils base on the particle size corresponding to 10% fines. Due to their low AEV, coarse-grained soils remain unsaturated above the ground water table with very little water retained by capillary action. In the other hand, fine-grained soils may remain saturated for several meters above the water table with pore water pressure continuing to decrease until the AEV is reached.

Table 2.1 Typical air entry values for soils.

Soil Type	D_{10} (mm)	AEV (kPa)
Coarse Sand	1	0.28 to 1.4
Clay	0.001	280 to 1400

2.2.2 Shear Strength of Unsaturated Soils

The shear strength of a saturated soil, τ, is typically expressed as a function of the effective stress, σ' applied to the soil:

$$\tau = c' + \sigma' \tan \phi' \qquad \textbf{(2.3)}$$

where, c' is the effective cohesion which occurs due to molecular attraction between soil particles, and φ' is the effective friction angle. The effective normal stress (σ') is defined by Terzaghi (1943) as the normal stress taken by the solid soil particles of a soil skeleton and is equal to the total normal stress applied to the soil (σ) less the pore-water pressure (u_w).

In this equation, the shear strength of the soil is dependent on only one stress state variable. Equation (2.3) is applicable to soils that are either completely saturated ($u_w > 0$) or

completely unsaturated (u_w = 0). The following paragraphs describe the shear strength principle as it applies to unsaturated soils.

For the more general case of an unsaturated soil, the shear strength is typically expressed in terms of the stress state variables as shown in the following equation after Fredlund et al. (1978):

$$\tau = c' + (\sigma - u_a)\tan\phi' + (u_a - u_w)\tan\phi^b \quad \textbf{(2.4)}$$

where, τ is the shear strength, φ' is the angle of friction for changes in the net stress ($\sigma - u_a$), and φ^b is the angle of friction for changes in matric suction ($u_a - u_w$), and c' is the effective cohesion.

In most cases, the pore-air pressure is taken to be atmospheric and set to zero for simplicity. Equation 2.4 can be used to define the shear strength of either saturated or unsaturated soils. For a saturated soil, u_w will be positive and there will be no additional contribution to shear strength from suction. In that case, φ^b is equal to φ' and the shear strength formulation will be equal to Equation 2.3. For an unsaturated soil, u_w will be negative and the contribution to shear strength from suction will be evaluated (Collins, 1995).

The shear strength envelope for Equation 2.4 takes on a three-dimensional form due to the presence of two stress state variables. Fredlund (1979) simplified this type of conceptualization by combining the first and last terms of the equation into one, termed the

total cohesion, c_t, which represents the cohesion intercept that combines the effective or true cohesion and a term related to the matric suction ($u_a - u_w$) level in the soil, as follows:

$$c_t = c' + (u_a - u_w)\tan\phi^b \quad \textbf{(2.5)}$$

This approach is widely used in interpreting shear strength data on unsaturated soils and it was the approach used in this study. From Equations (2.4) and (2.5) we can envision a shear strength envelope that will depend on the level of matric suction in the soil. This is shown graphically in Figure 2.5.

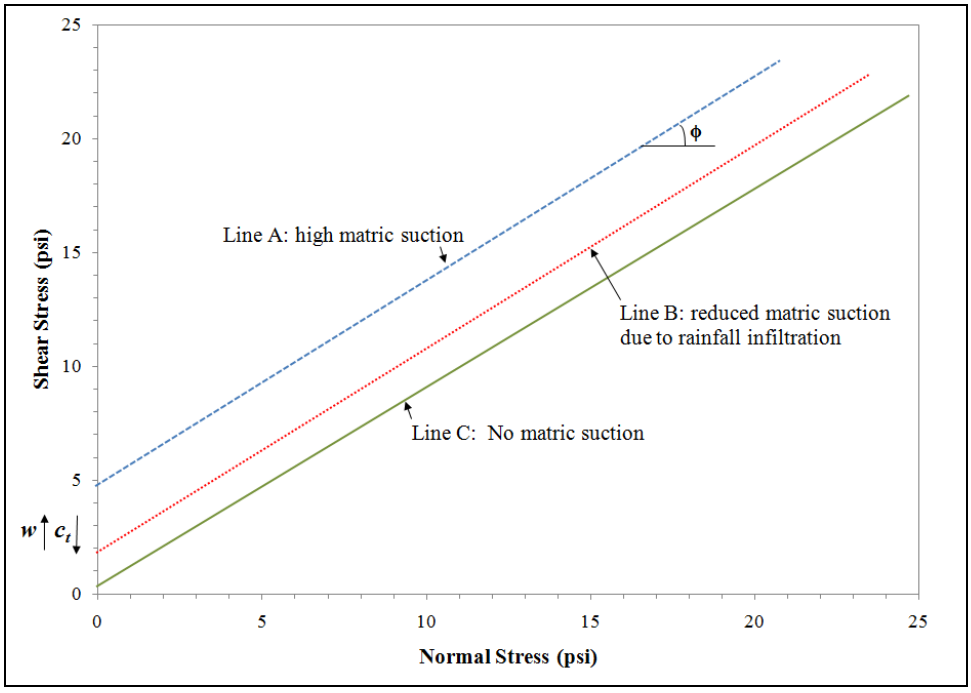

Figure 2.5 Shear strength envelopes for unsaturated soils under different suction conditions.

This figure shows a shear strength envelope (labeled line A) for an unsaturated soil sample. This line shows a relatively high cohesion intercept (c_t) due to a high matric suction level if the soil is at low moisture content (w). If the moisture content of this soil increases due to rainfall infiltration, then the shear envelope could drop to line B, which would correspond to a lower cohesion intercept. Some of this cohesion is due to matric suction if the soil is still unsaturated. Eventually, if the rainfall infiltration is high enough it could reach a shear strength envelope corresponding to line C, which would represent the envelope of a saturated soil with no matric suction. For this case, the cohesion intercept (if any) would be only due to true of effective cohesion.

To better illustrate the influence of matric suction on the shear strength envelope of unsaturated soils we can refer to Figure 2.6. This figure shows unpublished data in the form of Mohr circles obtained from suction controlled triaxial tests on a high-plastic sandy residual silt (Burrage et al., under review). The solid blue line represents the shear strength envelope obtained from tests on saturated soil samples (i.e., with no suction). The fine dotted red line represents the shear strength envelope obtained from triaxial compression tests carried out on soil samples tested under a constant matric suction of 10 psi. We can see that the two shear strength envelopes are parallel, but the envelope for 10 psi suction has a higher cohesion intercept.

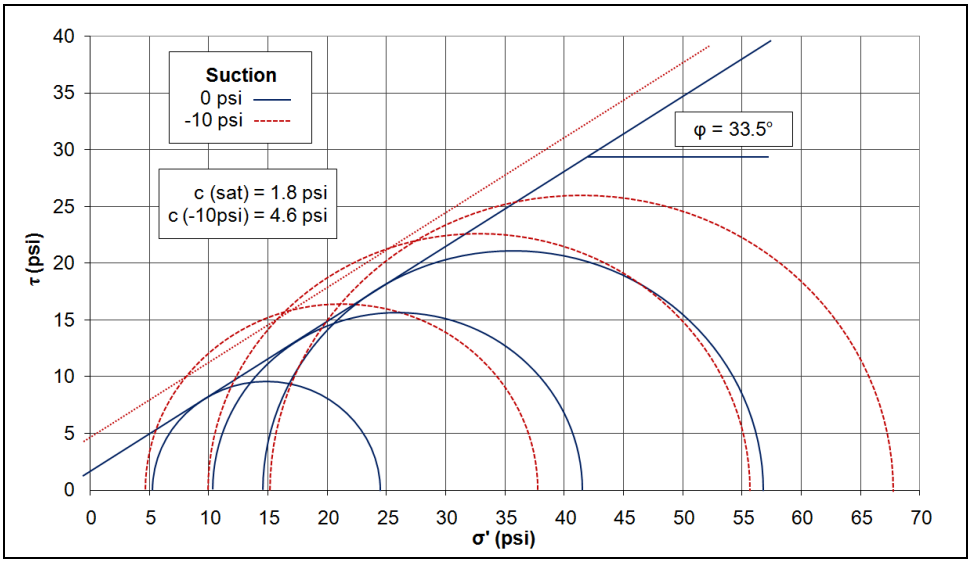

Figure 2.6 Mohr-Coulomb diagrams for triaxial tests (Burrage et al., 2011).

From Figure 2.6, it can be seen that the samples tested at a suction of 10 psi have on average an increased cohesion of approximately 2.8 psi over the saturated samples. Using this increase in cohesion, the parameter φ^b can be calculated using the following equation:

$$\varphi^b = \tan^{-1}\left(\frac{c_{unsat} - c_{sat}}{u_a - u_w}\right) \quad \textbf{(2.6)}$$

In this equation, c_{unsat}-c_{sat} represents the difference in cohesion between the saturated tests and the unsaturated tests, u_a-u_w represents the matric suction at failure, and φ^b is an angle that represents the rate of increase in shear strength as the matric suction increases. This is illustrated in a 3-D plot in Figure 2.7.

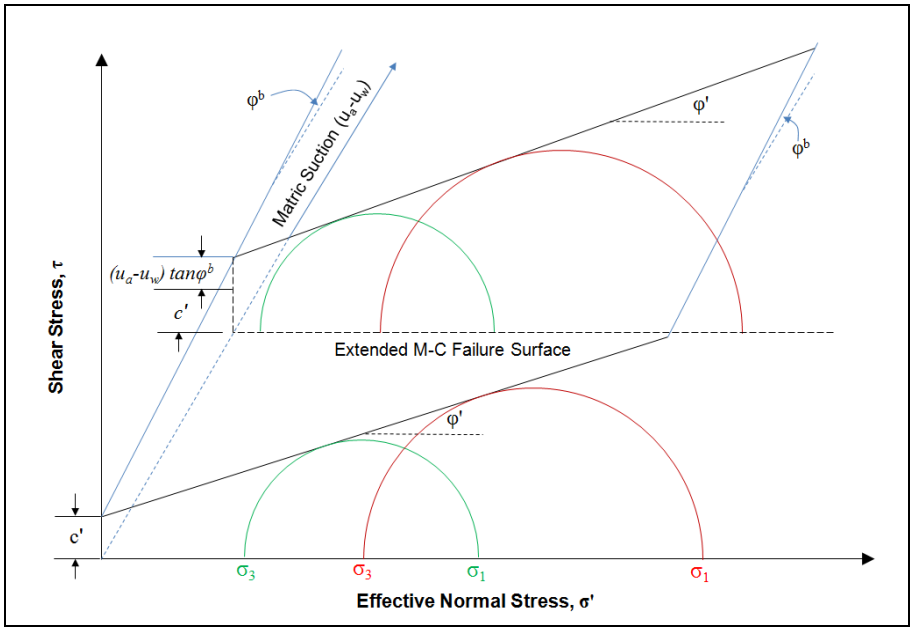

Figure 2.7 Extended Mohr-Coulomb failure surface (Burrage et al., 2011).

The value calculated for φ^b for the sandy residual silt tested by Burrage et al. (2011, under review) was found to be 15.64°. This value is comparable to values reported in the literature as summarized in Table 2.2. The shear strength evaluation for the soils involved in the case history slope is discussed in more detail in Chapter 7.

Table 2.2 Shear strength parameters for relevant unsaturated soils.

Soil Type	c' (psi)	φ' (deg)	φ^b (deg)	References
Undisturbed decomposed granite	4.19	33.4	15.3	Ho and Fredlund (1982)
Boulder clay; w = 11.6%	1.39	27.3	21.7	Bishop et al. (1960)
Madrid gray clay; w = 29%	3.44	22.5	16.1	Escario (1980)
Tappen-Notch Hill silt; w = 21.5%, ρ_d = 99.3 pcf	0.00	35.0	16.0	Krahn et al. (1989)

2.3 Summary

This chapter presented a brief overview of some basic concepts on unsaturated soil mechanics including definitions and shear strength. These concepts will help understand the formulations and procedures used for the stability analyses that are discussed later on in this thesis.

3 LITERATURE REVIEW

3.1 Introduction

This chapter presents the literature review carried out for this thesis. The literature review was carried out on the general subject of rainfall induced landslides, but with a emphasis on residual soil slopes. The literature review was subdivided into four main topics: empirical rainfall-duration intensity thresholds, effects of cumulative and antecedent rainfall, hydro-geological approach, and analytical approaches of the rainfall-stability problem. The following subsections present a summary of each of these four areas.

3.2 Empirical Rainfall Duration-Intensity Thresholds

A large percentage of the existing studies related to rainfall induced landslides have focused on the use of empirical rainfall thresholds. These thresholds typically consist of a relationship between the intensity of the rainfall event that triggered landslide events and its duration. These empirical relationships establish threshold values of rainfall above which a certain degree of landsliding can be expected, or below which no landslide activity will occur (Preston, 2000). Caine (1980) is considered the first researcher who proposed an empirical relation between rainfall characteristics (duration and intensity) and the occurrence of landslides to define a landslide triggering threshold. This author proposed a worldwide

intensity duration threshold by selecting heavy rainfalls which triggered landslides in a variety of locations around the world. Caine (1980) proposed a rainfall threshold as the straight line shown in Figure 3.1. This figure represents a double logarithmic plot of intensity and duration from 73 rainfall storms throughout the work that have triggered landslides. The author selected as the threshold a straight line that represents approximately the lower bound of most landslides triggering rainfall data in his database (n=73). These 73 locations included varying geologic and climatic characteristics, thus, the threshold proposed by Caine is supposed to be applicable throughout the World.

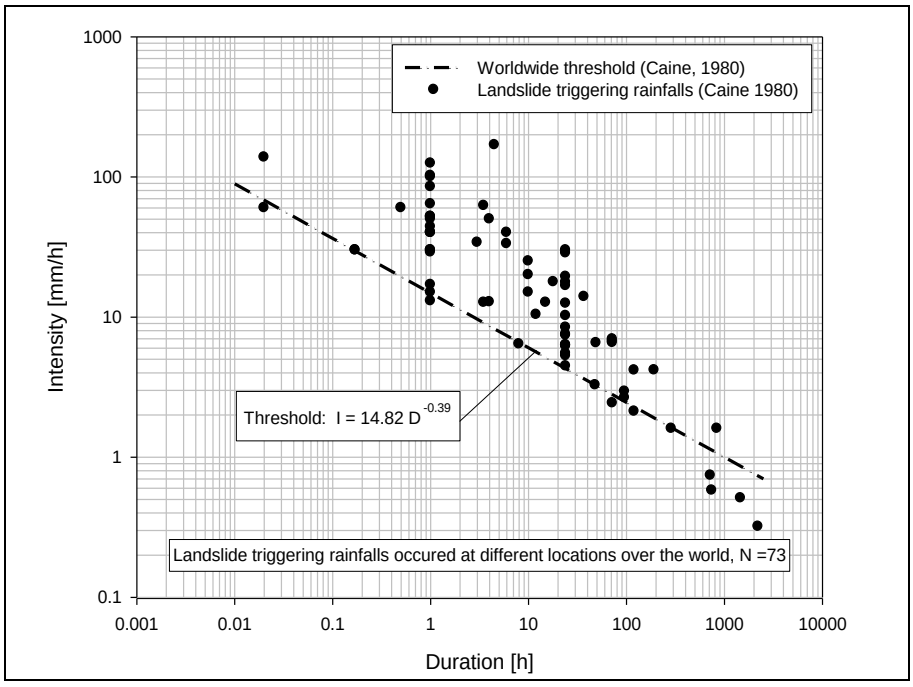

Figure 3.1 Intensity-duration threshold proposed by Caine (1980).

Although empirical rainfall thresholds have their limitations, they have been used successfully in landslide warning systems. For example, Keefer et al. (1987) describe the successful use of empirical thresholds in the San Francisco Bay area, California, where they developed a landslide warning system using a network of rainfall gauges. However, recent research recognizes regional variations in such thresholds, due to differences in lithology, soils, vegetation, climatic conditions and other similar factors (Polemio and Petrucci, 2000; Preston, 2000).

For Puerto Rico rainfall thresholds have been proposed by Larsen and Simon (1993) and more recently by Pando et al. (2005). An extensive compilation of storms that triggered landslides between 1959 and 1991 was published by Larsen and Simon (1993). A total of 41 storms were identified, each of which triggered 10's to 100's of landslides in Puerto Rico between 1959 and 1991. Using a similar approach as Caine (1980), these authors obtained a rainfall intensity-duration threshold for Puerto Rico. This rainfall threshold was recently updated by Pando et al. (2005) to include a total of 34 storms that triggered landslides for the period of 1993 to 2003. The revised threshold proposed by these authors is shown in Figure 3.2.

Although empirical rainfall threshold are useful for landslide mitigation strategies, this research was not focused very much on this aspect of the problem.

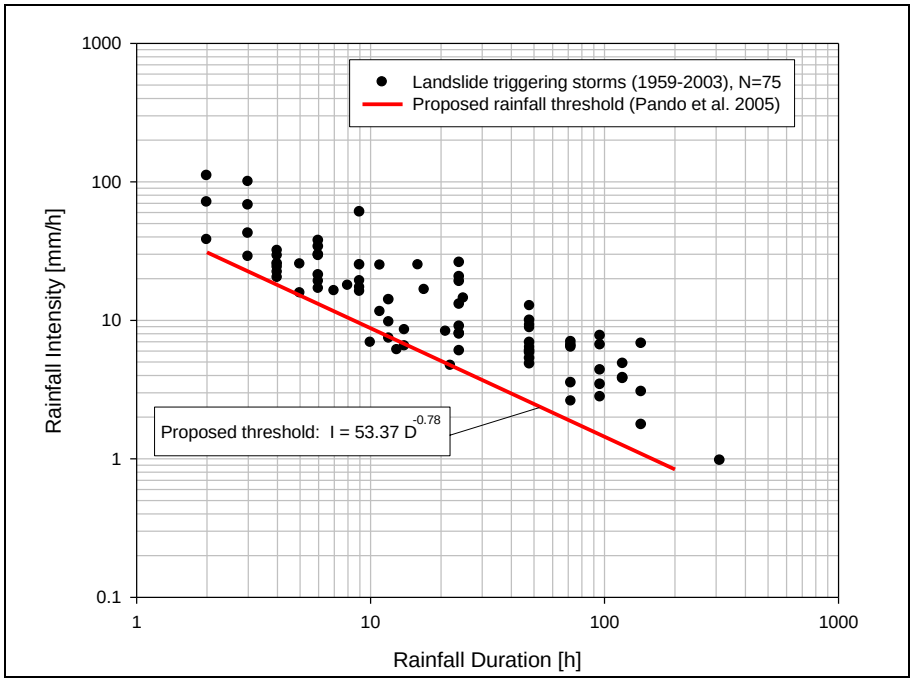

Figure 3.2 Puerto Rico Rainfall-Landslide Threshold (from Pando et al., 2005).

3.3 Effects of Cumulative and Antecedent Rainfall

The previous section presented an overview of generalized empirical rainfall threshold for landslides. Most of these thresholds only use the intensity and duration of the rainfall event that triggers the landslide. However, for unsaturated soil slopes the initial level of matric suction, which in turn is dependant of the soil moisture content, is a key variable. Thus, several researchers have incorporated the effects of antecedent or cumulative rainfall and not only the rainfall intensity and duration of the triggering event. A list of some studies related to this topic is presented in Table 3.1.

For example, Rahardjo et al. (2001) studied rainfall induced slope instabilities by considering the antecedent rainfall during the five days preceding a storm that triggered several shallow slides. Using numerical modeling of several of the of failed slopes the authors were able to simulate the changes in pore-water pressure due to different rainfall patterns, and calculated the associated changes in factor of safety of the slopes. The study revealed that factors of safety of unity, i.e. slope failure, were obtained satisfactorily when the analyses included the effects of antecedent rainfall and if not included, slope failure was not adequately predicted. The analyses also highlighted the importance of including the effects of having a heavier sliding mass as the soils increase in moisture content with rainfall activity.

Table 3.1 Some relevant studies that consider antecedent rainfall for stability analysis.

Reference	Description	Conclusions
Brand (1984)	Studied the relation between rainfall and slope failure for the area of Hong Kong.	• Antecedent rainfall could be a significant factor for slope failure only when the major rainfall event does not have a long duration or a high intensity.
Chatterjea (1989)	Studied the effect of antecedent rainfall on slope failures in Singapore.	• 5-days of antecedent rainfall should be sufficient to trigger landslides.
Rahardjo (1998)	Studied the rainfall characteristics that induced landslides in Singapore.	• Major landslides occurred after 24 hours rainfall of over 110 mm and minor landslides occurred after significant amounts of antecedent rainfall.
Rahardjo et al. (2001)	Studied rainfall induced slope instabilities by considering the antecedent rainfall during the five days preceding a storm.	• Slope failure, was obtained satisfactorily when the analyses included the pore-water pressure changes associated with the antecedent rainfall. • Analyses highlighted the importance of including the effects of having a heavier sliding mass as the soils increase in moisture content with rainfall activity.

Polemio and Petrucci (2000) pointed out the importance of recognizing that there is a rainfall intensity upper limit, above which runoff dominates as the rainfall intensity exceeds the infiltration rate. Wieczorek and Sarmiento (1988) highlighted the importance of considering accumulated rainfall as a controlling factor of rainfall induced slope stability particularly for regions where soils have low permeability.

The references summarized in this subsection highlight the importance of including the antecedent and cumulative rain in slope stability analyses. The slope failure studied in this project occurred during a heavy rain that was preceded by various episodes of rain, which is typical of the wet season in Western Puerto Rico. Therefore, based on these previous studies it was considered important to incorporate in this research the effects of antecedent rainfall (and moisture) prior to the actual slope failure event.

3.4 Hydro-Geological Approach

The literature on rainfall induced landslides also includes several studies that have tackled the landslides problem using a water balance approach. This approach considers the three main components of the water cycle: rainfall, runoff and infiltration. These studies mainly involved experimental studies where the project involved monitoring these three components on an existing slope. Thus, these types of studies required field measurements of rainfall and

runoff quantities, and in situ measurements of soil moisture and suction. A list of references that involved water balance based studies is listed in Table 3.2.

For example, Haneberg (1991) and Anderson and Thallapally (1996) carried out investigations at some experimental slope sites with different approaches, using piezometers, tensiometers and rain gauges and complemented with numerical modeling. These studies were useful for the design of the experimental program carried out for this MS thesis.

Table 3.2 Studies related to field instrumentation and soil-water balance analyses.

Reference	Description	Conclusions
Sweeney (1982)	Presents results of in-situ soil suction measurements with tensiometers in Hong Kong's residual soil slopes.	• Good performance of many steep, high slopes in Hong Kong over a long period of time indicates that some slopes may preserve significant suctions indefinitely.
Low (1992)	Studied the change in soil matric suction with the rainfall on a residual soil cut slope in Malaysia.	• Heavy rainfall intensity may not cause instability to slope, but prolong rainfall can be significant. • Bare surface causes higher reduction in matric suction during rainfall.
Haneberg (1991) Anderson and Thallapally (1996)	Investigated slope sites using piezometers, tensiometers and rain gauges and complemented with numerical modeling.	• The groundwater flow is mainly slope-parallel between two storms and vertical during a storm.
Li et al. (2005)	Monitored soil moisture and matric suction variations in a Saprolite slope using moisture probes, tensiometers, and piezometers.	• Actual infiltration rate was 70% of the total rainfall. • Antecedent rainfall had some influence on the increase in soil moisture content and a significant influence on the groundwater level at depth.
Zhan et al. (2007)	Conducted a full-scale field study to investigate the effects of rainfall infiltration on a natural grassed expansive soil slope in China	• Depth of influence of the rainfall varied, depending on the elevation within the slope, and ranged from 2.8 to 3.5 m. • Measurements indicated that the presence of grass significantly increased the infiltration rate and reduced surface runoff.

Another important water balance study was carried out by Zhan et al. (2007). This study involved a full-scale field study carried out to investigate the effects of rainfall infiltration on a natural grassed expansive soil slope in China. Furthermore the authors also compared the infiltration rates between a grassed area and a nearby bare area and measurements indicated that the presence of grass significantly increased the infiltration rate and reduced surface runoff.

3.5 Analytical Approaches of the Rainfall-Stability Problem

Several references reviewed involved analytical approaches to study the rainfall induced slope instability problem. Typically all studies used a two step approach. The first step involves solving the infiltration/seepage problem for a given slope geometry and set of boundary conditions. This step predicts pore pressures or suction levels within the slope during the rainfall event. The second step uses the results of the first step and the analyses evaluate the stability of the slope (Polemio and Petrucci, 2000). Table 3.3 lists several recent studies that involved an analytical approach to study the rainfall-stability problem.

Collins and Znidarcic (2004) outlined a procedural method for utilizing the analytical formulation to predict the change in the factor of safety for an infinite slope subject to infiltration and performed a detailed analysis of a case study to verify the method. The authors used a simplified approach based on one dimensional flow modeling and an infinite

slope analysis model. The study was successful in identifying the triggering mechanisms that lead to rainfall-induced slope failures.

Anderson and Howes (1985) coupled a general one-dimensional soil water infiltration model with an infinite slope stability model to understand why many Hong Kong slopes have a safety factor less than one. They demonstrated that it is due to the fact that shear strength related to in situ soil suction is generally neglected during slope design.

Table 3.3 Studies involving analytical approaches of the Rainfall-Stability problem.

Reference	Description	Conclusions
Collins and Znidarcic (2004)	Outlined a procedural method for utilizing the analytical formulation to predict the change in the FS for a slope subjected to infiltration.	• The study was successful in identifying the triggering mechanisms that lead to rainfall-induced slope failures.
Anderson and Howes (1985)	Combined a one-dimensional soil water infiltration model with an infinite slope stability model to determine why many Hong Kong slopes have FS<1.	• Factors of safety less than one are due to the fact that shear strength related to in situ soil suction is generally neglected during slope design.

3.6 Summary

The literature review presented herein summarizes relevant references available that are related to this broad subject. The studies presented highlight the world-wide interest in addressing the problem of rainfall-induced landslides. Although quite a bit of work has been done in many fronts, i.e. thresholds, field studies, and analytical studies, there is still need for further research particularly those involving full-scale studies of well instrumented slopes.

Furthermore, very little literature was found involving behavior of unsaturated tropical residual soils in the Caribbean including Puerto Rico. The research project presented in this thesis aims to contribute towards filling this knowledge gap.

4 DESCRIPTION OF THE CASE STUDY SLOPE

4.1 Introduction

This chapter presents general information and details of the case history involving a slope failure that occurred after a heavy rainfall event in the city of Mayagüez, in Western Puerto Rico. This chapter describes the area of study as well as the rainfall event that caused several slope failures in the area of Mayagüez, including the slope under study.

4.2 Slope Failure Events during the June 10, 2005 Storm

The slope failure that is the main focus of this project was triggered during a heavy storm that occurred on June 10, 2005. This storm induced over ten shallow landslides in the general area of Mayagüez, PR. The city of Mayagüez is located in the western coast of Puerto Rico as shown in Figure 4.1. The topography is variable from relatively flat in the coastal areas to hilly in the mountainous area towards the east. Figure 4.2 shows the location of five of the landslides which happened to be near the campus of UPRM. The slope failure selected for this thesis was site #5. This site was chosen because of its proximity to the UPRM campus, which allowed easy access and was convenient for long-term field monitoring. Further details about this slope failure are presented in Section 4.3.

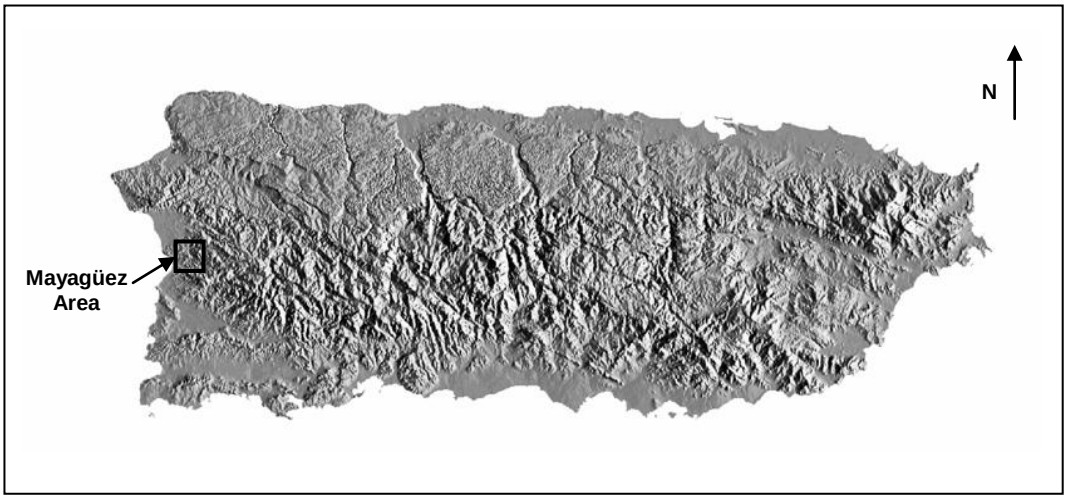

Figure 4.1 Location of the area of study in Mayagüez, Puerto Rico.

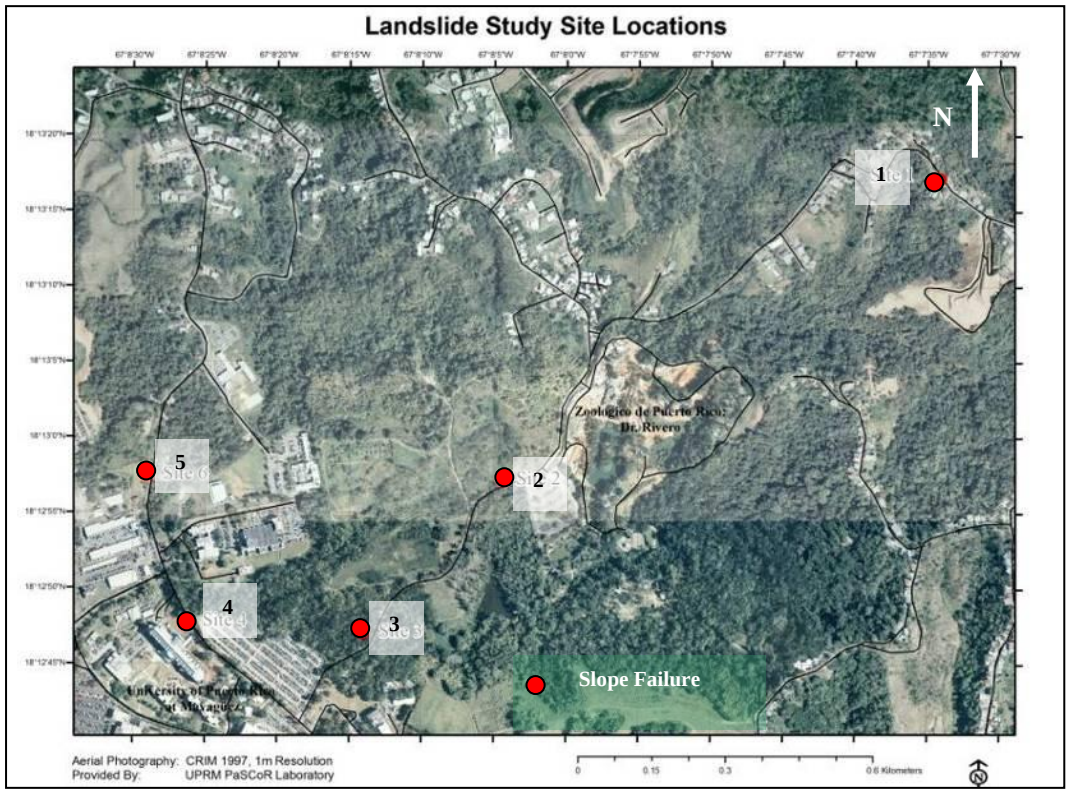

Figure 4.2 Locations of landslides events near UPRM due to the June 10, 2005 storm.

The rainfall of June 10, 2005 started at around 8 am and lasted for about 6 hours. The total rainfall for this storm was about 3.66 in. (9.3 cm) with a maximum intensity of 2.5 in./hr (6.7 cm/hr). A graph of cumulative rainfall for the June 10, 2005 storm is shown in Figure 4.3.

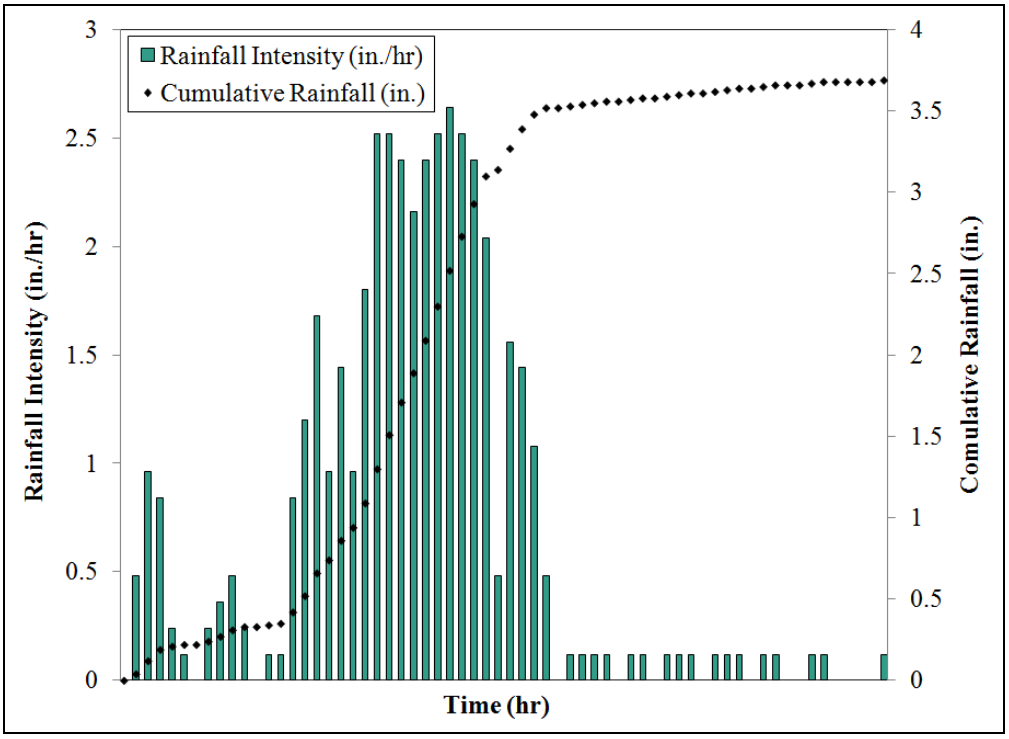

Figure 4.3 Cumulative rainfall for the June 10, 2005 storm (data collected and provided by the CID at UPRM).

In general, the area was affected by shallow slides that occurred just beneath the surface vegetation layer with depths typically ranging from 1.5 to 3.5 ft (0.46 to 1.07 m). Most of the slides were in relatively homogeneous soil slopes involving high plastic residual soils which are typical in the mountainous areas of Mayagüez. The residual soils were unsaturated, reddish brown with some sand content (typically less than 15%), and high contents of fines

classifying as high plasticity silts (MH) or clays (CH). Table 4.1 and Table 4.2 summarize provide information for five slides that occurred near the UPRM campus. The geology quadrangle for the city of Mayagüez (Figure 4.4) indicates that the parent bedrock formation is TKya, which consists of interbedded calcareous, vulcaniclastic sandstone, siltstone, claystone, limestone and mudstone. The mountainous terrain has several streams and ravines that promote depositation of alluvial material.

Table 4.1 Selected landslides near the UPRM triggered during the June 10, 2005 storm.

Site No.	Approximate Address	Geographic Coordinates		Original Slope Angle (°)	Failure Dimensions* ft (m)			Dominant Soil
		Latitude (N)	Longitude (W)		Length	Width	Depth	
1	PR-135 Km 1.3	18°13'17.9"	67°7'34"	41	17.8 (5.4)	14.0 (4.3)	1.3 (0.4)	Residual MH
2	PR-135 Front of PR Zoo	18°12'57"	67° 8'4.4"	43	14.6 (4.5)	6.4 (2.0)	1.7 (0.5)	Residual MH
3	PR-135 Km 200	18°12'47"	67°8'14"	48	20.2 (6.2)	13.0 (4.0)	3.3 (1.0)	Residual CH
4	PR-108 Front of Chemistry Bldg.	18°12'47.6"	67°8'26.4"	50	24.1 (7.3)	4.0 (1.2)	3.3 (1.0)	Residual MH
5	PR-108 Front of Plastic Arts Bldg.	18°12'58"	67°8'29"	42	20 (6.1)	19 (5.8)	2.75 (0.8)	Residual MH

* Landslide dimensions based on Cruden and Varnes (1992).
Notes: *Width* refers to the width of rupture surface; *Length* refers to the total length measured from the tip of the landslide to its crown; and, *Depth* refers to the depth of rupture surface measured perpendicular to the plane of the rupture surface.

Table 4.2 Classification soil test results at selected landslide sites.

Site No.	Atterberg Limits[a]		Percent Passing		
	LL	PI	% G[b]	% S[c]	% F[d]
1	65	24	6.6	5.9	87.5
2	70	21	0.0	4.3	95.7
3	79	47	0.0	5.5	94.5
4	64	19	2.7	10.8	86.5
5	61	26	0.0	14.2	85.8

[a] Atterberg Limits according to ASTM D 4318-93
[b] % G = percent of gravel sizes
[c] % S = percent of sand sizes
[d] % F = percent of fines (finer No. 200)

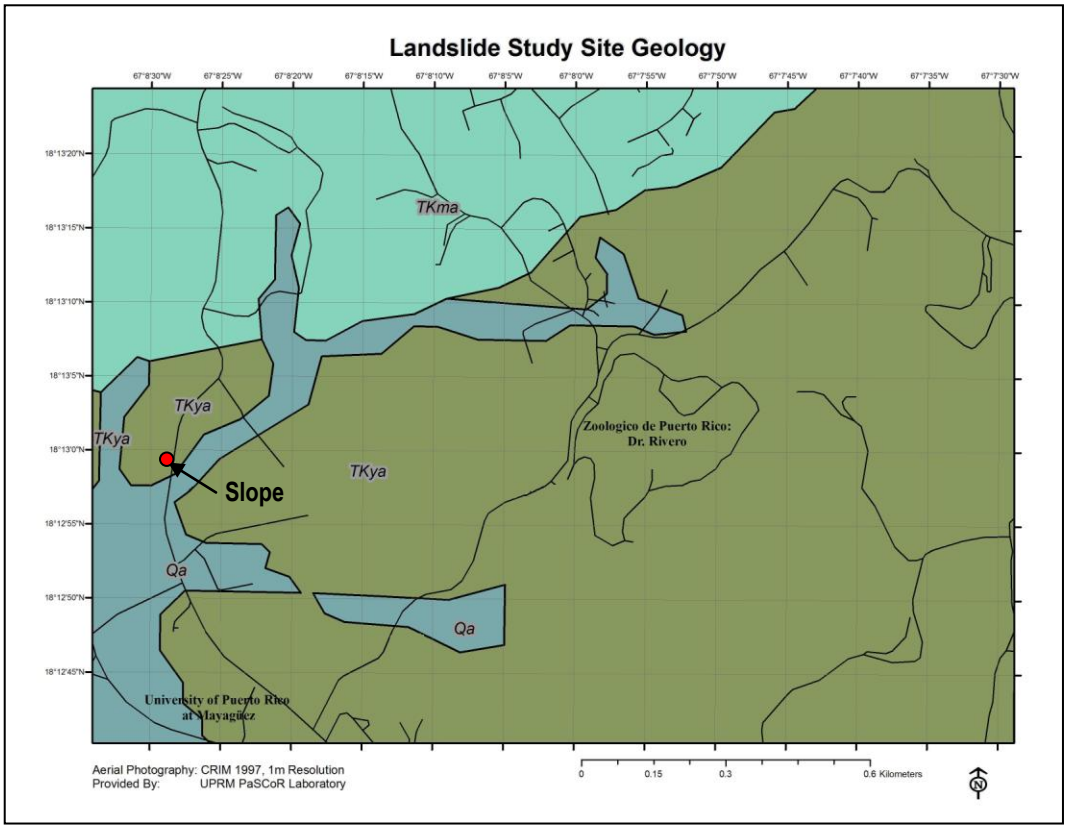

Figure 4.4 Geology of Mayagüez area.

4.3 Case study slope failure description

The slope failure case study selected for detailed study is located on the west side of road PR-108 in front of the Plastic Arts facilities. A general topographic map of the area is shown in Figure 4.5. This map represents a rectangle that represents the general location of the failed slope. An enlarged topographic map representing this rectangle is shown in Figure 4.6. An air photo is shown in Figure 4.7. A photo of the failed slope taken about one week after the failure is shown in Figure 4.8.

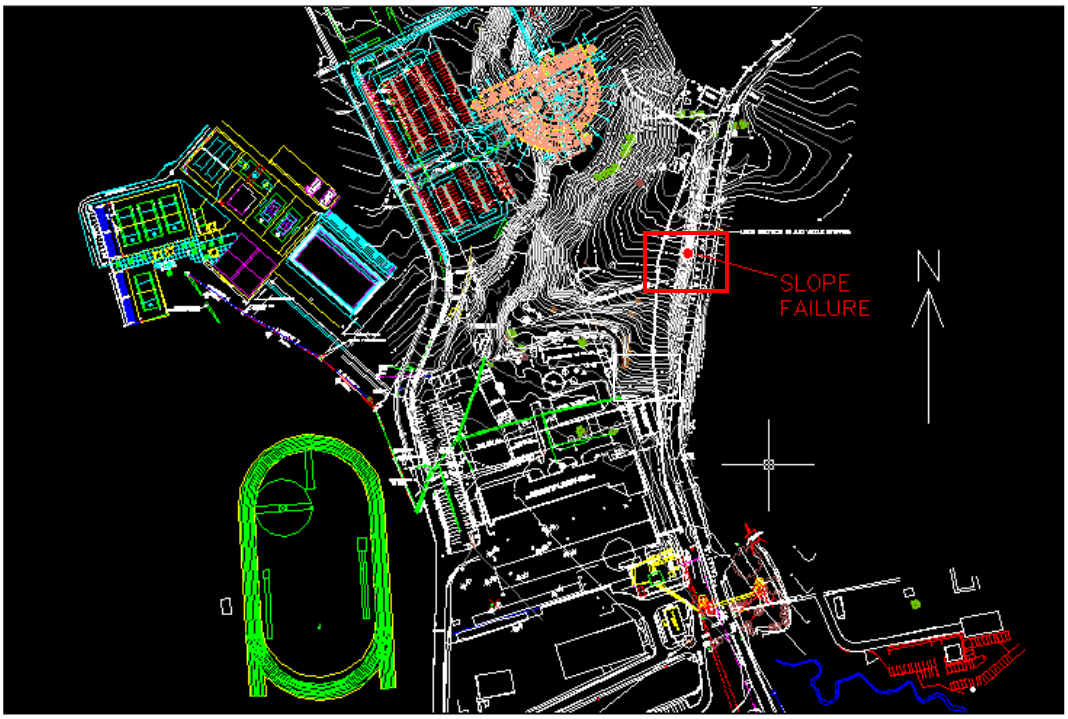

Figure 4.5 General topographic map of the UPRM Campus.

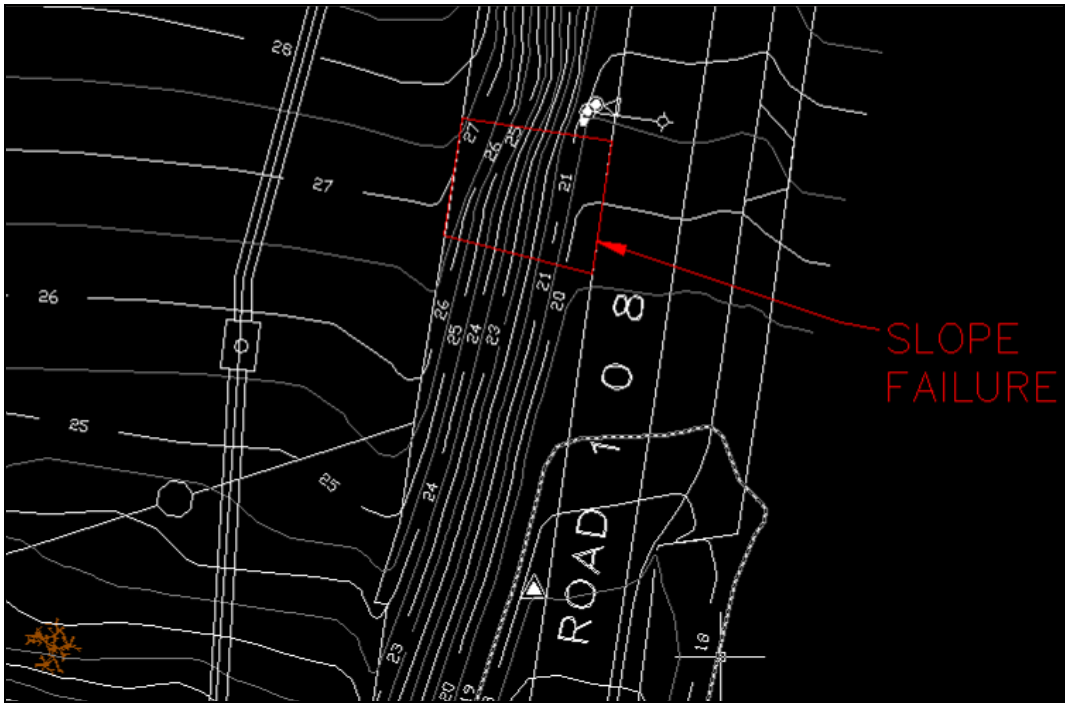

Figure 4.6 Topographic map of slope failure case study.

Figure 4.7 Location of the slope study (from Google, 2009).

Figure 4.8 Slope under study one week after failure.

The geometry of the slope was surveyed for this study and is shown in Figure 4.9. This figure shows the estimated original ground surface and also the topography of slope after failure. The original geometry was estimated based on the adjacent ground, which did not fail. On average the slope inclination of the adjacent slopes that did not fail was 42 degrees (i.e. approximately 1H:0.9V). The main scarp was at about 13 ft (4m) above the toe of the slope. The slope has an overall height of 15 ft (4.5 m). at the top of the slope there is an area of relatively horizontal ground. This horizontal ground extends at least 30 ft (9 m) behind the slope crest.

The slope failure is near the Quebrada Oro creek, which is about 40 ft (12 m) to the east of the site. However the alluvial deposit along the sides of this creek do not reach the slope site. Furthermore, the ground water table at the study slope is believed to be several feet below the toe of the slope and it is believed to be controlled by the quebrada Oro creek water level. Under heavy rainfall condition the Quebrada Oro water level typically remains about 2 to 5 ft (0.6 to 1.5 m) below the surface elevation of Road PR-108, which runs adjacent to the toe of the case study slope.

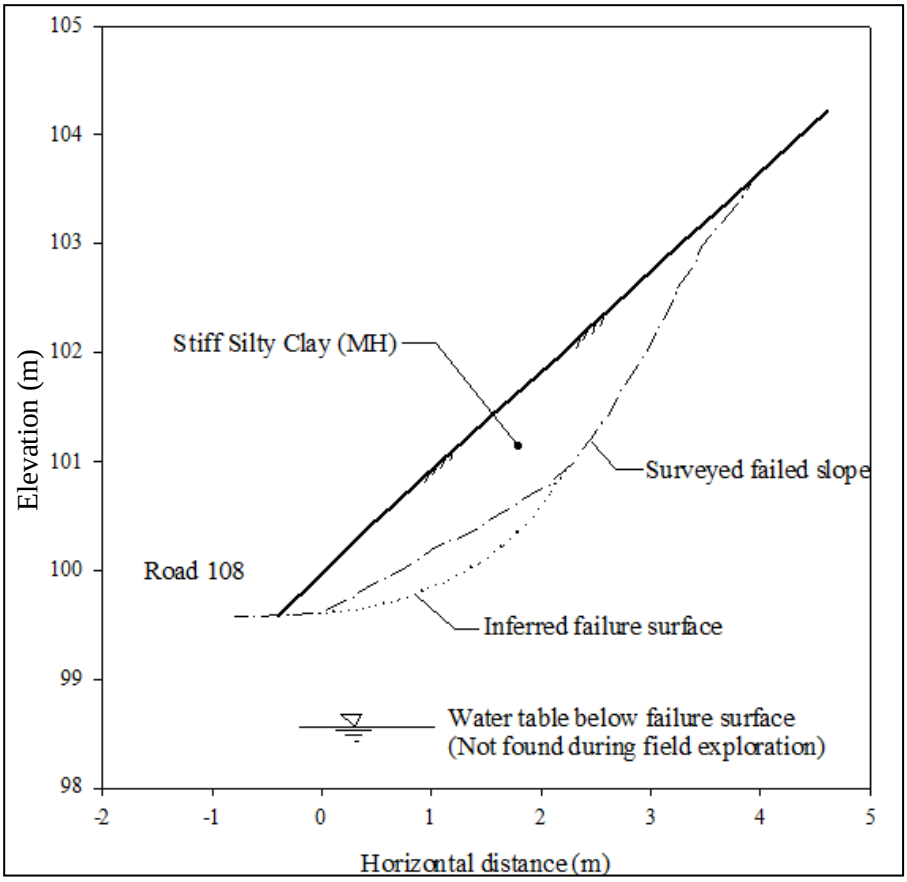

Figure 4.9 Original and failed slope average profiles (relative elevations).

As part of this research a conventional geotechnical borehole exploration was carried out. A schematic showing the approximate location of the borehole with respect to the failed slope is shown in Figure 4.10.

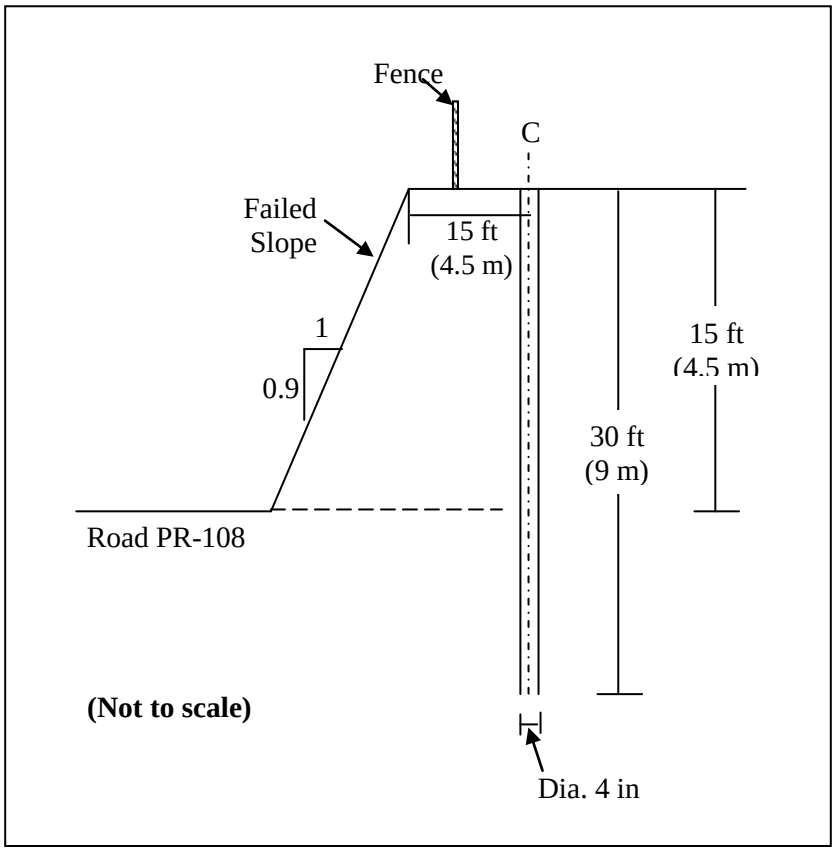

Figure 4.10 Schematic of location of geotechnical borehole.

The geotechnical borehole was drilled on January 14, 2008 by a CME-55 drill rig owned and operated by PIM Geotechnical Services. The borehole was carried out using standard 4-in. hollow stem augers to a final depth of 30 ft (9m). As shown in Figure 4.10, this depth was enough to extend below the elevation of the failed slope toe. The geotechnical investigation

included standard penetration tests (SPT) at depths of 1.5, 5, 11, 15, 20 and 25 ft (0.5, 1.5, 3.4, 4.6, 6.1, and 7.6 m). The SPT samples were used for soil classification, Atterberg limits, and moisture content evaluation. Undisturbed Shelby tube samples were retrieved at 3, 7, and 9 ft (0.9, 2.1, and 2.7 m) depths. The Shelby tube samples were used for shear strength evaluation. The Shelby tubes had a diameter of 3 in. and were 24 in. long.

Atterberg limits were determined and used to classify the soil at each layer using the Unified Soil Classification System (USCS). Three samples from the soil exploration were selected to conduct this analysis: #2, #7 and #10. Figure 4.11 presents the plasticity chart with the soil classification for each sample. Samples #2 and #7 are classified as high plasticity silts (MH) while sample #10 is classified as low plasticity silt (ML).

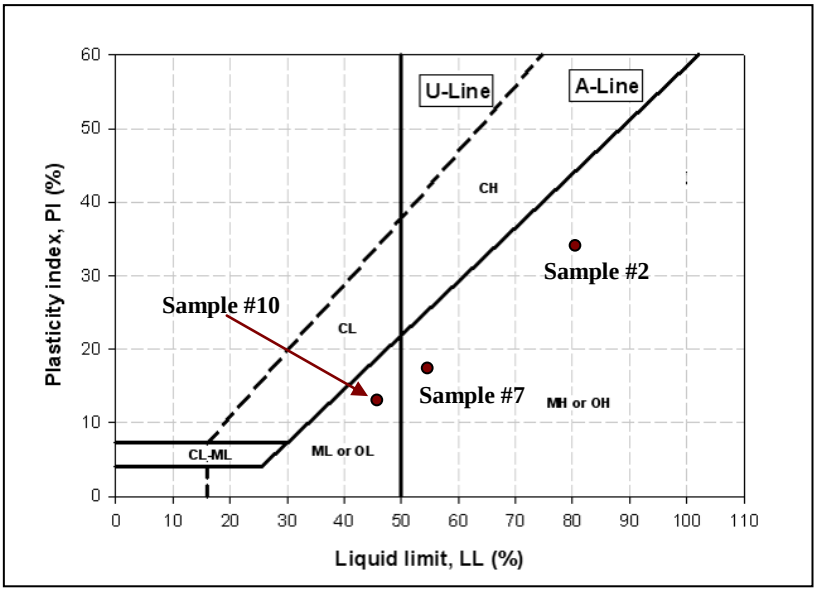

Figure 4.11 Plasticity chart for samples extracted from the slope.

The shear strength was evaluated in the laboratory by conducting the direct shear test. In this study, the direct shear tests were conducted using two different soil conditions to investigate the variation in soil shear strength as function of saturation. For this, soil samples with natural water content (as sampled), and soil samples saturated for 24 hours were evaluated. Table 4.3 presents the shear strength properties and Figure 4.12 presents the shear strength envelopes obtained in the direct shear tests for full suction (as sampled) and saturation condition (i.e. without suction).

Table 4.3 Shear resistance parameters from direct shear tests.

Unit Weight γ (kN/m^3)	Natural Water Content W_n (%)	Water Content 24 hrs Saturated W_s (%)	Direct Shear Test Results for W_n		Direct Shear Test Results for W_s	
			φ' (º)	c' (kPa)	φ' (º)	c' (kPa)
14.9	23.4	37.4	32	18.6	34	8.4

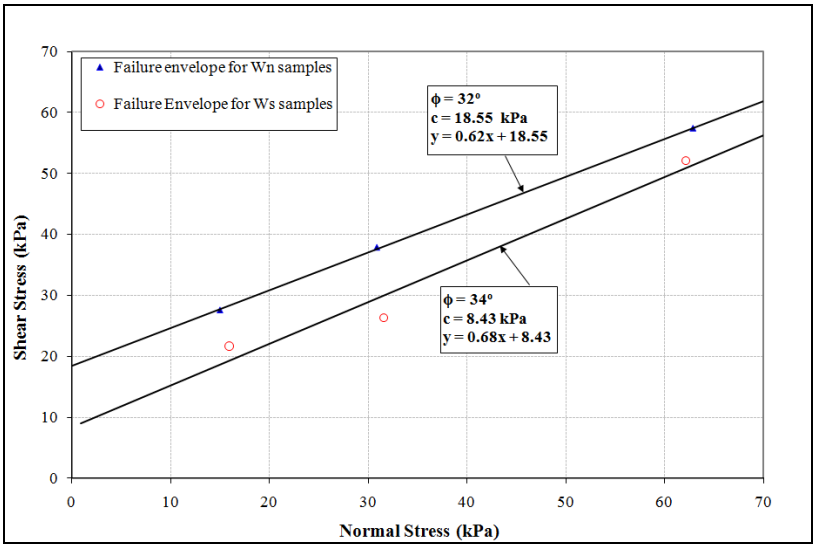

Figure 4.12 Shear strength envelopes determined from direct shear tests.

From Figure 4.12, it can be observed that the angle of internal friction (ϕ) did not vary significantly. However, the cohesion (c) was reduced by 55% when the samples were saturated for 24 hours. A greater change in cohesion would have been expected if the samples were saturated for a longer period of time. It can normally take several days for the samples to become completely saturated. At that point the cohesion is expected to be very low.

The boring log from the soil study is shown in Figure 4.13. No water table was found during the exploration, which indicates that these soils were in a partially saturated condition. In general, the predominant soil type in the slope is MH, and the soil properties determined from the soil exploration will be used for further analyses.

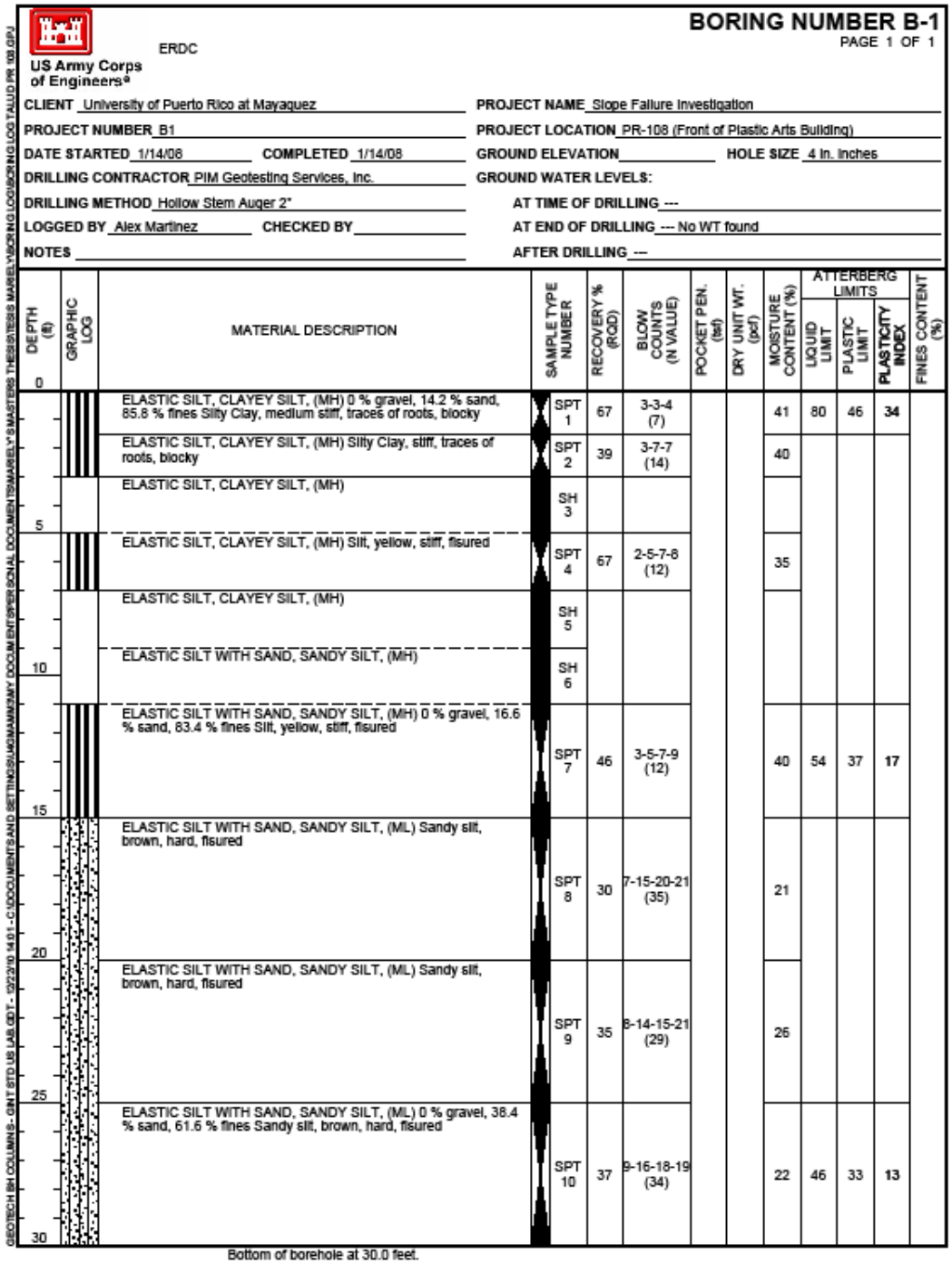

ERDC

US Army Corps of Engineers®

BORING NUMBER B-1

PAGE 1 OF 1

CLIENT University of Puerto Rico at Mayaguez

PROJECT NAME Slope Failure Investigation

PROJECT NUMBER B1

PROJECT LOCATION PR-108 (Front of Plastic Arts Building)

DATE STARTED 1/14/08 COMPLETED 1/14/08

GROUND ELEVATION _____ HOLE SIZE 4 In. Inches

DRILLING CONTRACTOR PIM Geotesting Services, Inc.

GROUND WATER LEVELS:

DRILLING METHOD Hollow Stem Auger 2"

AT TIME OF DRILLING ---

LOGGED BY Alex Martinez CHECKED BY _____

AT END OF DRILLING --- No WT found

NOTES _____

AFTER DRILLING ---

DEPTH (ft)	GRAPHIC LOG	MATERIAL DESCRIPTION	SAMPLE TYPE NUMBER	RECOVERY % (RQD)	BLOW COUNTS (N VALUE)	POCKET PEN. (tsf)	DRY UNIT WT. (pcf)	MOISTURE CONTENT (%)	ATTERBERG LIMITS: LIQUID LIMIT	ATTERBERG LIMITS: PLASTIC LIMIT	ATTERBERG LIMITS: PLASTICITY INDEX	FINES CONTENT (%)
0		ELASTIC SILT, CLAYEY SILT, (MH) 0 % gravel, 14.2 % sand, 85.8 % fines Silty Clay, medium stiff, traces of roots, blocky	SPT 1	67	3-3-4 (7)			41	80	46	34	
		ELASTIC SILT, CLAYEY SILT, (MH) Silty Clay, stiff, traces of roots, blocky	SPT 2	39	3-7-7 (14)			40				
5		ELASTIC SILT, CLAYEY SILT, (MH)	SH 3									
		ELASTIC SILT, CLAYEY SILT, (MH) Silt, yellow, stiff, fisured	SPT 4	67	2-5-7-8 (12)			35				
		ELASTIC SILT, CLAYEY SILT, (MH)	SH 5									
10		ELASTIC SILT WITH SAND, SANDY SILT, (MH)	SH 6									
15		ELASTIC SILT WITH SAND, SANDY SILT, (MH) 0 % gravel, 16.6 % sand, 83.4 % fines Silt, yellow, stiff, fisured	SPT 7	46	3-5-7-9 (12)			40	54	37	17	
20		ELASTIC SILT WITH SAND, SANDY SILT, (ML) Sandy silt, brown, hard, fisured	SPT 8	30	7-15-20-21 (35)			21				
25		ELASTIC SILT WITH SAND, SANDY SILT, (ML) Sandy silt, brown, hard, fisured	SPT 9	35	8-14-15-21 (29)			26				
30		ELASTIC SILT WITH SAND, SANDY SILT, (ML) 0 % gravel, 38.4 % sand, 61.6 % fines Sandy silt, brown, hard, fisured	SPT 10	37	9-16-18-19 (34)			22	46	33	13	

Bottom of borehole at 30.0 feet.

Figure 4.13 Boring log.

5 EXPERIMENTAL METHODOLOGY

5.1 Introduction

This chapter describes the experimental methodology used conduct the slope failure study presented in this thesis report. The methods and procedures carried out for the completion of this project were developed based on several sources of information including case studies found in the literature, considering the availability of instruments and equipment, and evaluating the site conditions.

5.2 Slope Instrumentation and Monitoring

The first part of this experimental component consisted of an instrumentation of the slope. The three main parameters that were evaluated were rainfall, soil suction, and soil moisture. This project aimed to conduct a complete monitoring of these three parameters to determine how variations of each one could have contributed to the slope failure.

5.2.1 Description of Instrumentation

The instruments used to monitor the slope included: septum tensiometers, TRIME-IPH moisture meters, and a rain gauge. Details of each instrument such as measurement range and estimated accuracy are summarized in Table 5.1.

Table 5.1 Instruments description.

Item No.	Measurement	Type of Instrument	Quantity	Measuring range/ Accuracy	References
1	Rainfall	Tipping bucket rain gauge with data logger	1	2.55 in per interval/+-2% @ 1 in per hour	Spectrum Tech. (2007)
2	Soil suction	Septum Tensiometer	20	0 to 1bar	Skye Instruments (2004)
3	Soil suction	Hydrosense Display Meter and Data Logger	1	1200 readings 2 channels	Skye Instruments (2004)
4	Volumetric Water content	TRIME-IPH with intelligent TDR	1	0 to 40%/+-2% 40 to 60%/+-3%	Mesa Systems

Rainfall was measured using a rain gauge from Spectrum Technologies, Inc. (Figure 5.1) that was installed at the top of the slope. The rain gauge consists of a self-emptying tipping bucket with an 8 in. diameter collector and data logger. The data logger records accumulated rainfall during each interval, with a maximum of 2.55 in. per interval.

Figure 5.1 Rain gauge used in this study (www.specmeters.com).

Tensiometers were used to monitor the soil matric suction within the slope. Tensiometers are instruments that are used to measure the potential of soil water and commonly used for plant irrigation purposes. Most of the tensiometers used in this study were constructed in-house. A tensiometer normally consists of a porous ceramic cup, connected through a rigid body tube to a vacuum gauge, with all components filled with water. The tensiometers used in this study consisted of a ceramic cup attached to a 0.5-in. diameter, Schedule 80, grey PVC pipe that was attached to a clear acrylic tubing with a septum stopper (Figure 5.2). These tensiometers were constructed in various lengths to meet the proposed depths for monitoring.

Figure 5.2 Septum tensiometer with needle sensor.

Instead of using one vacuum gauge per tensiometer, a Hydrosense Display Meter and Data Logger with a needle sensor from Skye Instruments Ltd. was used (Figure 5.3). This instrument provided the flexibility to monitor soil suction at multiple points with just one

meter by inserting the needle sensor through the septum stopper. This logger has capacity for 1200 readings of date, time, and two channels and has Windows compatible software to download the data to a computer.

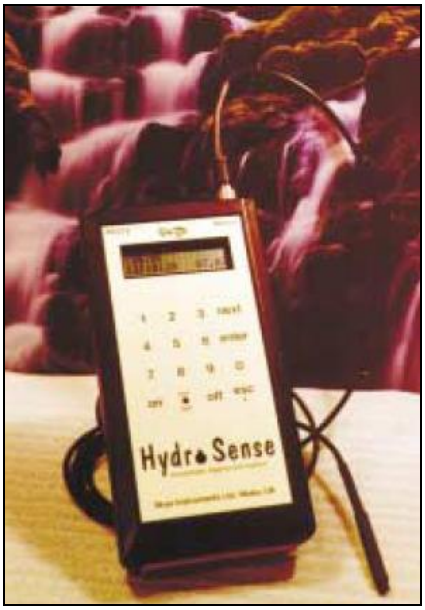

Figure 5.3 Hydrosense display meter and data logger.

For water content measurements the same approach of using one meter to monitor several locations was considered. In this case, polycarbonate tubes were installed in five different locations along the slope at a depth of 6 ft, and a TRIME-IPH probe from Mesa Systems was used to measure the volumetric water content (Figure 5.4). The sensor was connected to a 12 V battery and a multimeter to read voltage. The TRIME tube probe comprises a cylindrical PVC casing with four spring-mounted aluminum plates on opposite sides. The mode of operation of this mechanism consists of inserting the sensor through the polycarbonate tube

and taking readings at different depths. Once inserted in the tube the TRIME device generates a high frequency pulse (up to 1GHz) which propagates along the aluminum plates, generating an electromagnetic field around the probe (Figure 5.4). At the end of the plates, the pulse is reflected back to its source. The resulting transit time (3ps to 2ns) can be measured and the propagation velocity is determined, which is primarily dependent on the water content. The probe converts the signal reflected to a voltage reading, which is immediately read in the multimeter. The probe has an internal calibration that converts the voltage to the soil moisture, so that the voltage reading in the multimeter is actually moisture in the soil. For example, if the soil is fully saturated or if the probe is inserted in water the voltage reading would be 1. In the other hand, if the soil is completely dry or if the probe is exposed to the air, the reading should be 0.

The internal calibration of the probe does not apply to all soil types. Therefore, a calibration curve was developed for the soil material predominant in the slope. Three soil samples were collected from the slope in 5-gal buckets and each sample was conditioned to a different water content. Small samples of known volume were extracted from the cylinders and the volumetric water content was determined. Then, the TRIME-IPH was inserted in the access tube inside each cylinder and the voltage readings for each cylinder were recorded. These readings were plotted against the volumetric water content to determine the linear relationship between the instruments voltage reading and the actual soil moisture for this type

of soil. The calibration curve developed is shown in Figure 5.5. The regression data was included in this curve just to show the relationship, and not for statistic purposes.

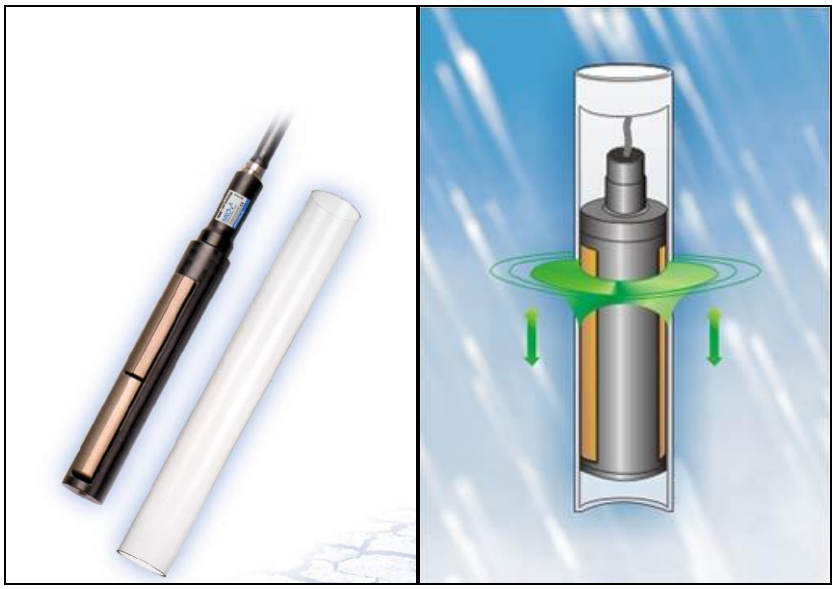

Figure 5.4 TRIME-IPH probe with polycarbonate access tube and operating principle.

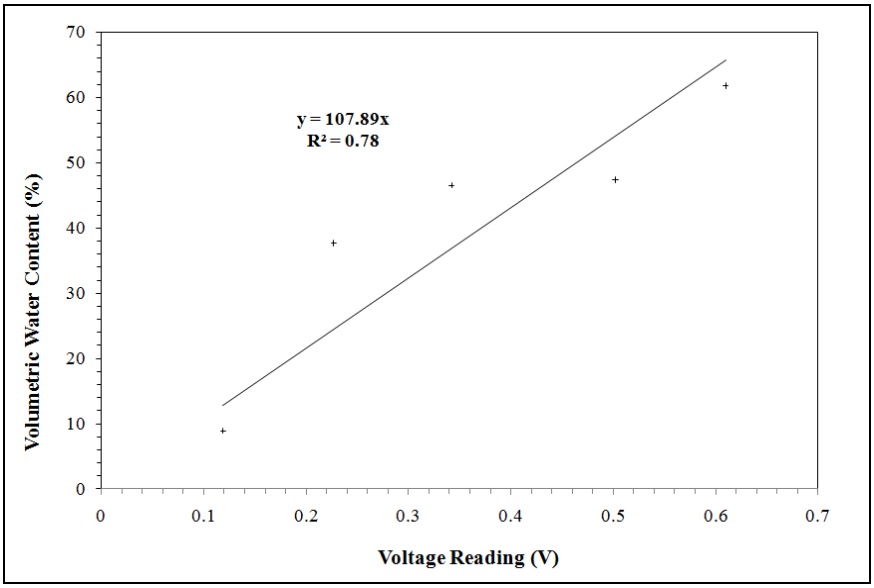

Figure 5.5 Calibration curve of the TRIME-IPH for the soil in the slope.

5.2.2 Instrumentation Layout and Installation

To access the failed part of the slope and to facilitate the installation of the instruments, a 15 ft wide by 20 ft high area was cleared of vegetation as shown in Figure 5.6. The failed part of the slope originally consisted of an area 19 ft by 19 ft, as measured by Pando et al. (2007). Clearing and instrumentation of the slope took place between July and August 2007.

Figure 5.6 Slope cleared of vegetation for instrumentation.

Instruments were then installed (Figure 5.7) following the instrumentation layout shown in Figure 5.8. A total of 20 tensiometers, 5 polycarbonate tubes for soil moisture measurements, and one rain gauge were installed in the slope. Four tensiometers were installed around each

polycarbonate tube at each point of observation at depths of 0.75, 1.5, 3, and 6 ft. In this study the tensiometers were installed perpendicular to the slope surface (Figure 5.9) to reduce the head of water. Figure 5.9 shows the actual vertical depth of each tensiometer.

Figure 5.7 Instruments installed in the slope.

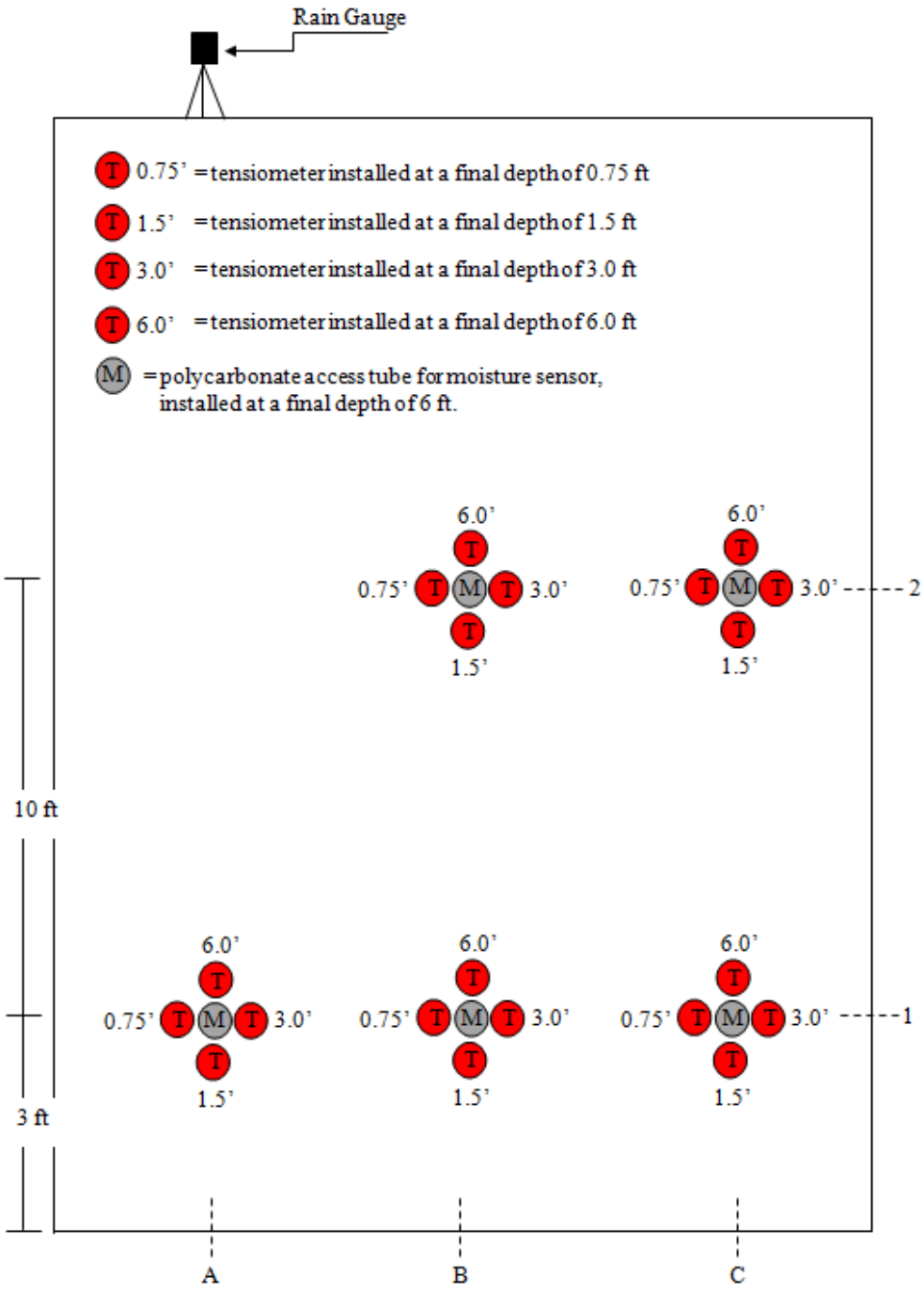

Figure 5.8 Plan view of slope instrumentation layout.

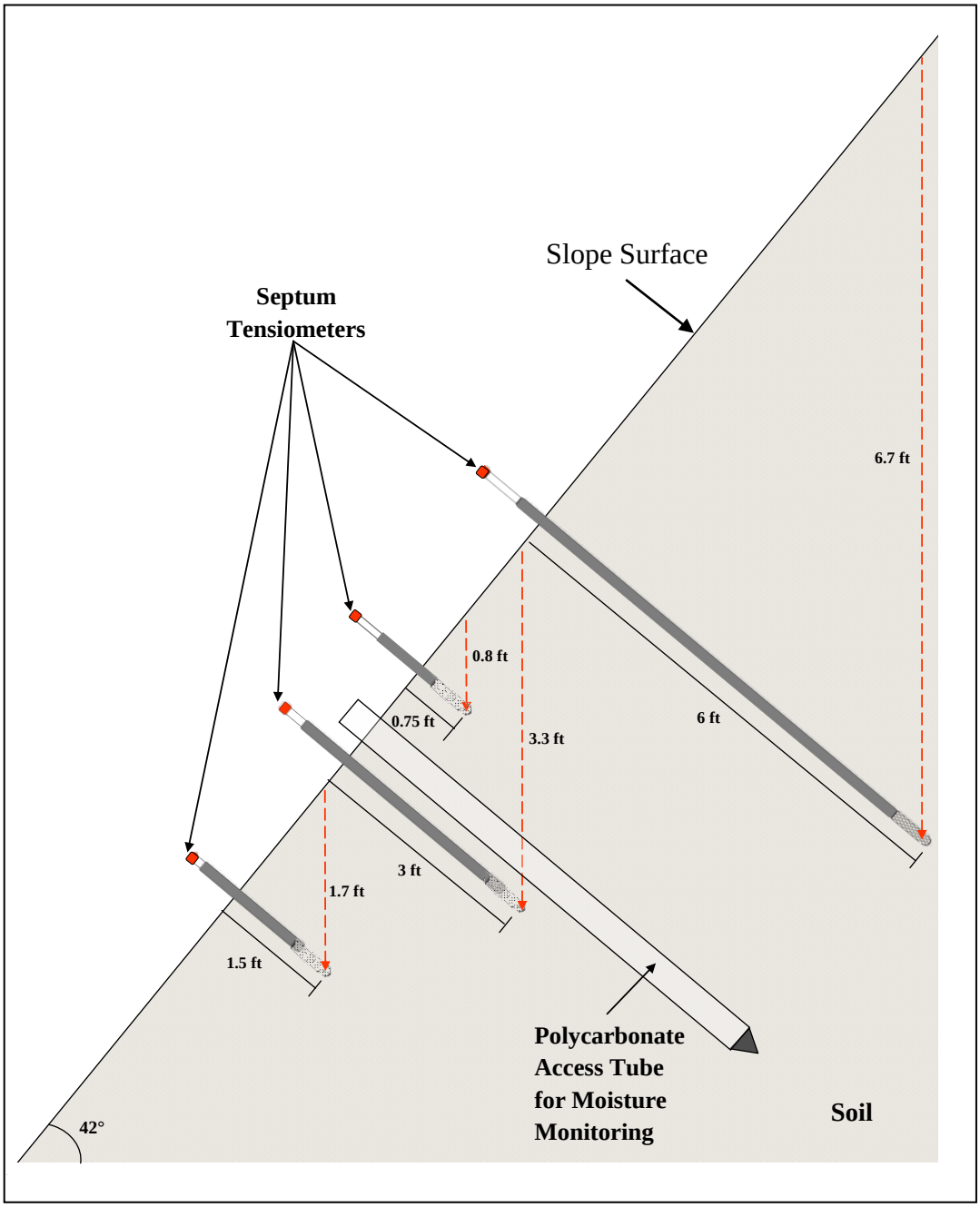

Figure 5.9 Instruments layout at each observation point and vertical depth of tensiometers.

5.2.2.1 Tensiometers

Before installation, the tensiometers were placed vertically in a bucket with water at the bottom, to saturate the ceramic cups for 24-hrs. To install each tensiometer, an access hole was drilled with a 0.94-in.-OD auger. The access hole was drilled approximately 2 in. above the desired depth to have undisturbed soil through which the ceramic cup would penetrate. The tensiometer was placed in the hole and pushed to its final depth. This allowed a good contact between the ceramic cup and the surrounding soil. Once the tensiometer was in place the soil removed from the hole during the drilling was used to seal the gap between the tensiometer and the wall of the hole. This prevented rainwater from leaking into the installation hole through the shallow cracks, which could cause a bypass water flow through the gap between the tensiometer tube and the walls of the hole. This procedure was used when installing the shallower tensiometers (0.75, 1.5 and 3 ft deep).

To install the deeper tensiometers (6 ft deep) a second installation method was used (Figure 5.10). A 2-in.-diameter auger was used to drill each access hole and then a 1-in.-diameter PVC tube was placed centrally in the hole. The gap between the pipe and the wall of the hole was backfilled with moist soil at the bottom and bentonite at the top to prevent the hole from becoming a water passage. Then the tensiometer was pushed into the bottom of the hole to its final depth and a seal was placed on top of the PVC tube to prevent rain from entering the hole.

Once in place, the tensiometers were filled with distilled water till 0.75 in. below the top and the septum stoppers were placed. To protect the septum stoppers from exposure to sunlight, a 2.5-in. section of a 0.75-in-diameter Schedule 40, white, plastic tube with an end cap was placed at the top of each tensiometer.

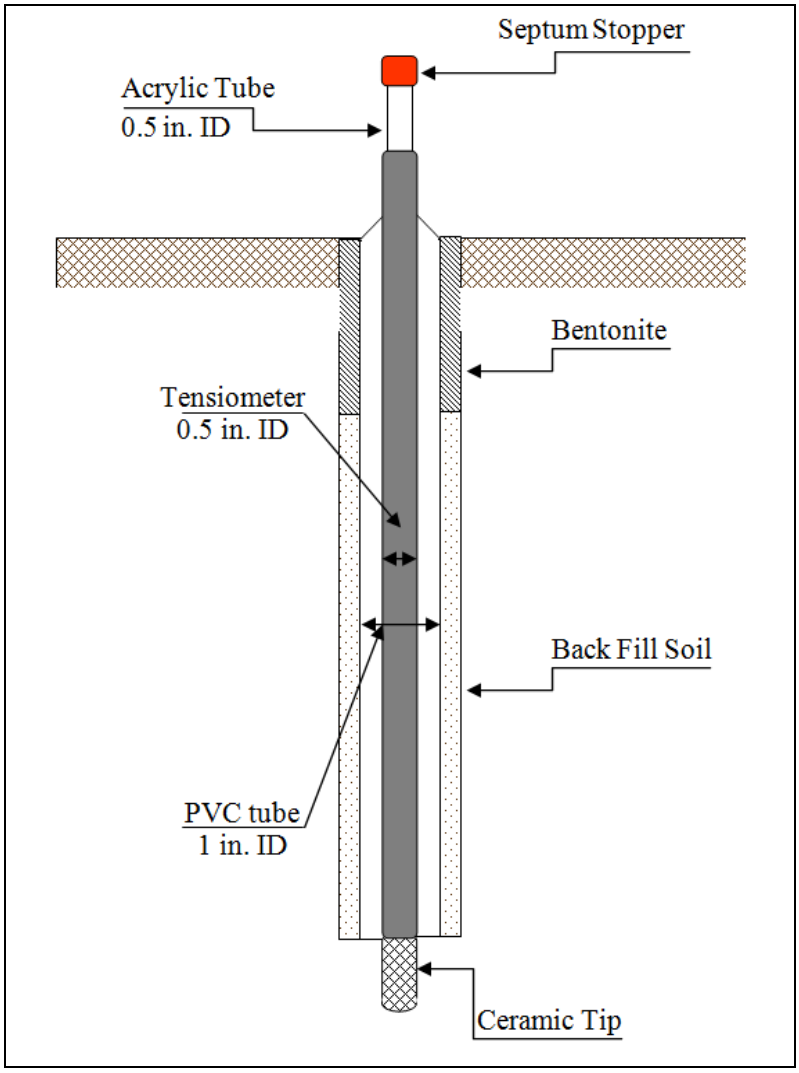

Figure 5.10 Diagram showing the arrangement of sealing the installation hole.

After installation, 24 hours were required before the tensiometers read the correct soil suction. This was because of the disturbance to the soil caused by the installation procedure, and because of the need for water to move through the ceramic cup before equilibrium was reached. After this initial equilibrium period, the tensiometers indicated more accurately the soil suction and they followed more closely the changes in suction as they occurred in the soil. The tensiometers were filled with water periodically as needed. The dryer the soil was the more frequently the tensiometers needed to be refilled.

5.2.2.2 Moisture Sensor

The polycarbonate tubes were installed using a method very similar to the installation of the tensiometers. The same 2-in.-diameter auger was used to drill a hole to a depth of 6 ft. Then the polycarbonate tube was placed in the hole and the gap between the tube and the walls of the hole was filled with the soil cuttings from the drilling of the hole at the bottom and bentonite at the top to prevent the hole from becoming a water passage. Once the tube was in place a PVC end cap was placed at the top of the tube to prevent any moisture to enter the tube.

5.2.3 Monitoring Plan

All the instruments required manual monitoring. Therefore, a monitoring plan was necessary to be designed in such a way that soil suction and moisture were measured adequately to assure that any changes in these two parameters due to rainfall were captured.

Due to the steepness of the slope and the height of the instruments locations, a wooden ladder was fabricated to get access to the higher instruments and take measurements. For security reasons, traffic cones were placed in the road to deviate the traffic while measurements were taken. For these same reasons and because the slope was located at a highly trafficked road, the monitoring of the slope could not be as frequent as wanted. In regular days when no rain was observed in the area, the slope was monitored once a day. When rain events were forecasted for the area, measurements were taken early in the morning and then in the afternoon, or before and after the daily rain event. Measurements were continued with the same frequency for the proceeding 3 to 5 days.

The data logger in the rain gauge was programmed to record data every 5 minutes. Data was downloaded to a computer every week.

Taking the measurements from all the instruments was a two people job. One person measured the soil suction with the Hydrosense while the other measured the soil moisture with the TRIME-IPH probe. All the measurements were taken in the following order of points of observation: 1A, 1B, 1C, 2B, and 2C. Suction measurements were taken in order of instrument's depth. In other words, suction was measured at the tensiometer installed at 0.75 ft, then at the one at 1.5 ft, and so forth. The Hydrosense recorded each reading with the time and date when it was taken, and the data was downloaded to a computer at the end of each monitoring.

Soil moisture measurements were taken in the same order; this is, at 0.75 ft first, then at 1.5 ft, and so forth. In this case the voltage readings were recorded in a field book, and then were uploaded to a spreadsheet for volumetric water content calculations.

5.2.4 Difficulties during Instrumentation and Monitoring

This project attempted to conduct a complete monitoring of rain, soil suction, and soil moisture to determine how variations of each one could have contributed to the slope failure. However, security and logistics issues as well as issues related to the performance of the instruments made it difficult to address the full evaluation of the slope failure.

The moisture sensor used was not new and a little after the slope monitoring started it got damaged, making it difficult to collect moisture data for the rest of the monitoring periods. Therefore, a reduced amount of moisture data was collected and the variation of soil matric suction as a function of soil moisture content was not possible to be assessed. However, the matric suction measurements were considered sufficient and important for the analyses carried out in this study.

5.3 Soil-water Characteristic Curve Determination

5.3.1 Significance and Description

The soil water characteristic curves (SWCC) describes the relationship between suction and volumetric water content, gravimetric water content, or degree of water saturation. SWCC is

fundamental to hydrological characterization of unsaturated soils and is required for most analyses of water movement in unsaturated soils. The SWCC is also used for characterizing the shear strength and compressibility of unsaturated soils.

The test mechanism used in this project was the Tempe pressure cell. The Tempe cell consists of top and bottom Plexiglas plates, a porous ceramic plate, a brass cylinder, and sealing and connecting hardware as shown in Figure 5.11. An external pressure source is connected to the Tempe cell using Neoprene tubing. The test procedures used to conduct this test are described in the next section.

Figure 5.11 Tempe cell

5.3.2 Test Set-up

The Tempe cell consists of top and bottom Plexiglas plates, a porous ceramic plate, a brass cylinder, and sealing and connecting hardware. A test setup for soil-water characteristic curve determination was especially constructed for this project. As shown in Figure 5.12, the test setup consisted of an air compressor, a regulator, and a series of pressure gauges, including water columns, connected by Neoprene tubing to apply air pressure to the Tempe cells. The regulator controlled how much air pressure was entering the system from the air compressor. This pressure was equal to the desired pressure increment for each data point. The precision of the gauge in the regulator was 1 psi. Therefore, to get better precision, digital pressure gauges with a precision of 0.01 psi were used. The gauges were installed at each connection to the Tempe cells; that way if there was any leak it could be detected because the readings in the gauges would be different when it was supposed to be the same when the system is in equilibrium. The water columns served as a second regulation method to maintain the pressure going into the system.

Figure 5.12 Test set-up for soil-water characteristic curve determination.

5.3.3 Tempe Cell Test Procedure

The soil-water characteristic curve was determined using the method described by the ASTM D 6836 (2002). The test was performed using Tempe Cells. Tempe Pressure Cells provide a

simple method to determine the soil moisture-retention curves or the "moisture characteristic" of undisturbed soil cores in the 0-1 bar range. This moisture characteristic of field soils is determined by weighing the complete cell at pressure equilibrium points.

Undisturbed soil samples were obtained from three different points in the slope using a soil sampler with 2.25-in.-diameter by 2.35-in.-tall cylinders (Figure 5.13). As many hammer blows as it was necessary to fill the cylinder with soil were used. Once the cylinder was filled with soil, it was extracted from the sampler and placed in a plastic bag to preserve the moisture. Then natural water content was determined for each sample.

Figure 5.13 Sampler with cylinder used to collect samples for Tempe Pressure Cell.

The soil samples collected from the field were trimmed to match the cylinders dimensions and then weighted. Volume was calculated by averaging three diameter measurements and

three height measurements. This sample volume was then used to calculate the volumetric water content from the gravimetric moisture values.

The porous ceramic plates were saturated 48 hrs before the samples were mounted in the cells. Then the samples were placed in the cell with the porous ceramic plates and everything was submerged in water for saturation. Two saturation levels were applied to the cells: full and partial saturation. Full saturation consisted on placing the cell in a container and filling the container till the top of the cell was covered with water. After 24 hrs the cells were removed from the container and any air bubbles trapped in the cell were extracted. The cells were weighted to monitor the change in weight due to saturation. Then partial saturation was applied. This consisted of filling the container until the water level reached the level of the bottom ceramic plate. Again, the cells were saturated for 24 hrs, and bubbles were extracted and the cells were weighted. Once the saturation was complete the cells were placed in the test apparatus for air pressure application.

Seven pressure increments were applied to the samples during this test: 0.14, 0.28, 0.57, 1.14, 2.27, 4.54, 9.09, and 14.7 psi (1, 2, 4, 8, 16, 32, 64, 100 kPa). The test duration was approximately four months, from October 20, 2007 to February 21, 2008.

When each pressure increment was applied the cells were constantly weighted to monitor how the weight was reducing and to determine when the pressures were in equilibrium. Once the equilibrium was established, the total weight of the cell and the sample was recorded with

the corresponding pressure increment. Then the next pressure increment was applied and the procedure was repeated for each pressure increment.

At the end of the test, the samples were extracted from the cell and dried. Then the volumetric water content at equilibrium for each pressure increment was calculated with the recorded moist weight, the dry weight of the samples, and the sample dimensions determined at the beginning of the test. These data was plotted to obtain the soil-water characteristic curve.

5.4 Summary

This chapter summarized the methodology used to conduct the research investigation presented in this thesis report. Several literature references as well as experts in the topic were consulted to determine the best way to achieve the goals of this project. The instruments, layouts and methods used to carry out the field investigation were selected based on the properties to be measured, the geometry of the slope, the availability of instruments, and the scope of the project. The test setup used to conduct the soil-water characteristic curve test in the laboratory was especially designed for the requirements of this project.

Next chapter will present the results of the laboratory and field tests described before.

6 EXPERIMENTAL RESULTS

6.1 Introduction

This chapter presents the laboratory and field measurements collected as part of the proposed experimental program. The experimental results will shed light on the causes and triggering mechanisms for the slope failure under study. Results from the laboratory-based Soil-Water Characteristic Curve tests are presented and discussed first. Then field data collected is discussed in terms of field suction as function of rainfall and volumetric water content.

6.2 Laboratory Soil-Water Characteristic Curve

As discussed in the previous chapter, the soil-water characteristic curve for the soils of the study slope was determined using undisturbed samples tested with Tempe pressure cells. SWCC's were determined for three undisturbed samples extracted from the same soil unit that failed at the test site. The natural soil properties of the three undisturbed samples measured after extracted from the failed slope are listed in Table 6.1. The set up and procedures of these tests were described in Chapter 5. Table 6.2 shows the initial soil properties of the three samples after the saturation process.

Table 6.1 Natural soil properties of samples for soil-water retention test.

Sample No.	Date Sampled	Void Ratio e_0	Natural Water Content, w (%)	Natural Saturation, S (%)
1	9/9/2007	1.05	35.3	90.0
2	9/9/2007	0.94	27.3	78.1
3	9/11/2007	1.15	27.0	62.9

Table 6.2 Initial soil properties of samples for soil-water retention test after saturation.

Sample No.	Initial Volumetric Water Content (θ_0)	Initial Percent Saturation (S_0)	AEV (kPa)
1	55.6	99.6	20
2	49.2	98.0	10
3	51.0	93.9	2

Each Tempe pressure cell was subjected to seven levels of pressure. For each level of applied pressure the soil weight (i.e. moisture) was tracked with time until equilibrium was reached. The time to reach this equilibrium state is often called equalization time. Figure 6.1 shows the pressure increments and the time of equalization for the seven pressure levels applied to the three samples. The best fit line was included in this figure just to show the tendency, not for statistical meaning. Usually the equalization time is longer for higher applied pressures. Higher pressures cause a larger amount of water movement through the soil media and out the sample. Therefore, it takes longer to reach equilibrium up to certain pressure level. Various factors can affect this relationship, including pore size distribution and permeability.

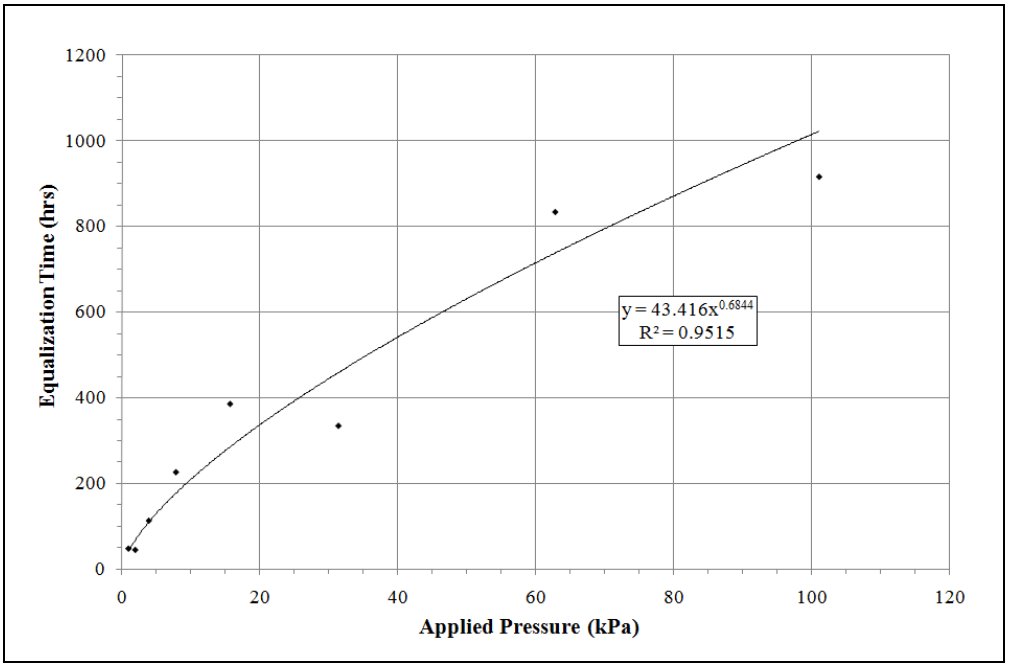

Figure 6.1 Required time to reach equilibrium after each pressure increment was applied.

Figure 6.2 presents the SWCC's obtained for the three samples tested in terms of volumetric water content, and Figure 6.3 shows the SWCC in terms of percent saturation. The range of suction feasible with Tempe cell devices is relatively small compared with the total range often measured in generating the SWCC (i.e. 0 to 1,000,000 KPa). However, the SWCC data collected with the Tempe Cell devices was sufficient to characterize the first two stages of SWCC, i.e., the stage of "Capillary Saturation" and the stage of "Desaturation Zone". The transition between these two zones is typically referred to as the *Air Entry Value* (AEV). As mentioned in Chapter 2, the AEV is considered a very important parameter in unsaturated soil mechanics as it marks the matric suction pressure value beyond which the degree of

saturation starts to drop rapidly. Figure 6.2 shows the AEV values for the 3 soil samples tested. The AEV values shown were determined using the graphical method proposed by Fredlund and Xing (1994). It can be seen that AEV values ranged from 2 to 20 kPa for the 3 soil samples tested. This range of values is believed to be related to differences in void ratio and initial volumetric moisture content for the three samples and also small variations in soil composition, which is normal in natural soil slopes. In general, the smaller the sample void ratio (i.e., the denser the soil) the higher the AEV, which means that at low void ratio values, small changes in degree of saturation can be assumed at low suction.

Figure 6.2 also shows the initial water contents for each sample, i.e. the water content at full saturation. It can be observed that the higher the initial water content the steeper the SWCC is. The AEV also increases with initial water content. The effect of de-saturation is more obvious for soils with high initial water content, especially at low suction values. It is expected that the three curves shown in Figure 6.2 converge at high suction values.

From Figure 6.2, it can also be observed that when the samples are fully saturated at the beginning of the test, the shape of the SWCC is smoother. This is the case for Sample 1, with an initial percent of saturation of 99.6. Samples 2 and 3 had initial saturations of 98.0% and 93.9%, respectively.

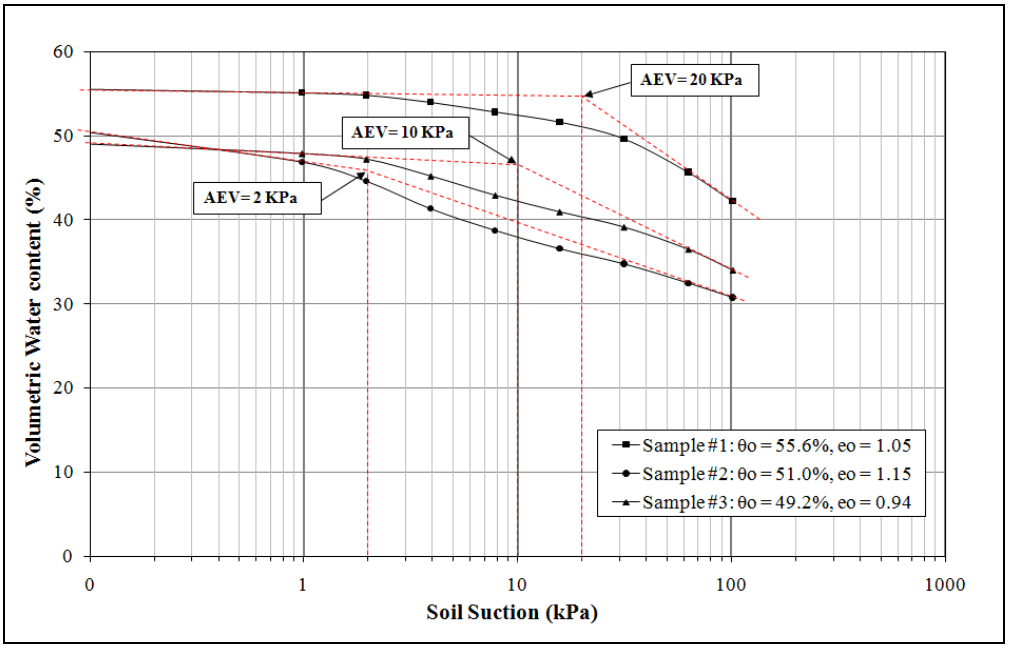

Figure 6.2 SWCC for the three samples tested in terms of volumetric water content.

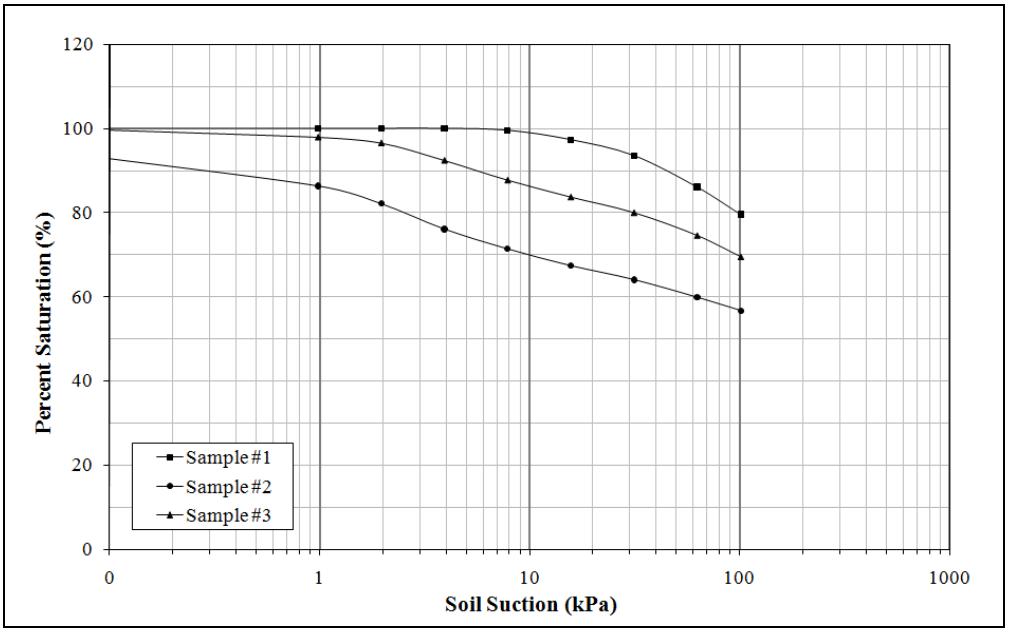

Figure 6.3 SWCC for the three samples tested in terms of percent saturation.

The SWCC results from the laboratory tests can be compared with empirical SWCC. For example Figure 6.4 compares the average laboratory SWCC with the van Genuchten model. The van Genuchten model curve shown was produced by using the saturated volumetric water content determined from laboratory results and the rest of the parameters were estimated from empirical data. It can be observed the model produced using these parameters yields a curve that is higher than the laboratory based SWCC.

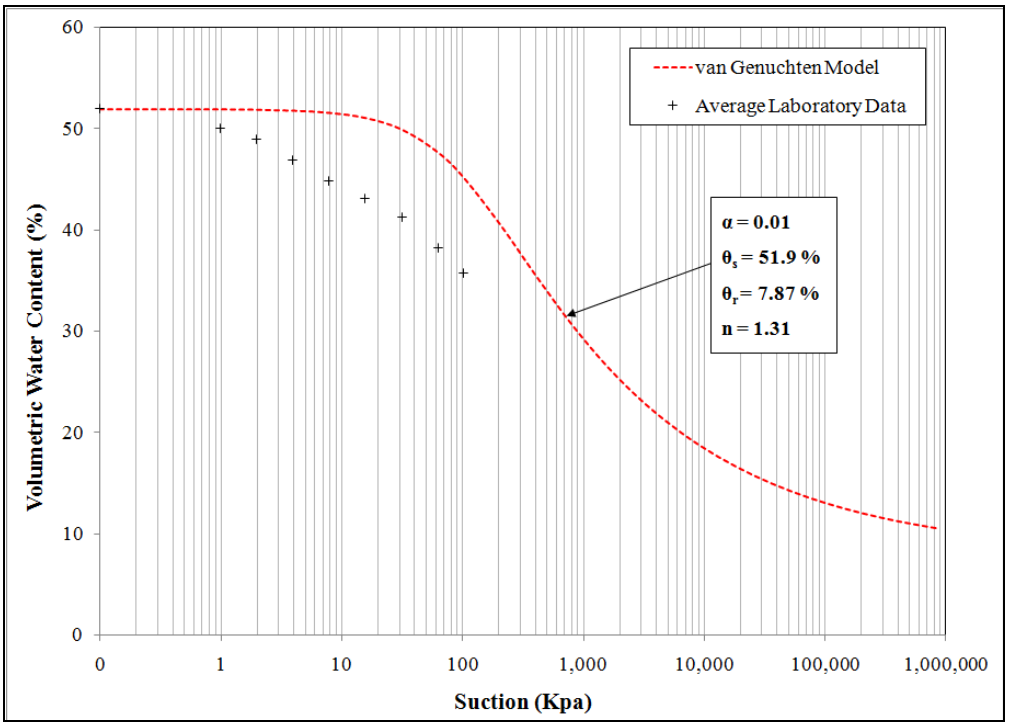

Figure 6.4 Comparison of the laboratory SWCC data and the van Genuchten model.

To better fit the model to the laboratory data, a parametric analysis was performed. The hydraulic parameters in the van Genuchten model were varied to fit the laboratory data, so that the laboratory results could be used for further analyses. Table 6.3 lists the parameters

used for the parametric analysis compared to the empirical parameters used in Figure 6.4. The model produced by the best combination of parameters is presented in Figure 6.5.

Table 6.3 Hydraulic parameters used to predict SWCC.

Parameter	Figure 6.4	Figure 6.5
θ_s	51.9 %	51.9 %
θ_r	7.87%	9.15
α	0.01	0.06
n	1.31	1.25

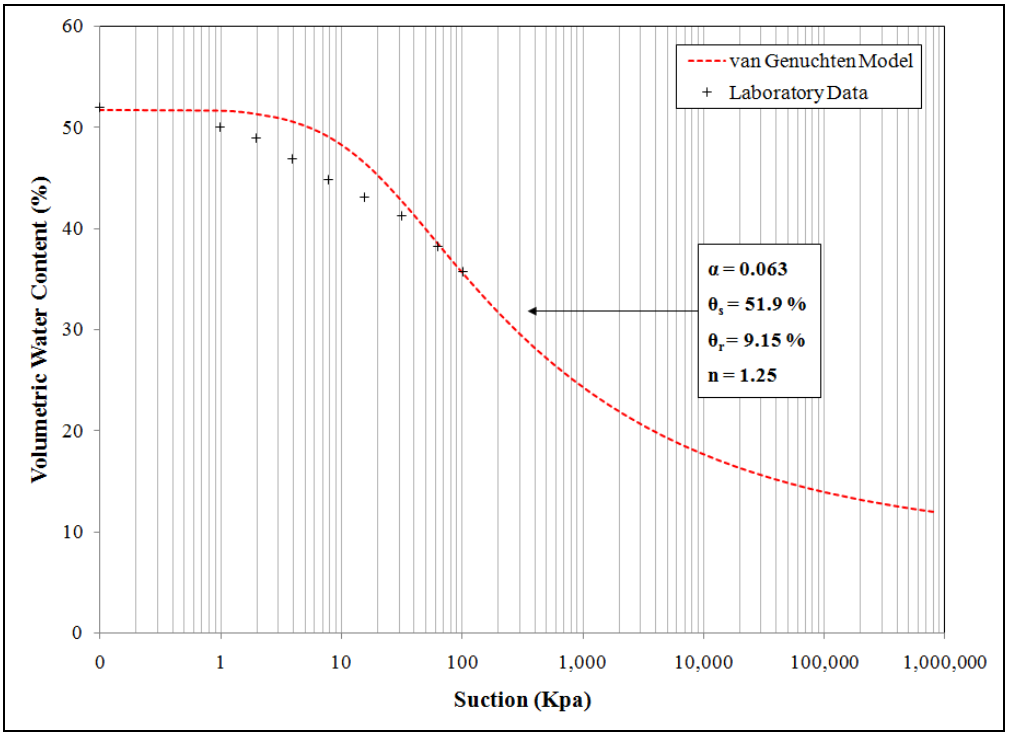

Figure 6.5 Predicted SWCC produced by varying the parameters of the van Genuchten model to fit the laboratory results.

Figure 6.6 presents a typical range of SWCC's for a silty clay loam consisting of 2.3-12.9 % sand, 29.5-36.9 % clay and the rest silt. Table 6.4 lists the hydraulic parameters for this soil

type as determined by Carsel and Parrish (1988). These parameters were determined for the van Genuchten's mathematical model for SWCC. It is important to note that the value called "Upper Limit" refers to the parameter's value that corresponds to the upper limit curve, and the value called "Lower Limit" refers to the parameter's value that corresponds to the lower limit curve of the SWCC range shown in Figure 6.6. And these values are not always the high and low value, respectively. In the case of *n* and α, the "Upper Limit" value corresponds to the low value of *n* and α, because the lower *n* is the less steep the curve is and the lower α is the higher the AEV is. And these conditions are the ones that define the upper and lower limit curves for the range of SWCC of the silty clay loam.

Table 6.4 Typical range of hydraulic parameters for a silty clay loam (adapted from Carsel and Parrish, 1988).

Parameter	Mean Value	Standard Deviation	Upper Limit SWCC	Lower Limit SWCC
K_s (cm/hr)	0.070	0.190	0.120	0.260
α	0.014	0.006	0.004	0.020
θ_s	0.430	0.070	0.500	0.360
θ_r	0.089	0.009	0.098	0.080
n	1.230	0.060	1.170	1.290

For comparison purpose, the laboratory SWCC is also included in Figure 6.6, and it can be observed that it tends to be steeper and the saturated water content is outside the range given by Carsel and Parrish (1988). This can be attributed to the fact that the percent of sand in the soil under study is higher (percent sand = 14.2 %) than the 7.6% that corresponds to the silty

clay loam. This higher percent of sand causes the soil to lose moisture more rapidly during the drying process; therefore, the AEV is lower in this case.

This range of SWCC's was considered more adequate to be used in the modeling of water flow processes since they were determined from a greater amount of testing and are statistically justified by Carsel and Parrish (1988). The laboratory results obtained in this study could have been affected by quality control issues at the time of the soil sampling or by the variability of the test itself. Moreover, only three samples were evaluated in the laboratory and no repetitions were performed to increase the statistic reliability of the results. However, the SWCC obtained was mostly within the range of curves established by Carsel and Parrish (1988).

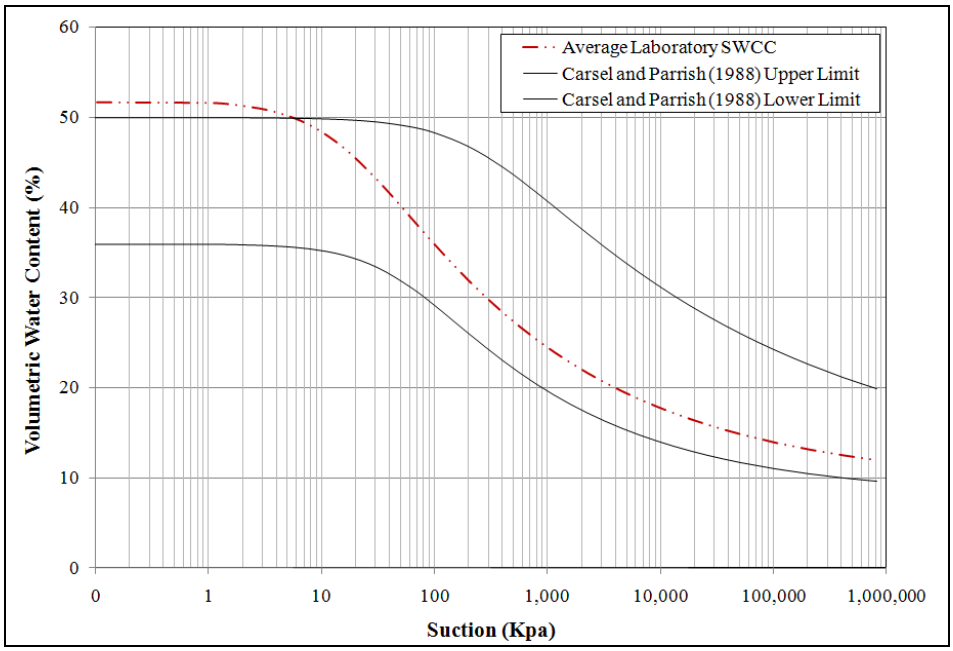

Figure 6.6 Comparison of laboratory SWCC and data from Carsel and Parrish (1988).

6.3 Filed Monitoring of Failed Slope

6.3.1 Suction Measurements

As described in Chapter 5, field suction measurements were taken at four different depths and at five different locations within the slope. Figure 6.7 shows the variation of suction measurements taken after the first set of instruments were installed, for a period between August 26 and September 11, 2007. Rainfall data collected during this period is also shown in Figure 6.7. Only one rain event was recorded for this period and it was observed that the suction values decreased after this event for all four depths. Although no great amounts of rain were recorded during the preceding five days, the low suction values during those days are indicative of an earlier rain activity. The range of suction values for this period was from 10 cm (0.15 psi) to 127 cm (1.81 psi).

Another monitoring period that was evaluated included the months of April, May and June of 2008. Figure 6.8 shows the suction variation with rainfall for this period. A very wide range of suction values was observed during this period. Suction values ranged from 3 cm (0.04 psi) to 900 cm (12.92 psi). Generally, it was observed that the suction values dropped when rainfall was measured and the more drastic changes in suction where observed at the shallower depths. The greatest drop in suction during the rain event on May 2, 2008 was experienced at the 23 cm (0.75 ft) depth. Near the surface the matric suction drops rapidly as the rain water infiltrates the soil.

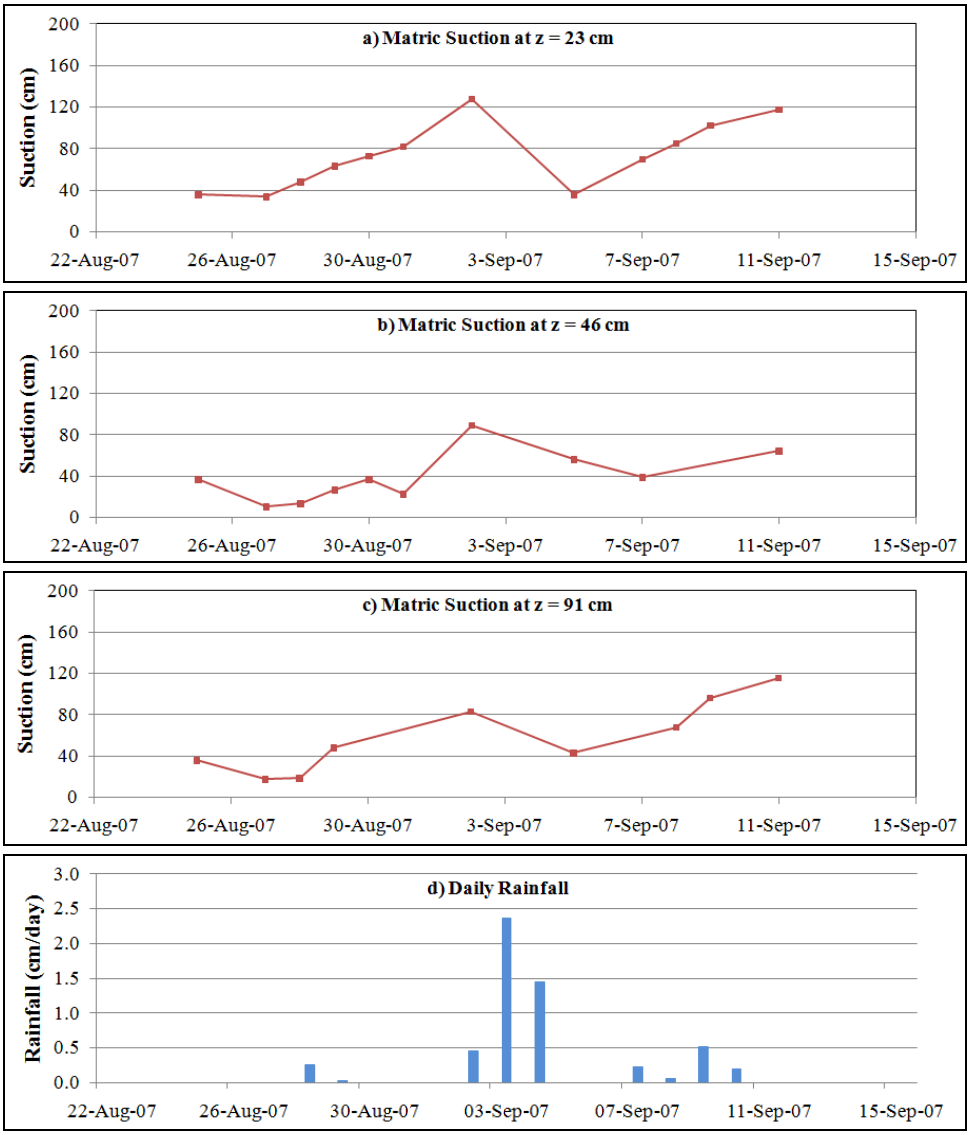

Figure 6.7 Suction measurements at each depth and rainfall distribution at the beginning of the monitoring program.

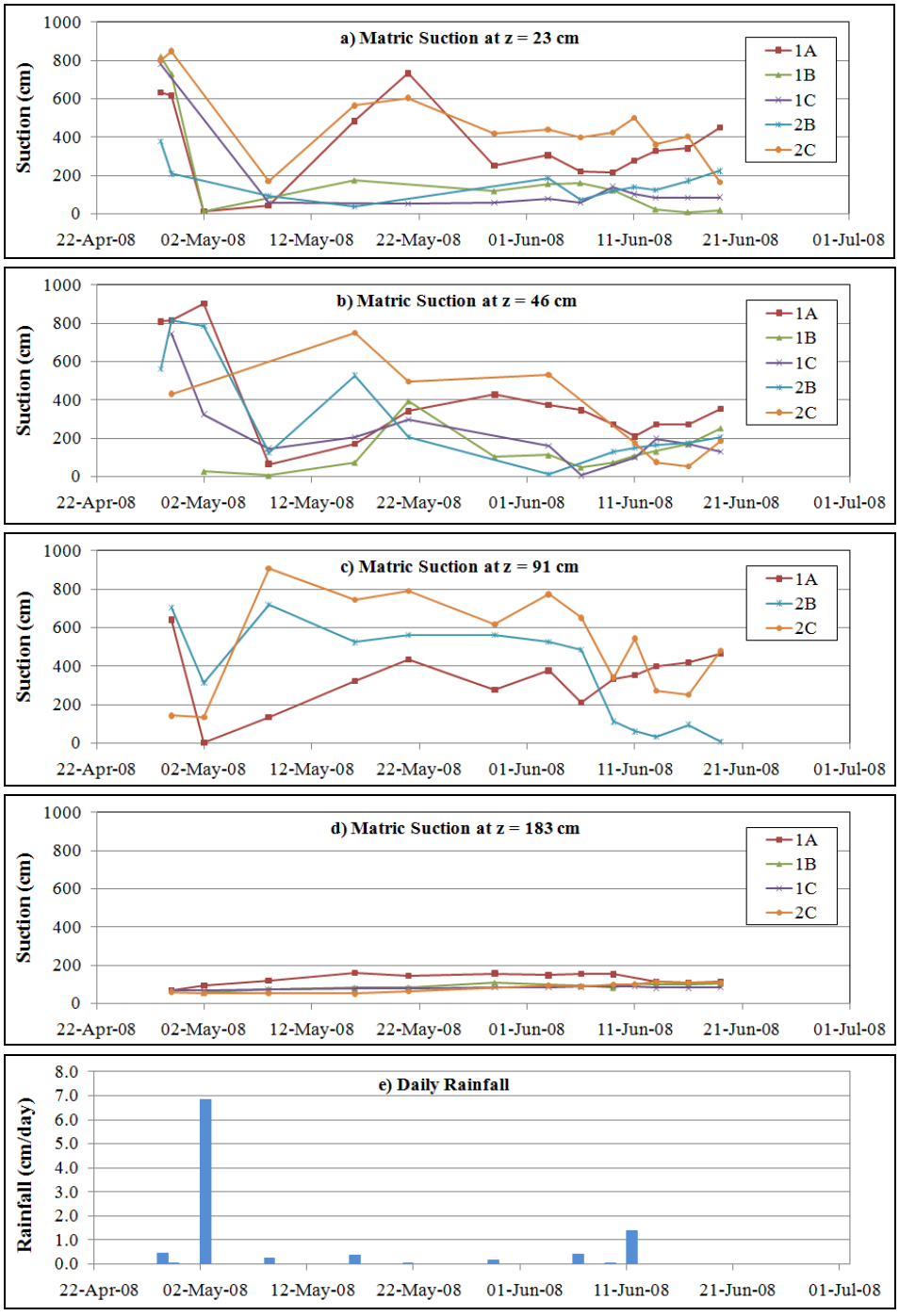

Figure 6.8 Suction measurements at each depth and rainfall distribution during the period of April to July, 2008.

No significant changes were observed at 183 cm (6 ft) of depth where the suction remained in a constant range of low suction (52–160 cm). This can be better observed in Figure 6.9, where the variation of matric suction as function of depth is presented. This could be attributed to the possibility that the wetting front was located at 183 cm (6 ft) from the slope surface. This behavior was expected as the slope is very steep and, thus, the rainfall is expected to runoff more than to infiltrate through the soil even more considering that the data was collected during the beginning of the rainy season. In this case the reduce amount of water that infiltrated the soil only affected a few feet below the slope surface and did not penetrate very deep into the soil.

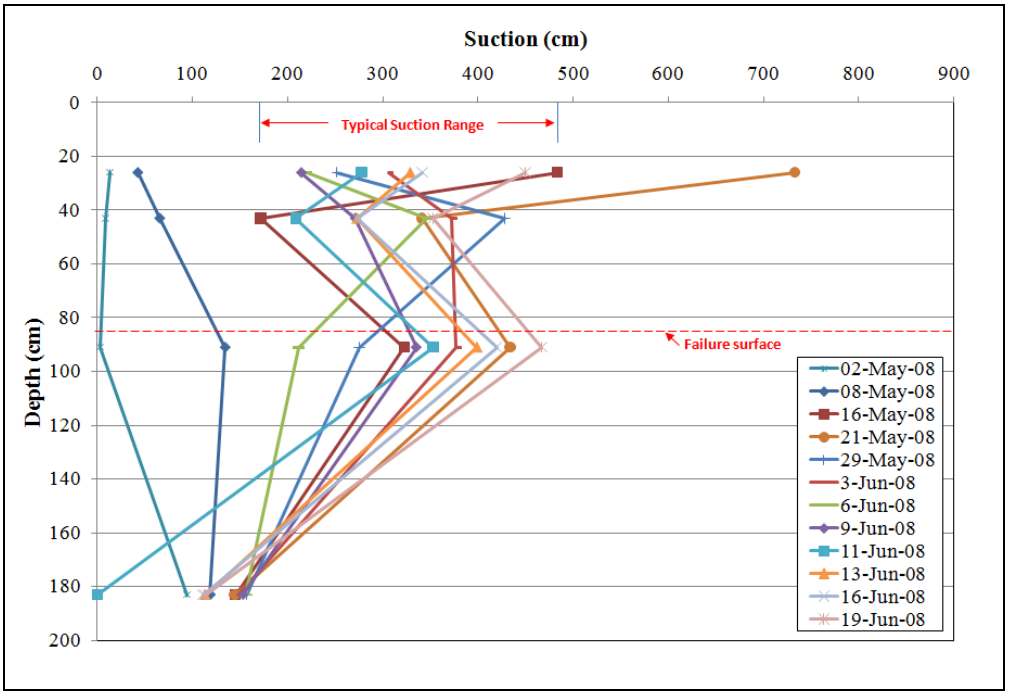

Figure 6.9 Variation of matric suction as function of depth at point 1A.

It can be observed in Figure 6.9 that as expected field suction fluctuates considerably and will depend to a large extent on the rainfall activity at the time of the measurement. The higher the recent rainfall activity the lower will be the corresponding suction measurement. For the range of depth of interest, suction values ranged from below 100 cm (1.4 psi) to higher than 500 cm (7.1 psi). For example, on May 2, 2008 the rainfall activity was 6.8 cm (refer to Figure 6.8) and the corresponding suction was very low (less than 100 cm); whereas for days with less rain activity, or even no rain, the suction measurements could be in excess of 500 cm. The field monitoring program revealed matric suction values ranging from 170 to 480 cm within the depth inferred of the failure surface.

7 ANALYTICAL STUDY

7.1 Introduction

This chapter presents the numerical analyses that were carried out to investigate the triggering mechanisms involved in the rainfall-induced slope failure case study. First, a slope stability back-analysis was carried out in Slope/W to determine the mobilized soil shear strength at the time of the slope failure. A seepage/infiltration analysis was then conducted using Hydrus 2D to estimate the levels of loss of soil suction that could have occurred during the rain storm of June 10, 2005.

The following sections describe the modeling procedures used for both types analysis and summarize and discuss the main results.

7.2 Slope Stability Back-Analysis

A slope stability back-analysis was conducted to determine the mobilized shear strength of the soils along the inferred failure surface. As discussed in Chapter 4, the shear strength of the MH residual soil, which was the predominant soil in this case study slope, was evaluated by means of laboratory shear tests. The shear strength properties determined in the laboratory were used for the slope stability back-analysis.

For all the models the water table was assumed to be very deep. This assumption was based on the knowledge of the existence of creek called “Quebrada de Oro” that runs very close to the area where the slope under study is located. This creek is located at a lower elevation than the toe of the slope. It was expected that the ground water table in this area is controlled by the water elevation of this creek. This assumption was corroborated during the geotechnical soil exploration, where no water table was found despite drilling to a depth of 3 m below the elevation of the toe of the slope.

The analysis type used was the combination of Bishop, Ordinary and Janbu, with a direction of movement from right to left. Then, the slope geometry was defined using the slope survey data given in Chapter 4. Only one material was used for the analysis and it was defined using the soil properties from the soil exploration and the direct shear tests. The slip surface was “fully specified” using the survey information presented in Chapter 4.

The slope stability was first evaluated using the shear strength properties determined from the samples with natural water content (see Table 4.3). These properties were believed to represent the original soil conditions corresponding to high suction values and apparent cohesion.

Figure 7.1 shows the results for this analysis. It can be observed that the soil properties corresponding to high suction and apparent cohesion produced a factor of safety higher than 3. This confirms that these properties were not the soil properties that led to the slope failure, and thus, can be considered the soil properties before the rain storm.

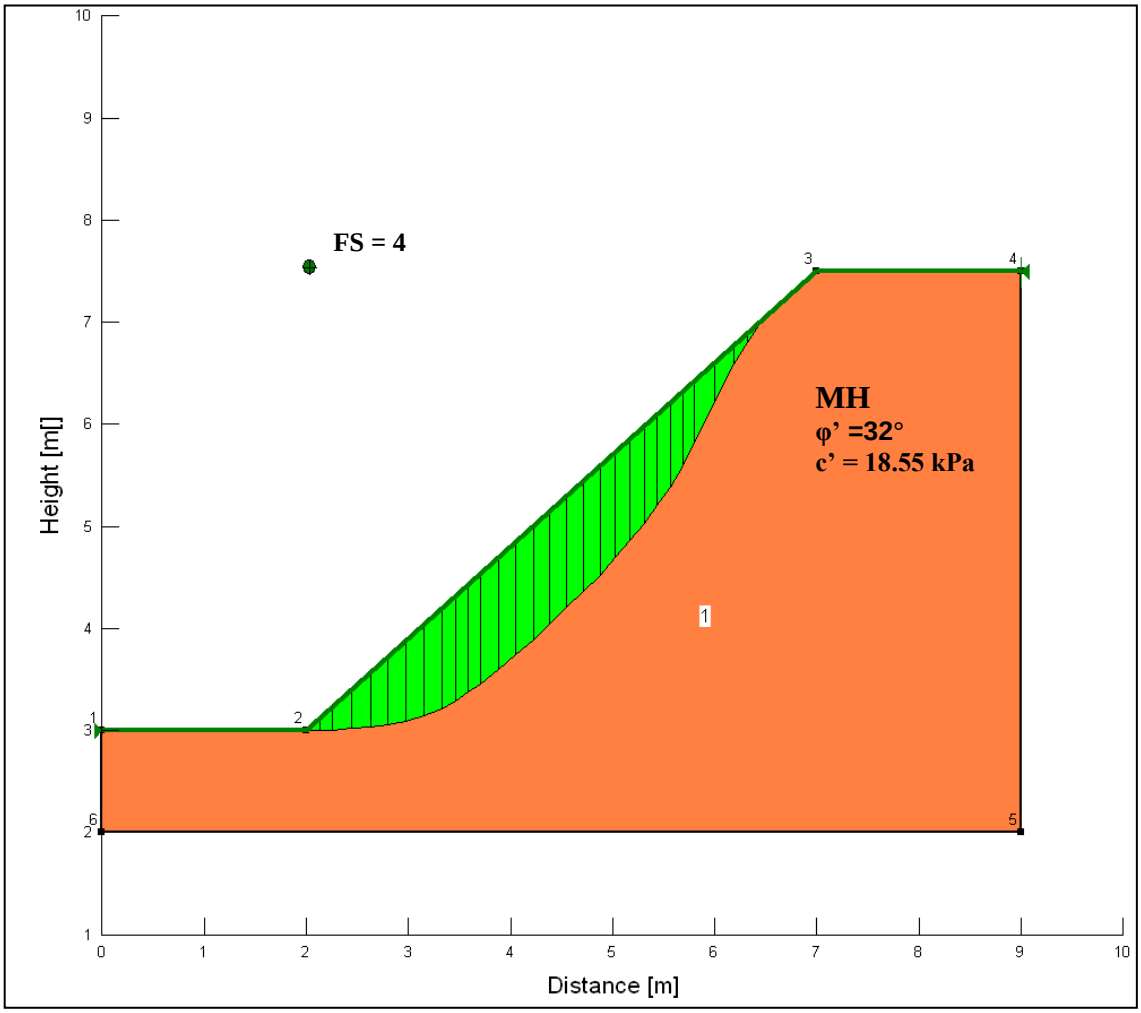

Figure 7.1 Initial slope stability analysis using peak shear strength properties and full apparent cohesion.

A back-analysis was carried out to determine the mobilized shear strength properties that generated the slope failure. For this, soil conditions were varied until failure was achieved (FS = 1). The soil properties corresponding to a FS equal to 1 were considered the failure properties. The results of the back-analysis are presented in Figure 7.2.

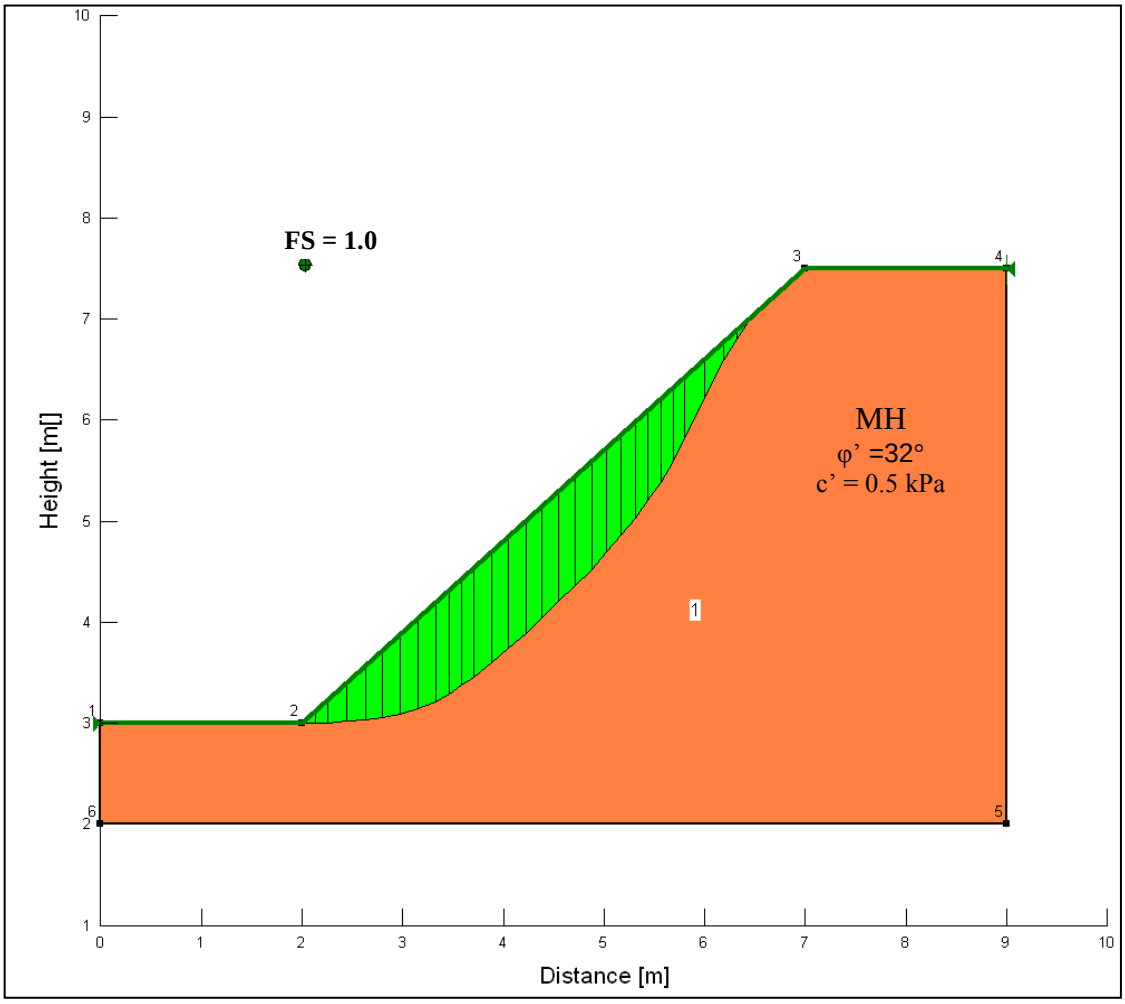

Figure 7.2 Back-analysis of the slope failure to target FS=1.

The back-analysis yielded a mobilized shear strength of φ'_m=32° and c'_m=0.5 kPa. Figure 7.3 shows the shear strength envelope of this mobilized strength and it compares it to the shear strength envelopes obtained in the laboratory tests for full suction (as sampled) and saturated condition (i.e. without suction). It can be seen that the slope failure back-analysis requires some loss of suction to explain its occurrence. The following subsections will investigate the

levels of suction los that can be expected for this soil slope site based on the SWCC, the soil type (MH), the geometry, and the rainfall/infiltration conditions typical for this region of Puerto Rico.

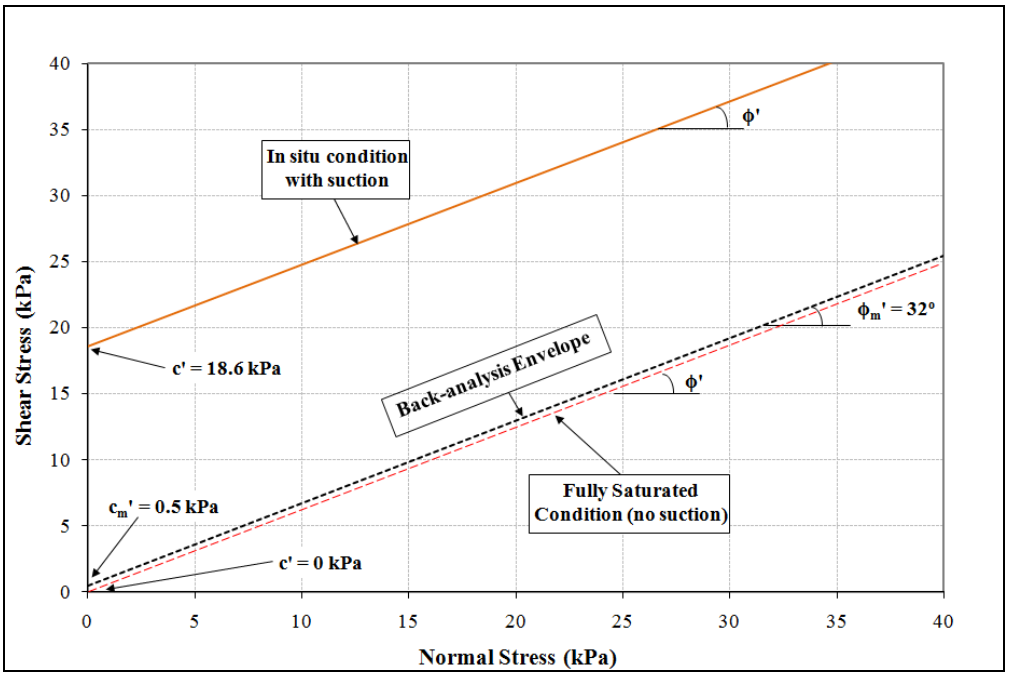

Figure 7.3 Comparison of the shear strength envelope obtained from the back-analysis with the envelopes obtained in the laboratory shear tests.

7.3 Seepage/Infiltration Analysis

As described in the preceding section, an important factor that appears to have triggered the slope failure is the shear strength decrease related to a drop in apparent cohesion, which in turn is related to the in situ matric suction. Thus, this section will investigate numerically

whether in-situ matric suction values could have dropped substantially in the field during the June 10, 2005 rainfall storm.

This section is divided into 3 subsections: i) general description of the numerical models used including boundary conditions, ii) results from analyses that included initial soil matric suction values based on average in situ measurements; iii) and results from analyses that included antecedent rainfall conditions based on historical rainfall records. The chapter ends with a summary section and conclusions.

7.3.1 General Description of Models Used

The seepage/infiltration analyses were carried out using the software Hydrus 2D. This software solves the governing differential equation using the finite element method (FEM). The finite element mesh used for the analyses is shown in Figure 7.4. This finite element mesh consisted of 219 1-D elements 1357 2-D elements and a total of 789 nodes. For all analyses suction values were tracked at the three observation nodes shown in Figure 7.5. These three nodes were selected to represent actual instrumentation installed in the field.

The Hydrus analyses were carried out using the software option "water flow," which is used for transient analyses. For transient analyses the program required specifying the initial and final time for calculations and also the time steps. For the analyses carried out here in, the time step ranged from $\Delta t = 0.00008$ to $\Delta t = 0.008$.

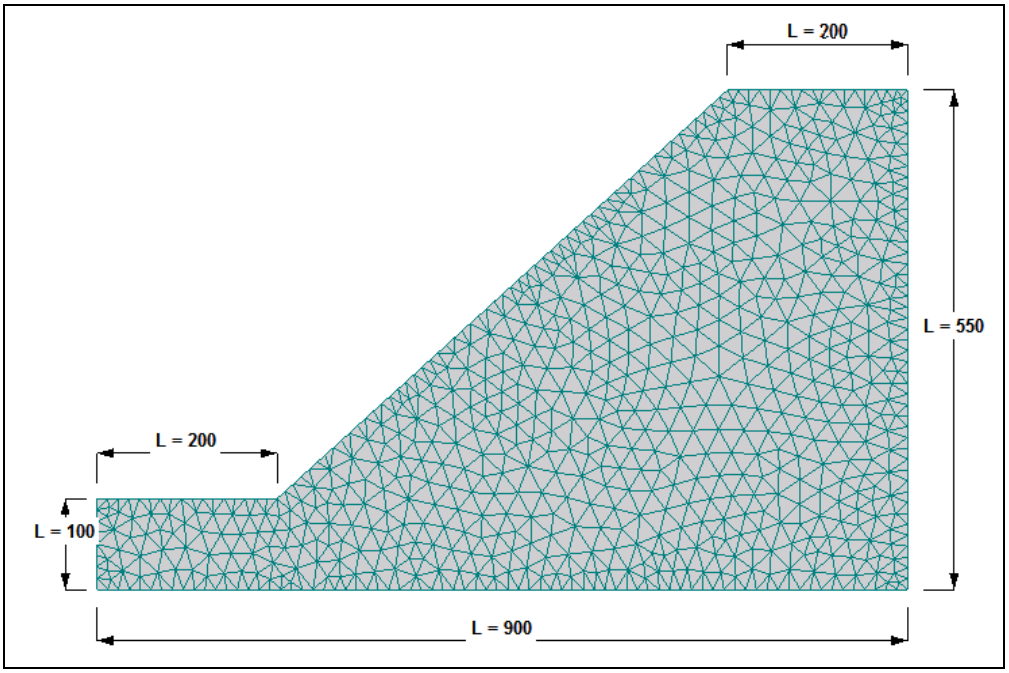

Figure 7.4 Finite element mesh used for infiltration analyses (dimensions in cm).

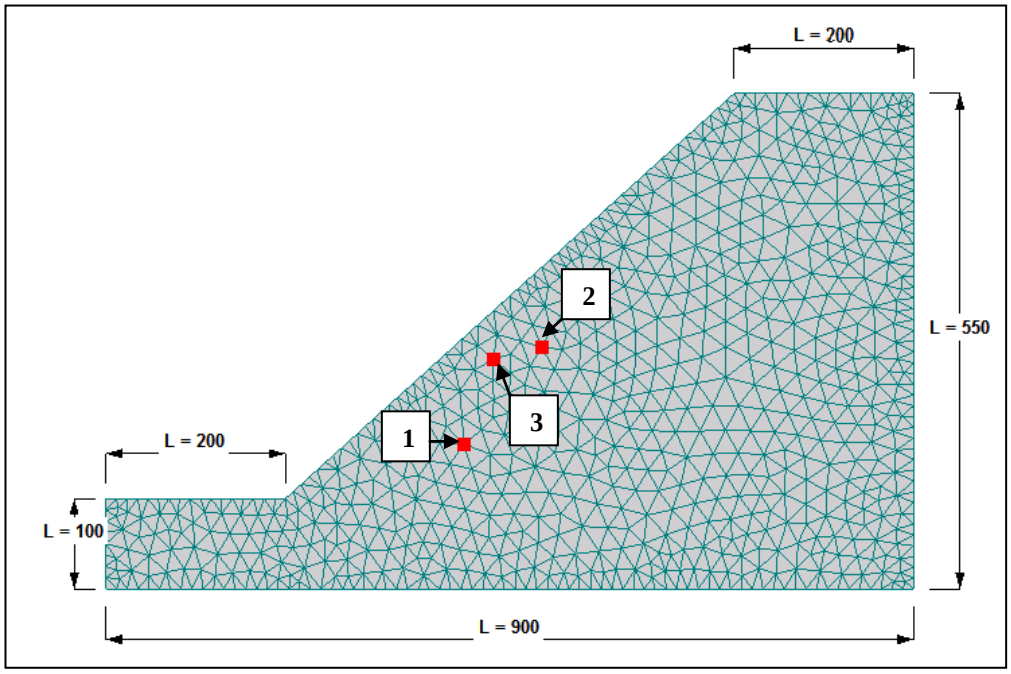

Figure 7.5 Observation nodes (dimensions in cm).

Most Hydrus analyses were carried out assuming a homogeneous slope as the slope failure was relatively shallow and the field investigation showed that the upper soils were fairly uniform.

The results presented in subsections 7.3.2 and 7.3.3 will correspond to different initial conditions and soil properties. For each soil type the program requires a different SWCC, a saturated volumetric water content (θ_s), a residual volumetric water content (θ_r), and a saturated hydraulic conductivity. The analyses were carried out with three sets of input soil properties: i) best estimate (based on lab SWCC); ii) higher bound SWCC; and, iii) lower bound SWCC. The higher and lower bound SWCC correspond to the upper and lower SWCC bounds based on published data corresponding to soil types similar to the ones encountered at the slope study site. Table 7.1 lists the parameters used for these analyses and Figure 7.6 shows the SWCC used.

Table 7.1 Hydraulic parameters used for seepage/infiltration analyses

Parameter	Best Estimate of Lab SWCC	Upper Limit* SWCC	Lower Limit* SWCC
K_s (cm/hr)	0.210	0.120	0.260
α	0.063	0.004	0.020
θ_s	0.519	0.500	0.360
θ_r	0.092	0.098	0.080
n	1.250	1.170	1.290
* Data published by Carsel and Parrish (1988).			

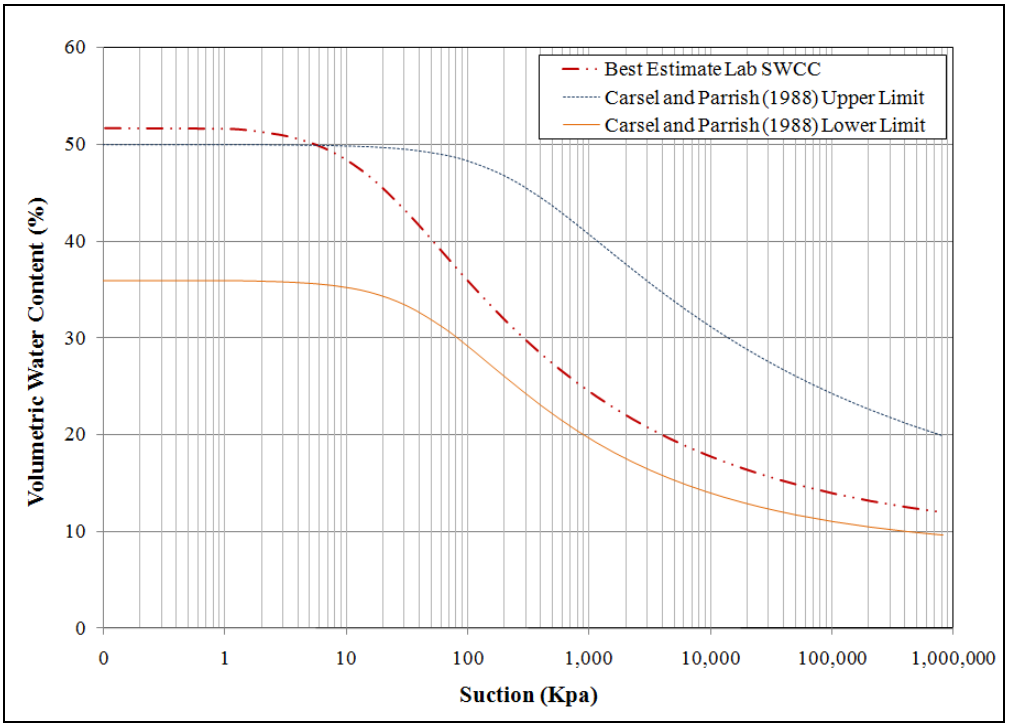

Figure 7.6 SWCC's used for seepage/infiltration analyses.

The boundary conditions used for the numerical analyses are shown in Figure 7.7. The figure shows the different boundary conditions with a color scheme. The right and left vertical boundaries of the model shown in Figure 7.7 were assigned as no flux borders. The horizontal surface to the left of the toe of the slope was also assigned as no flux boundary as it corresponds to an impervious asphalt paved roadway (PR-108). To avoid accumulation of water inside the model, the bottom of the model was assigned a free-drainage boundary. Free drainage is simulated in terms of a unit total vertical hydraulic gradient (i.e., a zero pressure head gradient). This situation is often observed in field studies of water flow during

drainage/redistribution in the vadose zone, as it is the case of this study (Sisson, 1987; and McCord, 1991). McCord (1991) states that the most pertinent application of a free drainage boundary condition is its use as a bottom outflow boundary condition for situations where the water table is situated far below the domain of interest.

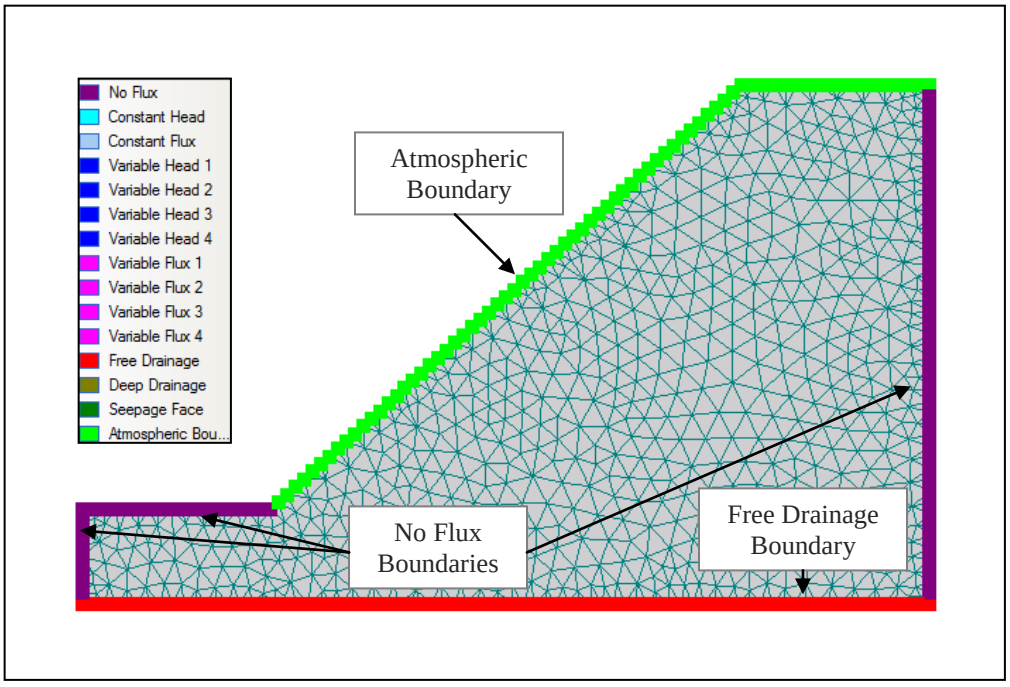

Figure 7.7 Boundary conditions applied to the slope for the water flow simulation.

An important boundary condition was the rainfall event and the corresponding infiltration. The rainfall event was specified using the Hydrus option of a time-variable boundary condition. This condition is applied by the software to all atmospheric boundaries specified. The default option of Hydrus is that precipitation water infiltrates into the soil at a rate controlled by the infiltration capacity of the soil. The analysis will assign all water in excess

of the infiltration capacity as surface runoff. For all the analyses of the slope study, the rainfall histogram corresponding to the June 10, 2005 storm was used (Figure 7.8) as the time-variable boundary condition. As observed from the rain histogram, the maximum intensity of the rain event occurred after 2 hours and 15 minutes. It was expected that the maximum loss of suction would occur after that time. After 3 hours, the intensity remained constant, thus no much suction variation would be expected after that.

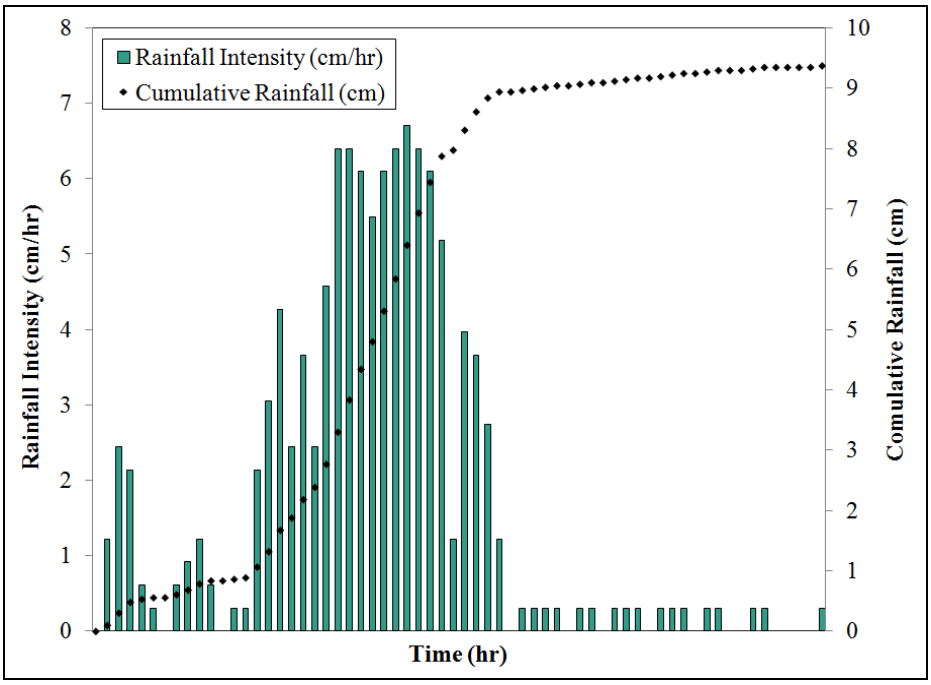

Figure 7.8 Rain histogram for the event that caused the landslides on June 10, 2005 (data collected and provided by the CID at UPRM).

The initial conditions of the slope, prior to rainfall exposure, were entered manually in the models. Two distinct cases were modeled: 1) initial properties based on best estimates from field suction measurements; and, 2) lower suction initial values based on consideration of

antecedent rainfalls that preceded the June 10, 2005 storm. These two cases are discussed in subsections 7.3.2 and 7.3.3, respectively.

7.3.2 Hydrus Results based on Range of Measured In Situ Suctions

The first set of Hydrus analyses were based on assuming soil properties to reflect our best estimate of the initial soil suctions in the slope. These values were based on the range of values measured with field instrumentation and monitoring. For example, field suction measurements from the range of depths of interest for this shallow slope failure are shown in Figure 7.9. These measurements are for the period of May to June 2008, and the corresponding rainfall activity is shown in Figure 7.10. These field measurements revealed matric suction values ranging from 170 to 480 cm within the depth inferred of the failure surface.

For this first set of Hydrus analyses three initial suction conditions were considered: 1) initial suction corresponding to low rainfall activity preceding the June 10, 2005 storm (this case used an initial suction of -480 cm); 2) initial suction corresponding to moderate rainfall activity preceding the June 10, 2005 storm (this case used an initial suction of -170 cm); and, 3) average initial suction of -325 cm, which was simply the average value of cases 1) and 2).

The results obtained in terms of suction values at the end of the storm for the initial condition of a high suction of -480 cm are shown in Figure 7.11. This figure shows the results for the analyses using SWCC's of upper bound, lower bound, and the lab curve.

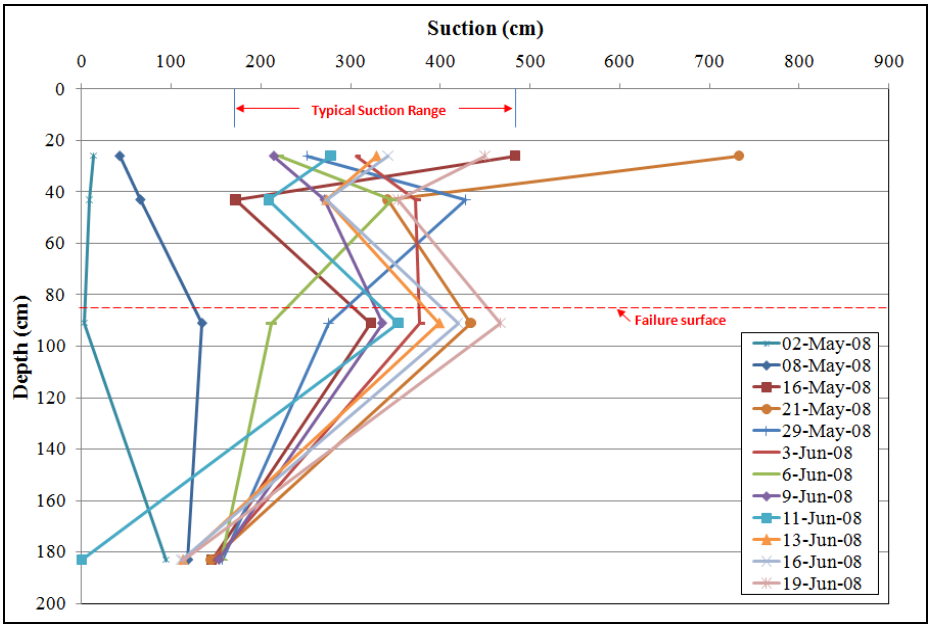

Figure 7.9 Profile of suction in the slope for a period from May to June 2008.

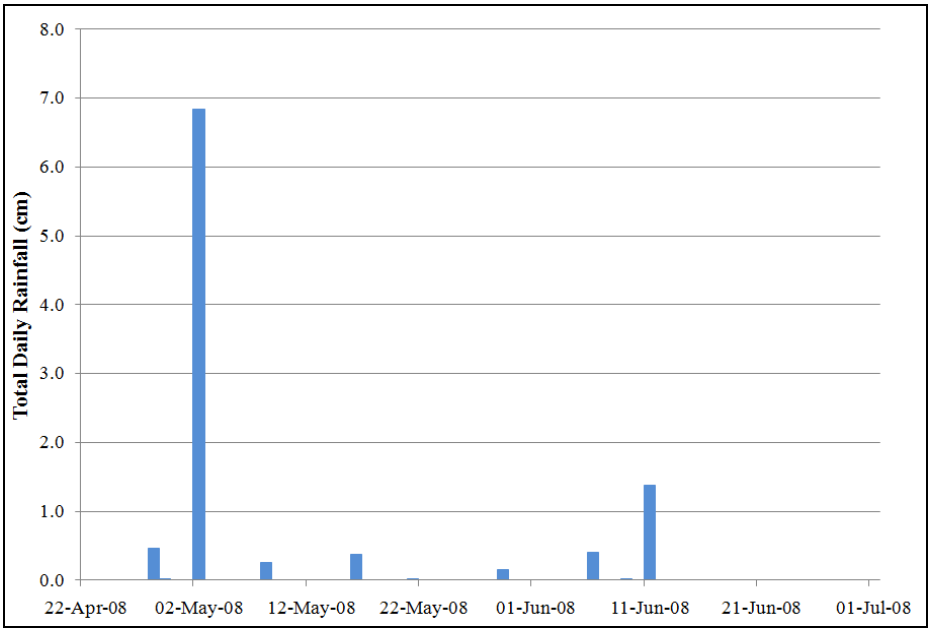

Figure 7.10 Rain data for the period of May-June 2008.

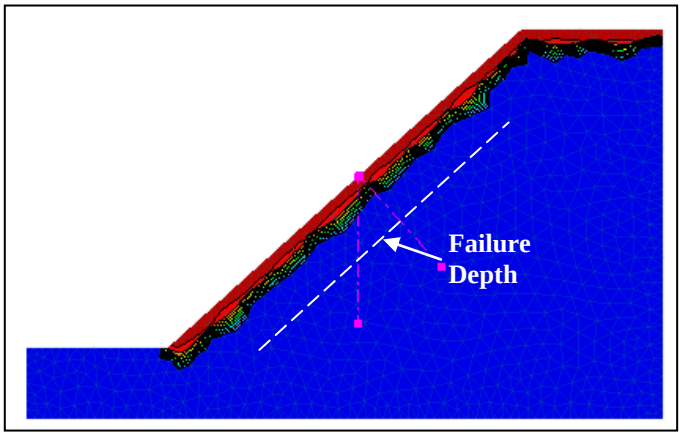

a) Lab SWCC

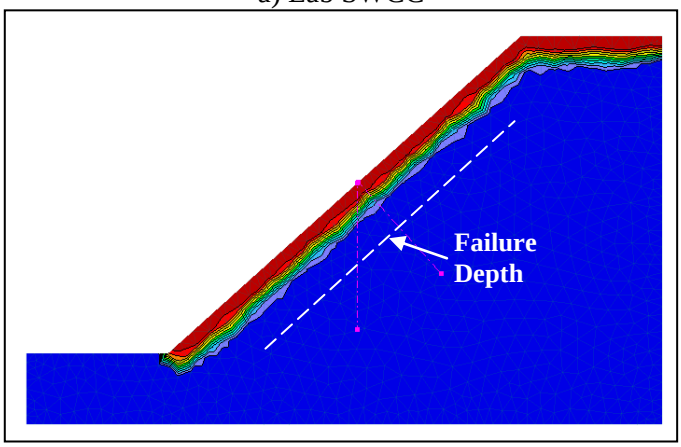

b) Lower Bound SWCC

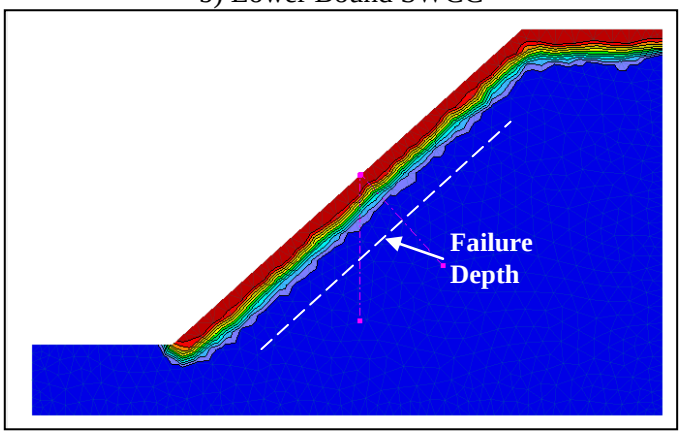

c) Upper Bound SWCC

Figure 7.11 Suction values at the end of the storm for initial suction of -480 cm.

It can be observed that there is not a significant difference between the three models. The three models show that the loss of suction during the storm using this initial condition of high suction is not low enough to explain the slope failure. Figure 7.12 shows an example of the variation of suction for the observation nodes at 40, 60 and 84 cm depth for the upper bound SWCC. It is observed that only a 27% loss of suction was experienced and it was not even at the failure depth.

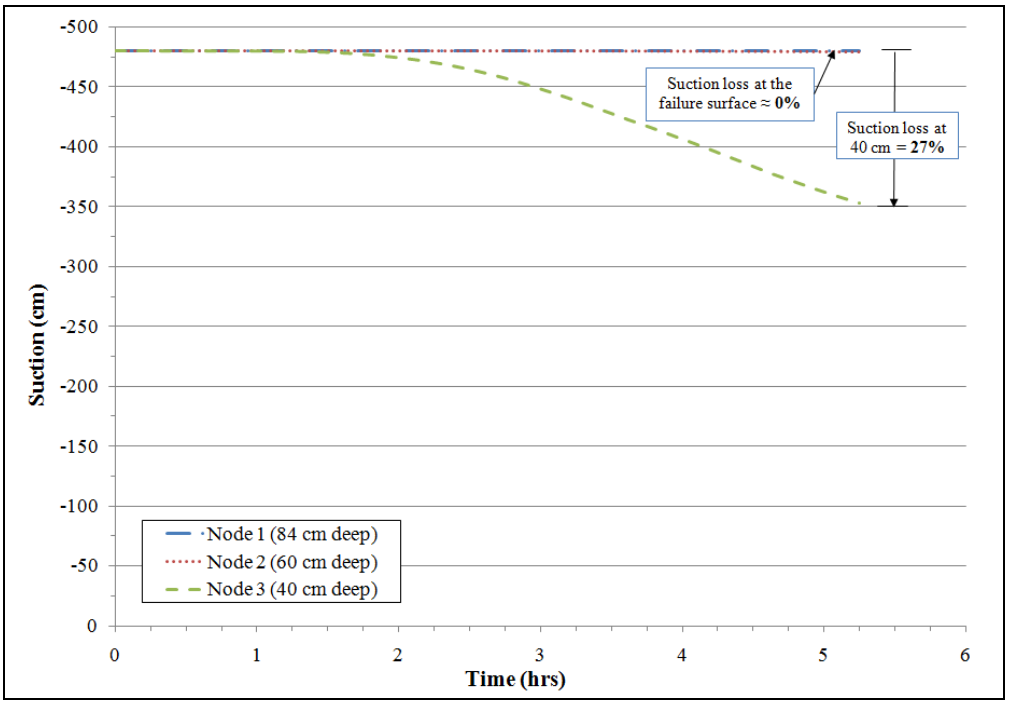

Figure 7.12 Suction variation at the observation nodes for high suction initial condition and upper bound SWCC.

The results obtained in terms of suction values at the end of the storm for the initial condition of an average suction of -325 cm are shown in Figure 7.13. Results are presented for the SWCC's of upper bound, lower bound, and the lab curve.

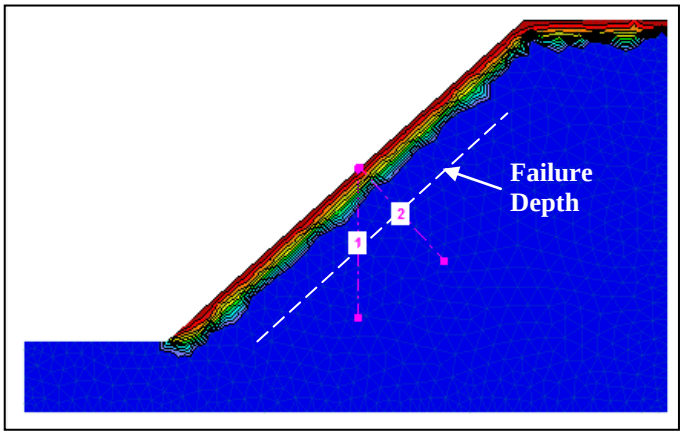

a) Lab SWCC

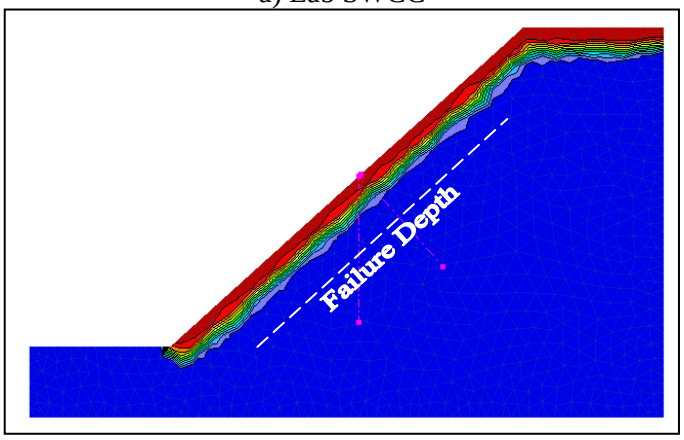

b) Lower Bound SWCC

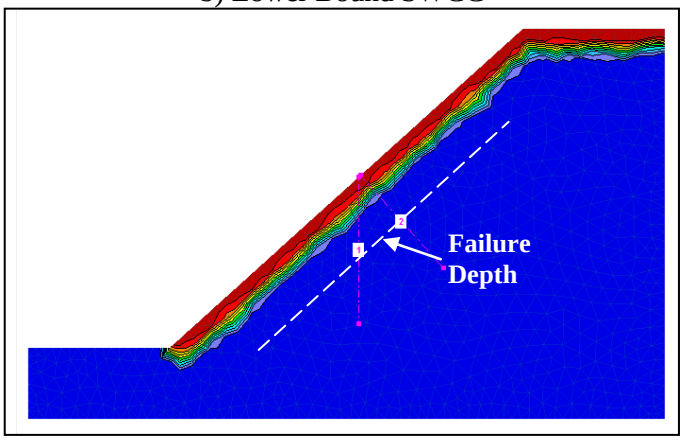

c) Upper Bound SWCC

Figure 7.13 Suction values at the end of the storm for initial suction of -325 cm.

It can be observed that the difference between models starts to be noticeable, but it is still not significant. The three models show that the loss of suction during the storm using this initial condition of average suction is not low enough to explain the slope failure. Figure 7.14 shows an example of the variation of suction for the observation nodes at 40, 60 and 84 cm depth for the upper bound SWCC. It is observed that only a 30% loss of suction was experienced (at 40 cm depth) and it was not even at the failure depth.

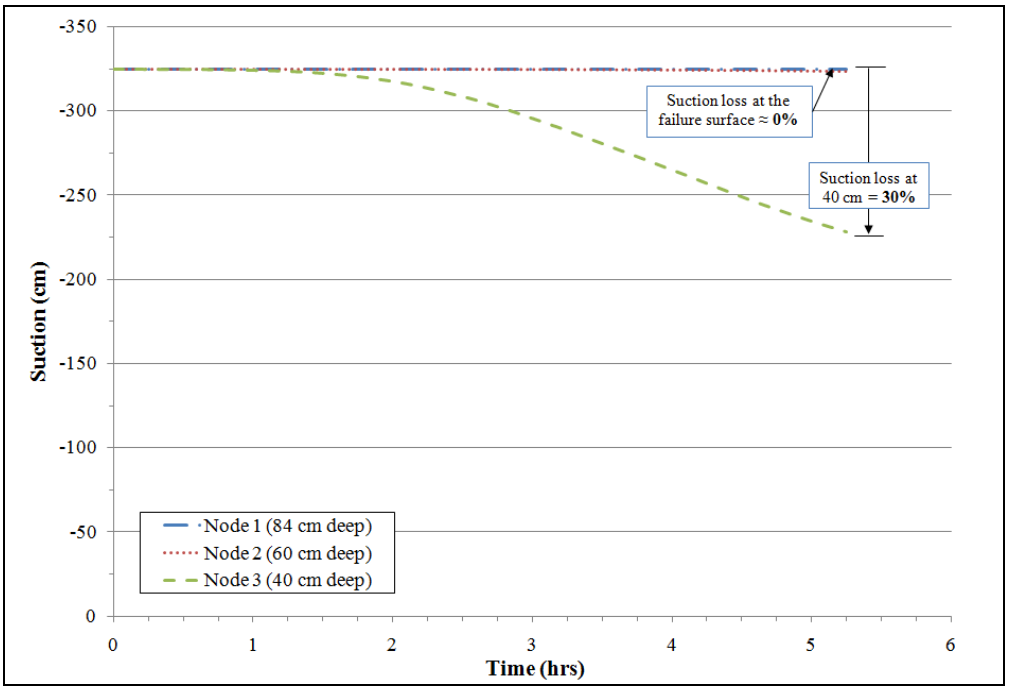

Figure 7.14 Suction variation at the observation nodes for average suction initial condition and upper bound SWCC.

The results obtained in terms of suction values at the end of the storm for the initial condition of a moderate suction of -170 cm are shown in Figure 7.15. Results are presented for the SWCC's of upper bound, lower bound, and the lab curve.

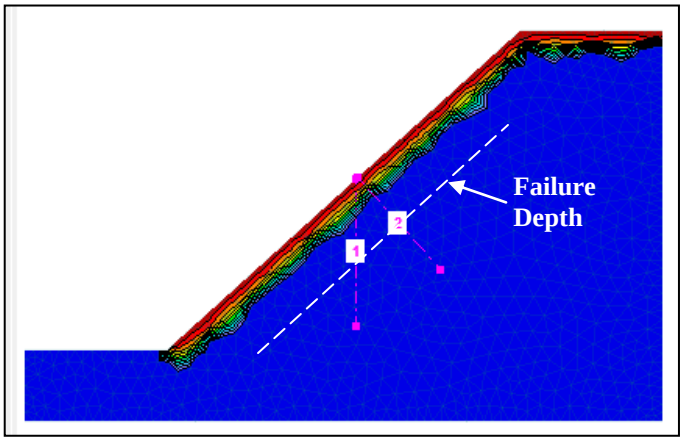

a) Lab SWCC

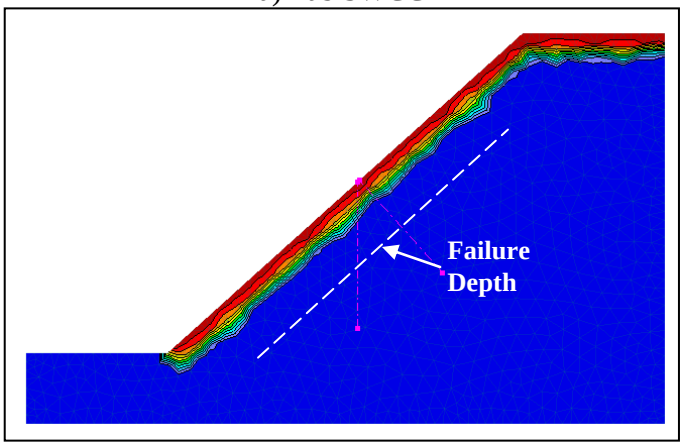

b) Lower Bound SWCC

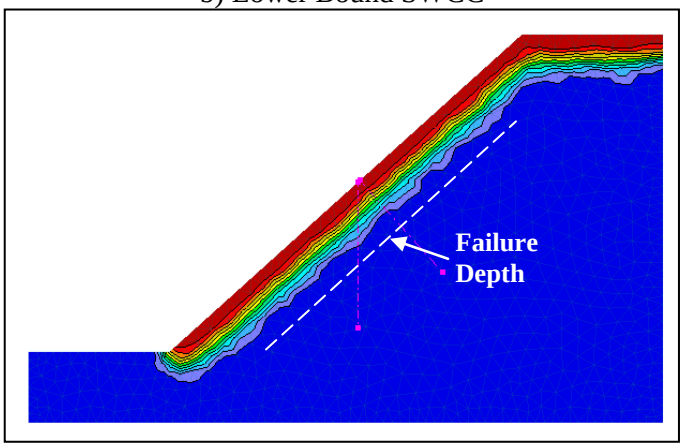

c) Upper Bound SWCC

Figure 7.15 Suction values at the end of the storm for initial suction of -170 cm.

It can be observed that difference between the three models is more noticeable. However, the three models still show that the loss of suction during the storm using this initial condition of moderate suction is not low enough to explain the slope failure. Figure 7.16 shows an example of the variation of suction for the observation nodes at 40, 60 and 84 cm depth for the upper bound SWCC. It is observed that only a 38% loss of suction was experienced and it was not even at the failure depth. However, it can be observed that as the initial suction decreases the loss of suction after the storm increases.

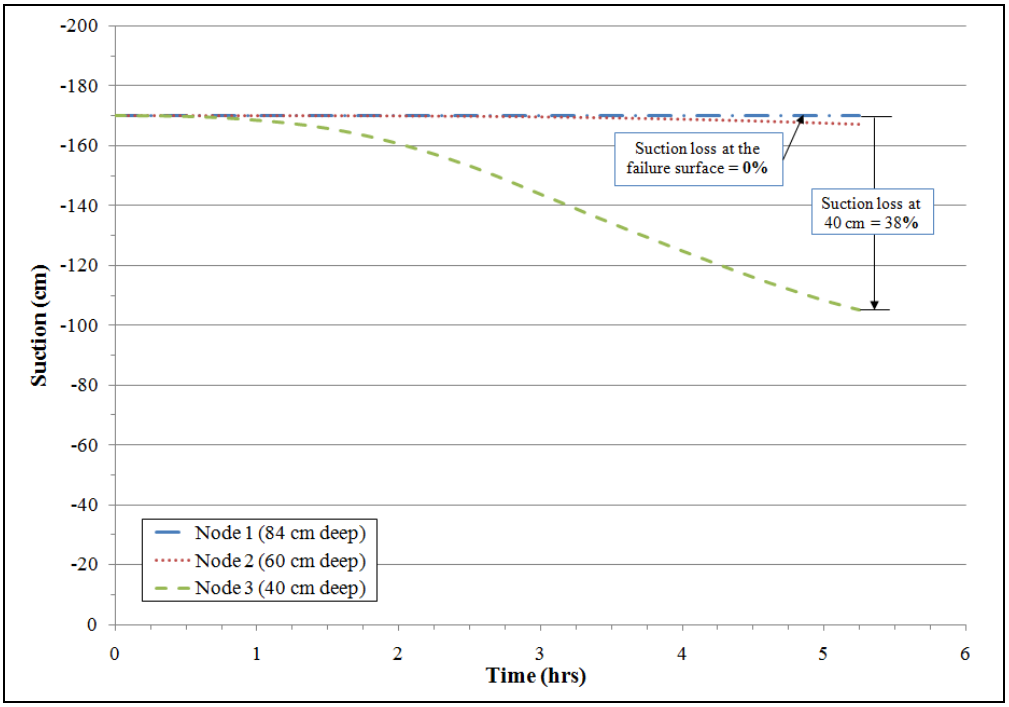

Figure 7.16 Suction variation at the observation nodes for moderate suction initial condition and upper bound SWCC.

7.3.2.1 Discussion of Results Using Initial Suction Estimate from Field Data

The range of suction values obtained from the three set of analyses (initial suction of -480, -325, and -170 cm) for the observation node located at the failure depth at the end of the June 10, 2005 storm was from -106 cm to -350 cm. This range of suction is not low enough to explain the observed slope failure. Therefore, it appears that the initial suction values within the region of the eventual failure mass of the slope had to be lower than what was assumed for the set of analyses presented in this subsection. Lower in situ suction values are justified if we consider that prior to the June 10, 2005 storm there was antecedent rainfall activity. The following subsection presents Hydrus analyses for the case when antecedent rainfall is considered.

7.3.3 Hydrus Results Considering Antecedent Rainfall

As discussed in the literature review chapter, Rahardjo et al. (2001) found that the rainfall activity 5 days preceding the landslide event were significant in excusing the landslide events. This precedent combined with the results presented in Section 7.3.2 justifies the set of analyses presented herein.

The rainfall activity preceding the main triggering event of June 10, 2005 is shown in Figure 7.17. For this period of five days the accumulated rainfall was 6.6 cm (2.6 in.). In contrast the June 10, 2005 event alone had a total of 9.3 cm (3.7 in.) of rainfall in a period of 5.25 hours.

The initial suction values were selected based on the field data collected for this thesis. The database of field data was reviewed to find field suction data for dates with an antecedent 5-day rainfall activity similar to the one of the June10, 2005 event.

From the field data collected for this project, a period of observation with a total rain in 5 days of 6.6 cm (2.6 in.) was isolated. The period of observation selected for this analysis was from April 28 to May 3, 2008. The total rainfall in five days caused a 94% reduction in the matric suction of the soil (measured at 23 cm from the surface) as shown in Figure 7.18.

From this, it was determined that the 6.6 cm (2.6 in.) of rain that fell during the 5 days preceding the landslide event, could have caused a total soil suction reduction of 94%. This information was used to vary the initial conditions in the hydraulic model. For this the average high suction (-325 cm) was reduced by 94% to obtain the initial condition of suction of -20 cm for the models considering antecedent rainfall. The analyses were carried out using the three SWCC's: upper bound, lab SWCC and lower bound.

The results obtained in terms of suction values at the end of the storm for the initial condition of a suction of -20 cm are shown in Figure 7.19. This figure shows the results for the analyses using SWCC's of upper bound, lower bound, and lab curve.

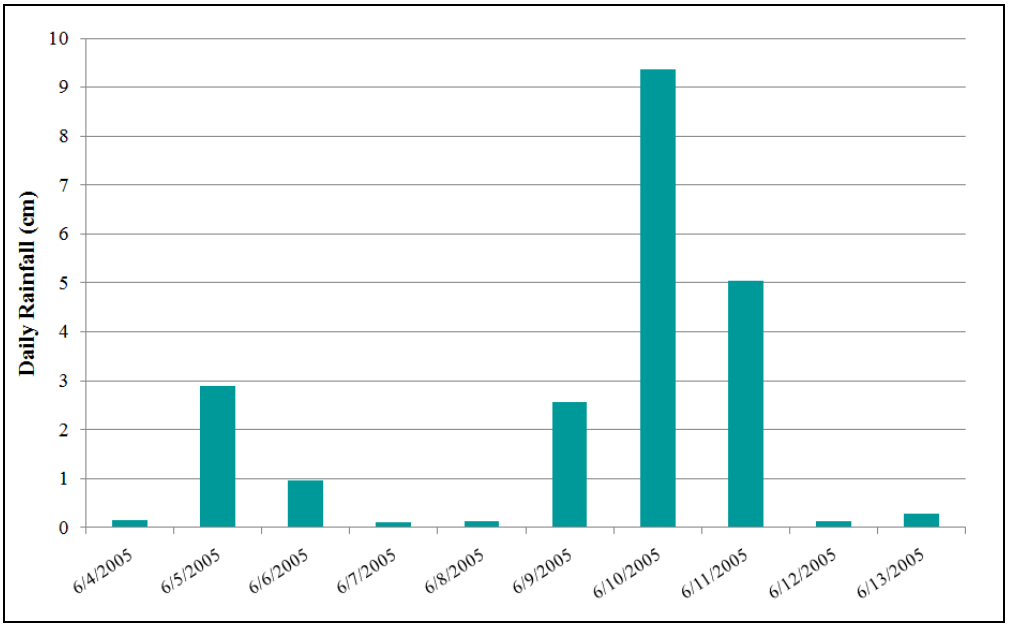

Figure 7.17 Antecedent rainfall to the June 10, 2005 storm (data collected and provided by the CID at UPRM).

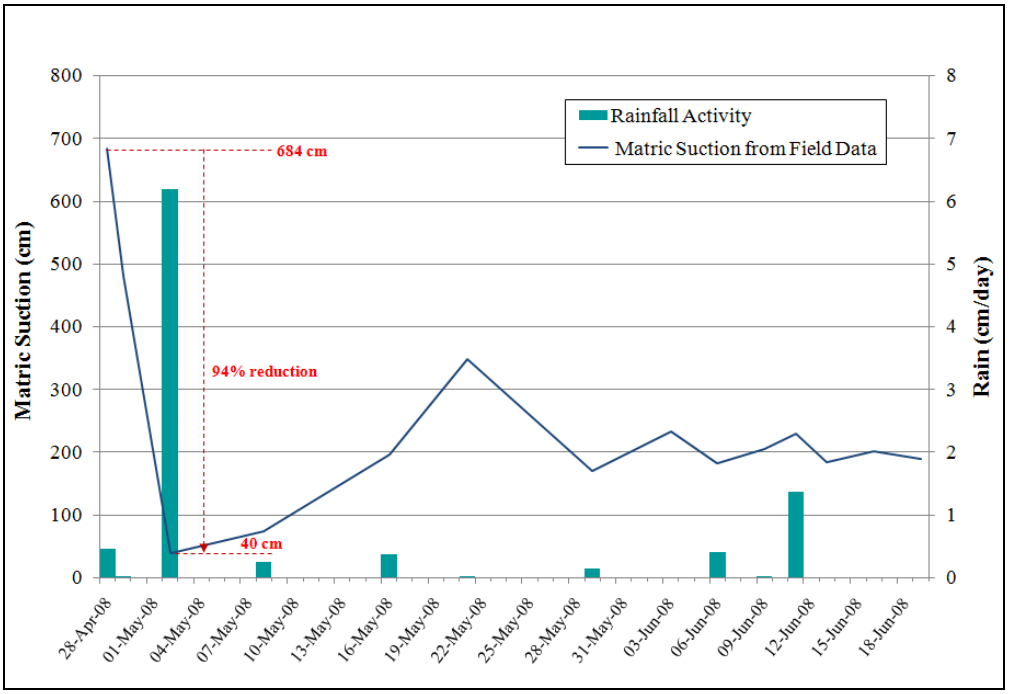

Figure 7.18 Field data showing suction variation with rainfall activity.

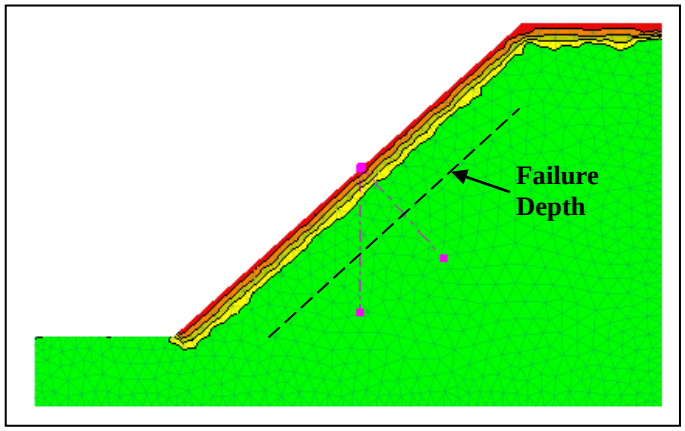

a) Lab SWCC

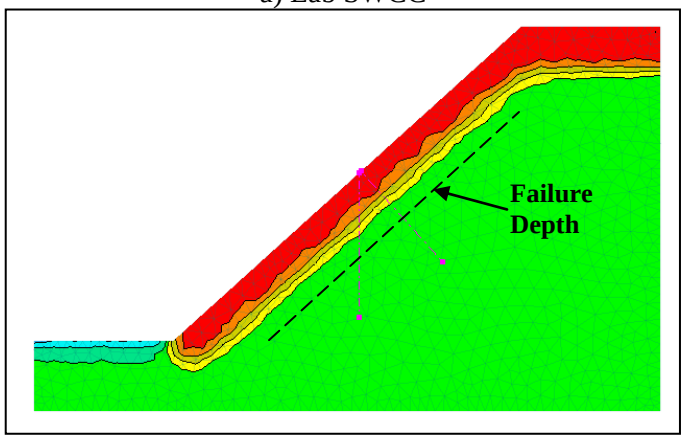

b) Lower Bound SWCC

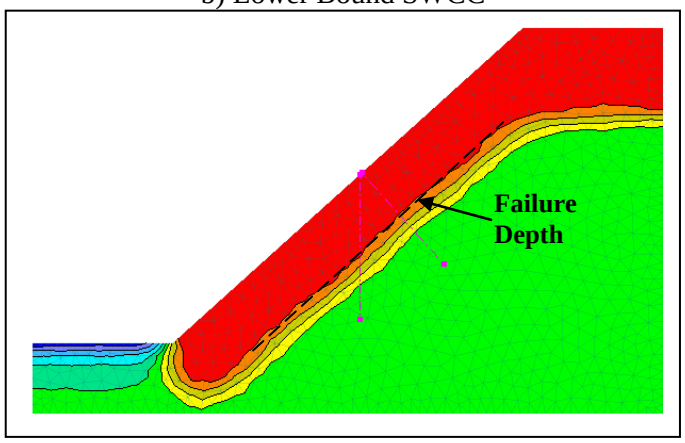

c) Upper Bound SWCC

Figure 7.19 Suction values at the end of the storm considering a 5-day antecedent rainfall.

The final conditions presented in Figure 7.19 show that the suction variation was significant when antecedent rainfall was considered in the analyses. The suction variation at the failure surface was significantly different from the suction obtained from the models that did not consider antecedent rainfall. This fact can be better observed in Figure 7.20, where an example of the change in suction with time is shown for the three observation nodes from the model using the upper bound SWCC. From this figure it can be seen that there is around 78% loss of initial suction at the failure surface depth. This suction loss represents a 98% of total suction loss if it is considered that the original soil suction in the slope without the antecedent rainfall was the average value of -325 cm (4.6 psi).

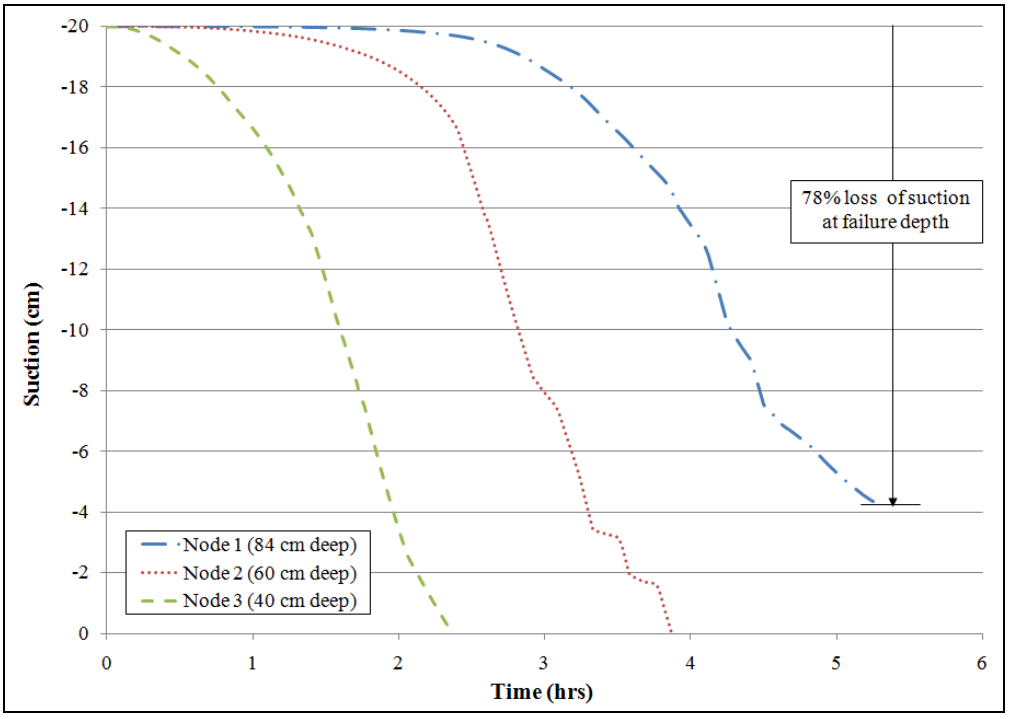

Figure 7.20 Soil suction variation at observation nodes considering 5-day antecedent rainfall and upper limit SWCC.

Figure 7.21 shows a comparison of all of the models that were analyzed in this section. It can be observed from the figure that the combination of hydraulic parameters in the upper SWCC produces a greater loss of suction at the failure surface for all cases than the lab and the lower SWCC's. All the models using suction values from field data produced the same results at the failure surface: no suction change. In the models considering antecedent rainfall, the upper SWCC produced a 78% loss of initial suction during the storm, while the lab SWCC and the lower SWCC produced 0% and 1% loss of suction at the failure surface, respectively.

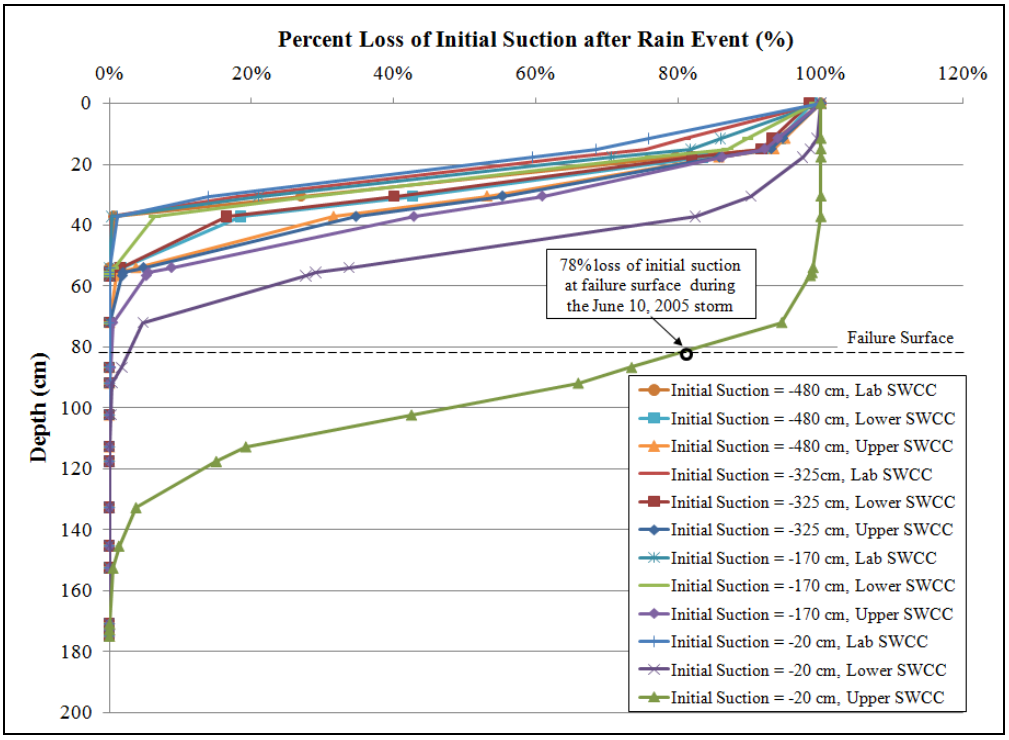

Figure 7.21 Comparison of suction loss profiles after the June 10, 2005 storm.

If the loss of suction produced by the model using the upper SWCC and antecedent rainfall is considered representative of the failure conditions, and if the average suction value of -325 cm is used as the base value, the total change in suction due to the total rain (5-day antecedent rainfall + storm rainfall) is 98%. This percent loss of suction is believed to be the cause for the almost complete loss of cohesion of the soil in the inferred failure surface that resulted from the slope stability back-analysis.

It can be concluded that the antecedent rainfall had a significant influence on the initiation of landslides. In this case study, the 5-day antecedent rainfall of 6.6 cm combined with the June 10, 2005 rainfall of 9.3 cm were sufficient to cause the complete loss of suction in the soil slope.

7.4 Summary

This chapter presented the analytical modeling that was performed to determine the possibility of loss of soil suction during a rain storm and the effects of that loss on the soil strength and stability of the slope. First, a stability analysis was carried out to determine the soil strength properties that led to the slope failure. It was observed that a 97% loss of strength was the cause for the slope instability.

A water flow analysis was then conducted to determine the possibility that the loss of strength was due to a loss of soil suction during the rain storm. It was observed that the loss of suction was not only influenced by the daily rain that was accumulated during the storm,

but also to antecedent rainfall. A 98% loss of suction was produced by the total rain, which is demonstrated that an almost complete loss of suction was possible at the failure surface due to the rainfall infiltration. Therefore, a major finding was that this case study slope instability was triggered by the combination of the rainfall infiltration during the June 10, 2005 rain storm and the effects of the 5-day antecedent rainfall. Analyses without antecedent rainfall were notable to capture the observation of this slope failure.

7.5 Uncertainties Related to the Analysis

The analyses presented in this chapter are valid for the conditions modeled and the assumptions made. For future investigations it should be considered that these analyses did not include capillarity elevation, which is a very important aspect in seepage/infiltration modeling, especially for clay soils. Also, it should be noted that the analyses assumed isotropic and homogeneous soil conditions, which is a simplification very commonly used in practice. And, finally, seepage/infiltration in the slope was modeled using transient analysis. A different type of analysis would probably produced different results.

8 SUMMARY, CONCLUSIONS AND RECOMMENDATIONS

8.1 Summary

This MS thesis presented the results of a research carried out to determine the triggering mechanisms for a rainfall-induced slope instability on a residual soil slope located in the city of Mayagüez, PR. The slope failure investigated was triggered by a heavy rainfall event that occurred on June 10, 2005 triggering at least ten landslides in the city of Mayagüez, PR. This particular slide chosen occurred near the UPRM campus facilitating field work and long-term monitoring. The slide was surveyed shortly after the rainfall event to determine the failure geometry and at that time soil samples were taken for determination of soil properties.

In 2007, an experimental program was designed to study more closely the soil properties and to analyze the possible triggering mechanisms of the failure. The slope was instrumented and monitored for different periods of time to observe changes in soil suction with rainfall. Observations showed reductions in soil suction after episodes of rainfall throughout different periods of time. This data was valuable and was used as reference for the seepage/infiltration modeling.

The laboratory test program carried out allowed soil classification, soil properties determination, and in particular the determination of the SWCC. For SWCC determination

three undisturbed samples were extracted from the slope area and tested using Tempe Cell devices.

Slope stability analyses were carried out to back-calculate the mobilized shear strength for the soil region along the inferred failure surface. The slope stability back-analysis indicated that the slope instability was a product of shear strength loss along the failure surface region. The shear strength back-calculated was found to correspond to an almost complete loss of the apparent cohesion, which is related to the matric suction present in unsaturated fine-grained soils at the site of the failed slope. The analytical component of this thesis also included a seepage/infiltration transient analysis to determine the possibility that the loss of strength was due to an almost complete loss of soil matric suction during the rain storm on June 10, 2005. It was observed that the loss of suction was possible, and that it was not only influenced by the heavy rainfall event on June 10, 2005, but also was related to antecedent rainfall. The next section summarizes the main conclusions of this study.

The results obtained from this project provide a contribution towards a better understanding of the triggering mechanisms for shallow slope instabilities involving unsaturated residual soils from tropical regions like Puerto Rico. This will help on the development of better schemes to mitigate the serious problem of rainfall-induced slope instabilities. For example, the models produced in this study can be applied to different slope geometries, soil types, and weather conditions to create a database that can be used to identify areas that are susceptible to rainfall-induced slope instabilities. Then, once these areas are identified the database can

be used in combination with a rainfall-landslide threshold to develop a warning system to alert the public about the areas that are prone to slope instabilities during a rainfall event.

8.2 Conclusions

The main conclusions drawn from this study include:

Field Instrumentation Plan:

- The field instrumentation plan worked satisfactorily for the purposes of this project. However, a continuous monitoring of the soil suction would have been more beneficial for a more detailed ground-water flow study.

Soil-Water Characteristic curve Determination:

- The experimental determination of the soil-water characteristic curve was important for the determination of the soil hydraulic properties to be used for the ground-water flow analyses.
- The SWCC determined in the laboratory was considered a good representation of the water retention properties of the soil.
- The lab-based SWCC compared well with published curves for similar soils. The analytical component used a range of SWCC's (lower bound, upper bound curves) to ensure the analysis covered a reasonable range of possibilities and soil variability issues.

Analytical Study:

- From the analytical component of this study it was shown that the soil could experience an almost complete loss of in situ matric suction due to rainfall infiltration for the June 10, 2005 storm. However the initial suction was a key consideration and it was necessary to include antecedent rainfall effects.
- The slope stability back-analysis showed that the failure properties corresponded to a loss of cohesion of 97%.
- The possibility of a loss in soil suction due to rainfall infiltration was shown possible through Hydrus seepage/infiltration flow modeling. However, it was shown that just the rainfall event of June 10, 2005 by itself was not enough to produce the required suction loss.
- The Hydrus analyses showed that antecedent rainfall of 5 days prior to the triggering event had a major influence on the loss of suction. When including 5-day antecedent rainfall effects a 98% loss of suction was found to be present in the soils along the failure surface. The Hydrus analyses showed that an almost complete loss of suction was possible at the failure surface due to this rainfall infiltration condition. Therefore, the slope instability was considered to be triggered by a combination of rainfall infiltration during the main June 10, 2005 rain storm and the 5-day antecedent rainfall.

8.3 Recommendations for Future Work

The main recommendations for future work include the following:

- Future studies would benefit from a continuous monitoring system that would record both soil suction and in-situ soil moisture.
- SWCC determination in the laboratory can be complemented by field-based SWCC's if both suction and moisture are measure in the field.
- A more detailed evaluation of the unsaturated shear strength of the involved soils is recommended, such as suction-controlled triaxial tests, which would be ideal for this type of research.
- It is also recommended to include in the study a water balance study to determine the percentage of infiltration relative to surface runoff.
- The hydrology around the slope under study should be evaluated and considered in the analyses to include effects of other sources of ground or surface water.

REFERENCES

Anderson, M. G., and Howes, S. (1985) "Development and application of a combined soil water-slope stability model," Q. J. Eng. Geol., London, 18, 225-236.

Anderson, S. A., and Thallapally, L. K. (1996) "Hydrologic response of a steep tropical slope to heavy rainfall landslides," landslides, Senneset (ed.), Balkema, Rotterdam, 1489-1495.

ASTM D 6836, (2002). "Standard Test Methods for Determination Of the Soil Water Characteristic Curve for Desorption Using a Hanging Column, Pressure Extractor, Chilled Mirror Hygrometer, and/or Centrifuge," ASTM International, US.

Bilskey, Jim. (2001). "Soil water status: content and potential," Campbell Scientific, Inc., http://www.campbellsci.com/documents/apnotes/soilh20c.pdf, downloaded on July 25, 2007.

Brand, E., W. (1984) "Relationship between rainfall and landslides in Hong Kong," *Proceedings of the 4th International Symposium on Landslides*, Toronto, Canada, 01:377-84.

Brooks, R. H., and Corey, A. T. (1964). "Hydraulic properties of porous media," Hydrology Paper No. 3, Colorado State Univ., Fort Collins, CO.

Brutsaert, W., (1966). "Probability laws of pore-size distributions," *Soil Sci.*, 101, 85-92.

Burdine, N. T. (1953). "Relative Permeability Calculations from Pore Size Distribution Data," Trans. AIME, 198, 71.

Caine, N. (1980). "The rainfall intensity-duration control of shallow landslides and debris flows," Geografiska Annaler. Vol. 62A, 23-27.

Carsel, R.F., Parrish, R.S., (1988), "Developing joint probability distributions of soil water retention characteristics," Water Resources Research, 24(5), 755-769.

Chatterjea, K. (1989). "Observations on the fluvial and slope processes in Singapore and their impact on the urban environment," Ph D thesis, National University of Singapore.

Collins, B. D., and Znidarcic, D. (2004) "Stability Analyses of Rainfall Induced Landslides," *J. Geotech. and Geoenviron. Eng.*, ASCE, 130(4), 362-372.

Cruden, D.M., and Varnes, D.J. (1992). "Landslide types and processes," Landslides: Investigation and Mitigation. Washington, DC: Transportation Research Board, National Academy of Sciences.

Fredlund, D. and Houston, S. (2009). "A Protocol for Assessment of Unsaturated Soils Properties for Geotechnical Practice," *Canadian Geotechnical Journal*.

Fredlund, D. G. (1979). "Appropriate concepts and technology for unsaturated soils," *Can. Geotech. J.*, 16, 121-139.

Fredlund, D.G. and N.R. Morgenstern (1977). "Stress state variables for unsaturated soils," *J. of the Geotechnical Engineering Division*, ASCE.

Fredlund, D.G. and Rahardjo, H. (1993). "Soil Mechanics for Unsaturated Soils," John Wiley and Sons, Inc., New York.

Fredlund, D.G., and Xing A. (1994). "Equations for the soil-water characteristic curve," *Canadian Geotechnical Journal*, 31: 521–532.

Gardner, W. (1956). "Mathematics of isothermal water conduction in unsaturated soils," Highway Research Board Special Report 40 International Symposium on Physico-Chemical Phenomenon in Soils, Washington D.C. pp 78-87.

Haneberg, W. C., (1991). “Observation and analysis of pore pressure-fluctuation in a thin colluviums landslide complex near Cincinnati, Ohio,” *Eng. Geol.*, 31(2), 159-184.

Keefer, D. K., Wilson, R. C., Mark, R. K., Brabb, E. E., Brown, W. M. III, Ellen, S.D., Harp, E. L., Wieczoreck, C. F., Alger, C. S., and Zatkin, R. S. (1987). “Realtime landslide warning during heavy rainfall.” *Science*, Vol. 238, 921-925.

Kosugi K (1994). “Three-parameter lognormal distribution model for soil water retention,” Water Resources Research 30, 891-901.

Larsen, M.C., and Simon, A. (1993), “Rainfall-threshold conditions for landslides in a humid-tropical system, Puerto Rico”, *Geografiska Annaler*, 75A(1-2), pp. 13-23.

Larsen, M.C., and Torres-Sánchez, A. J. (1998), “The Frequency and Distribution of Recent Landslides in three Montane Tropical Regions of Puerto Rico”, *Geomorphology*, 24, pp. 309-331.

Leong, E.C. and H. Rahardjo, 1997. Review of soil-water characteristic curve equations. J. Geotech. Geoenviron. Eng., 123: 1106-1117.

Li, A. G., Yue, Z. Q., Tham, L. G., Lee, C. F. and Law, K. T. (2005) “Field-monitored Variations of Soil Moisture and Matric Suction in a Saprolite Slope,” *Ca. Geotech. J.*, 42, 13-26.

Low, T. H., Faisal, H.A., Saravanan, M. (2000). “Suction and Infiltration Measurement on Cut Slope in Highly Heterogeneous Residual Soil,” *Asian Conference on Unsaturated Soils*, Singapore.

McCord, J. T. (1991). “Application of second-type boundaries in unsaturated flow modeling,” Water Resour. Res., 27(12).

McKee, C. R., and Bumb, A. C. (1987). "Flow-testing coalbed methane production wells in presence of water and gas," SPE Formation Evaluation, (Dec.), 599-608.

Mualem, Y. (1976). "A new model for predicting the hydraulic conductivity of unsaturated porous media," Water Resources. 12:513-522.

National Research Council (NRC) (2004). "*Partnerships for Reducing Landslide Risk-Assessment of the National Landslide Hazard Mitigation Strategy*," Washington, DC, National Academy Press, 131 pp.

Pando, M, Mejías, M., Molina, G., and Fernos, R. (2007). "Case Study of Rainfall Induced Instabilities on Unsaturated Residual Soils Slopes in Puerto Rico", *First North American Landslide Conference*, June, 2007.

Pando, M.A., Ruiz, M.E., Larsen,M.C. (2005), "Rainfall-induced landslides in Puerto Rico: An Overview", ASCE, Geotechnical Special Publication No. 140: "Slopes and Retaining Structures under Seismic and Static Conditions", 15 p.

Polemio, M. and Petrucci, O. (2000), "Rainfall as a landslide triggering factor: An overview of recent international research", in Landslides in Research, Theory and Practice, Vol. 3, pp. 1219-1226.

Preston, N.J. (2000), "Feedback effects of rainfall-triggered shallow landsliding", in Landslides in Research, Theory and Practice, Vol. 3, pp. 1239-1244.

Rahardjo, H., Leong, E. C., Gasmo, J. M., and Tang, S. K. (1998) "Assessment of rainfall effects on stability of residual soil slopes," *Proceeding of 2nd International Conference on Unsaturated Soils, Beijing, PR China, 01:280-5*.

Rahardjo, H., Li, X. W., Toll, D. G., and Leong, E. C. (2001) "The effect of Antecedent Rainfall on Slope Stability," *Geotech. and Geolog. Eng.*, 19, 371-399.

Rahardjo, H., Tsaparas, I., Toll, D. G., and Leong, E. C. (2002). "Controlling parameters for Rainfall-induced Landslides," *Computers and Geotechnics*, 29, 1-27.

Sisson, J. B. (1987). “Drainage from layered field soils: Fixed gradient models,” Water Resour. Res., 23(11).

Sweeney, D. J. (1982). “Some In Situ Soil Suction Measurements in Hong Kong's Residual Soil Slopes,” *7th Southeast Asian Geotechnical Conf.*, Hong Kong.

Terzaghi, K. (1943). “Theoretical Soil Mechanics,” John Wiley and Sons, New York.

Tsaparas, I., Rahardjo, H., Toll, D.G. and Leong, E.C. (2002). “Controlling Parameters for Rainfall-Induced Landslides,” Computers and Geotechnics, Vol. 29, pp. 1-27.

van Genuchten, M.Th. (1980). “A closed-form equation for predicting the hydraulic conductivity of unsaturated soils,” Soil Sci. Soc. Am. J. 44:892-898.

Wieczorek, G.F. and Sarmiento, J. (1988), “Rainfall, piezometric level and debris flows near La Honda, California, in storms between 1975 and 1983”, Ellen and Wieczorek eds., USGS Professional Paper 1434, 43-62.

Zhan, T. L., Ng, C.W.W and Fredlund, D. G. (2007). "Field Study of Rainfall Infiltration into a Grassed Unsaturated Expansive Soil Slope," *Canadian Geotechnical Journal*, 44(4), 392-408.